# Protecting Diamond Indenters for Nanoindentation between 400-750°C using Titanium PVD Coating

# PROTECTING DIAMOND INDENTERS FOR NANOINDENTATION BETWEEN 400-750°C USING TITANIUM PVD COATING

BY

ANDREW S. WEAVER, B.Eng., (Mechanical Engineering)

McMaster University, Hamilton, ON, Canada, M.A.Sc., (Mechanical Engineering)

McMaster University, Hamilton, ON, Canada

A THESIS

SUBMITTED TO THE DEPARTMENT OF MECHANICAL ENGINEERING

AND THE SCHOOL OF GRADUATE STUDIES

OF MCMASTER UNIVERSITY

IN PARTIAL FULFILMENT OF THE REQUIREMENTS

FOR THE DEGREE OF

DOCTOR OF PHILOSOPHY

Doctor of Philosophy (2022) McMaster University

(Mechanical Engineering) Hamilton, Ontario, Canada

| | |
|---|---|
| TITLE: | Protecting Diamond Indenters for Nanoindentation between 400-750°C using Titanium PVD Coating |
| AUTHOR: | Andrew S. Weaver<br>B.Eng., (Mechanical Engineering)<br>McMaster University, Hamilton, ON, Canada<br>M.A.Sc., (Mechanical Engineering)<br>McMaster University, Hamilton, ON, Canada |
| SUPERVISOR: | Dr. Stephen Veldhuis |
| NUMBER OF PAGES: | xviii, 175 |

**Dedications** *The fear of the Lord is the beginning of knowledge - Proverbs 1:7a*

*My Lord Jesus, thank you for this opportunity to learn a bit more of You through Your creation. This work is Yours.*

*Soli Deo Gloria*

# Abstract

The 400°C limitation to the most common nanoindenter material, diamond, is not due to diamond changing to graphite in air, which can happen above 750°C, but to the reaction of the nanoindenter with the sample, causing a change in the geometry. The nanoindentation methodology is very sensitive to a change in nanoindenter geometry, thus the typical solution for measurements above 400°C is to use a cBN nanoindenter. However, the cBN indenter that is commercially used at temperatures above 400°C is too soft for measuring hard coatings such as machine tool coatings. There is limited published research on improving nanoindentation measurements in this way. Thus, the objective of this thesis is to address whether a coated diamond could be used for nanoindentation between 400-750°C.

Due to the results of early experiments PVD titanium is the focus of this thesis as it will adhere to diamond by forming a carbide interlayer, TiC. A methodology to determine the best coating based on resistance to oxidation and robustness of the coating at temperature was used, allowing the exploration of several different titanium based alloys and coating thickness. The methodology used is as follows:

1. PVD coatings of titanium and titanium based alloys TiAl, TiN, and TiAlN

were oxidized at 500, 575, and 650°C. Measurements by SEM and EDS were taken after the oxidation at each temperature. Of the coatings tested, the pure titanium coating was determined to be the best coating.

2. The coating thickness of 0.25, 0.50, and 1.0 $\mu$m were evaluated with the same static oxidation test applied to the different alloys. It was determined that 0.50 $\mu$m was the best thickness. A duplicate 0.50 $\mu$m thick sample had a cross-section machined by FIB, and was examined by STEM, HAADF and EELS. The results confirmed that TiC was being formed at the expected rate.

3. To determine whether a coated nanoindenter could be used for measurements, a nanoindenter was first calibrated, coated by PVD with 0.50 $\mu$m thick titanium, and calibrated again. The results confirmed that a coated nanoindenter could be used for performing nanoindentation measurements.

4. To determine whether the titanium PVD coating would adhere to the diamond at temperature, a coated nanoindenter was used to measure fused silicon at 450°C. After each measurement, the nanoindenter was examined by SEM and EDS. The results confirmed that the titanium coating adhered to the diamond.

This thesis demonstrates that a titanium PVD coating can protect a diamond nanoindenter during measurements between 400-750°C. The primary contributions are that coated diamond nanoindenters can be used for nanoindentation measurements, and that titanium PVD coated nanoindenters can be used for nanoindentation measurements between 400-750°C. Additional contributions include the testing of adhesion of titanium PVD coating to diamond between 400-750°C, and a methodology of evaluating coatings.

# Acknowledgements

To my wife and children, this is as much yours as mine; without your patience and encouragement this would have never been completed.

To my extended family - my parents, my wife's parents, brother- & sister-in-laws - you have been a source of never ending support.

To Dr. Veldhuis, my mentor and advisor.

To Dr. Arif, my guide through this process.

To all those who assisted in my research, particularly Bipasha Bose, Jhoynner Martinez, Majid Abdoos, & Md. Shariful (Sharif) Chowdhury.

To Dr. Kirstein, my manager who encouraged me to do this, lead by example, and was always an encouraging phone call away.

To Candu Energy Inc., formerly Atomic Energy Canada Ltd., who have been supportive of my educational endeavours.

To all those who have offered support, encouragement, and help, thank you.

# Notation and abbreviations

cBN - cubic Boron Nitride

CVD - Chemical Vapour Deposition

DAF - Diamond Area Function

DTA - Differential Thermal Analysis

EDS - Energy Dispersive X-Ray Spectroscopy

EELS - Electron Energy Loss Spectroscopy

HAADF - High Angle Annular Dark-Field (Microscopy)

MMRI - McMaster Manufacturing Research Institute

nanoindenter - the indenter portion of the nanoindentation machine

PCD - Polycrystalline Diamond

PVD - Physical Vapour Deposition

SEM - Scanning Electron Microscopy

STEM - Scanning Transmission Electron Microscope

XRD - X-Ray Diffraction

# Contents

# List of Tables

# List of Figures

# Chapter 1

# Introduction

## 1.1 Problem Statement

Nanoindentation is commonly used for measuring the mechanical properties of PVD and/or chemical vapour deposited (CVD) thin coating such as those used on cutting tools. One of the advantages of nanoindentation is that the depth of penetration is so small that coatings can be measured with minimal secondary effects from the substrate. Of great interest are the material properties of the PVD cutting tool coatings at the temperatures they would experience during machining, which can exceed 1000°C (Fox-Rabinovich *et al.*, 2012; Trent and Wright, 2000; Ning *et al.*, 2001, 2008; Venkatesh *et al.*, 1993) in workpieces with poor heat distribution. Unfortunately, the experience with nanoindentation measurements at elevated temperature has shown that cBN indenters are too soft to measure these coatings. Diamond is known to transform directly into graphite in air at 750°C (Howe, 2001). However, it has been previously demonstrated that diamond will react with air and the sample at 400°C during nanoindentation (Wheeler *et al.*, 2010b), most likely due to the effect of the

high pressure experienced during the measurement. If the diamond could be protected such that it would be shielded from oxygen the hypothesis is that it will then be able to perform measurements between 400-750°C which would improve the capabilities of the nanoindentation instrument to measure hard samples. The ability to use a coated diamond in air would also create a lower price point for high temperature nanoindentation, as the vacuum chamber and other accessories would only be necessary for particularly reactive samples or for measurements above 750°C (the temperature that diamonds turns straight to graphite).

## 1.2 Background

This section will cover three areas that are crucial for understanding the scope and motivation of this work:

- Nanoindentation theory to understand the requirements,
- Current elevated temperature methodology, and
- PVD cutting tool coatings as an example of a high value application.

### 1.2.1 Nanoindentation

The use of indentation to characterize material was first introduced by Brinell in 1900 (Brinell, 1900) when he pressed a hardened sphere into a sample at a set load and measured the imprinted diameter. A similar methodology was published by Meyer in 1908 (Meyer, 1908).

The use of a pyramid instead of a sphere was introduced in 1908 by Ludwik (Ludwik, 1908), and then later by Smith (Smith and Sandland, 1925) in what would be called the Vickers test.

The mathematical relationship of a sphere indenting a surface was first explored by H. Hertz in 1881 and 1882 (Hertz, 1896a,b), mainly as a theoretical exercise. This was followed by the work of Boussinesq (Boussinesq, 1885), whose work determining the stress distribution within an elastic half-space when deformed by the normal pressure applied by a rigid punch, using the classic theory of elasticity, was applicable for several different indenter shapes. Partial numerical results based on his solution were later derived by Love for flat-ended cylindrical (Love, 1929) and conical punches (Love, 1939).

Further numerical methods were developed by Sneddon, published over several decades (Sneddon, 1946, 1948, 1951, 1960, 1965), while key experimental findings were published by Stilwell and Tabor (Stilwell and Tabor, 1961; Tabor, 1951).

Some of the earliest research into nanoindentation with a Berkovich indenter was by Pethica *et al.* (Pethica *et al.*, 1983), but it is the methodology of Oliver and Pharr (Oliver and Pharr, 1992), and their methodology refinement (Oliver and Pharr, 2004), that is used for current nanoindentation instruments. As the hardness, $H$, and effective elastic modulus, $E_r$, values are optimized in chapter 6 to show that a coated nanoindenter can be used for nanoindentation measurements, the full derivation of the formulas is shown here.

From the loading and unloading curve of the nanoindentation measurements, Oliver and Pharr determined a method to ascertain the effective elastic modulus, $E_r$, and the hardness, $H$. It is termed a $W - h$ curve, an example of the indentation load, $W$, versus displacement, $h$ can be seen in figure 1.1. The maximum load, $W_{max}$, maximum displacement, $h_{max}$, and stiffness, $S$, are all read from the graph used to calculate the effective elastic modulus, $E_r$, and hardness, $H$. The mathematics behind these evaluations will be described in the following sections.

**Effective Elastic Modulus Calculation**

The basis for the calculation to determine the effective elastic modulus begins with three assumptions:

1. That the Berkovich indenter geometry can be approximated by a conical indenter (Doerner and Nix, 1986; Pharr *et al.*, 1992).

2. That the initial contact area is constant, and, thus, the initial unloading is linear (Doerner and Nix, 1986).

3. That as the contact area is constant for the initial unloading, Sneddon's (Sneddon, 1965) equation for a cylindrical punch can be used instead of a conical punch, which greatly simplifies the analysis.

The beginning of the analysis of the $W - h$ curve starts with the derivation of the total load from Sneddon (Sneddon, 1965),

$$W = \frac{4\mu r}{1-\nu} \int_0^1 \frac{x^2 f'(x)\, dx}{\sqrt{1-x^2}}, \tag{1.1}$$

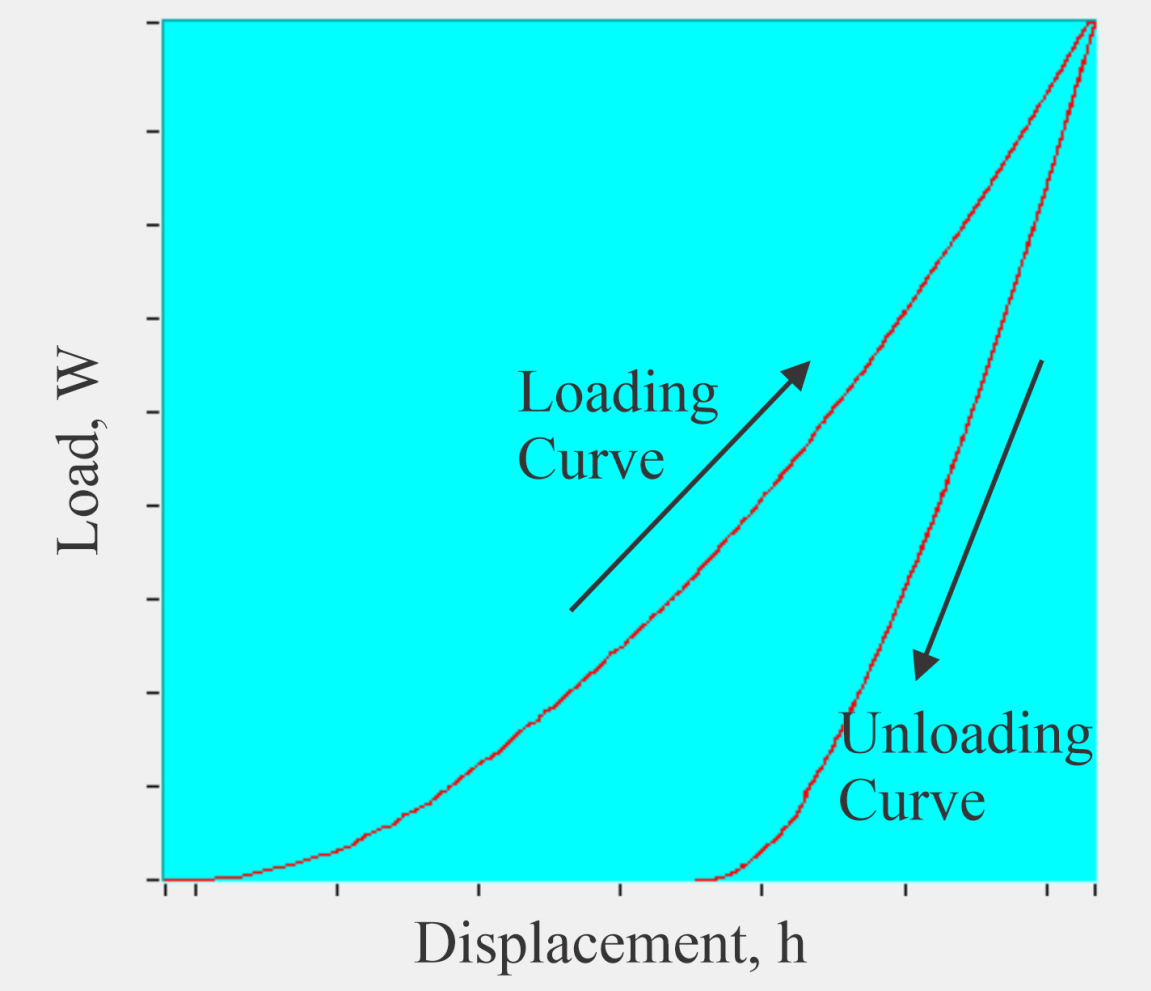


Figure 1.1: Example of load ($W$) - displacement ($h$) curve

where $\mu$ is the rigidity modulus, $\nu$ is the Poisson ratio of the sample, $r$ is the radius of the circle of contact, and $f$ is the equation representing the punch (with $f'$ the derivative).

By assuming an isotropic elastic material, Loubet et al. (Loubet *et al.*, 1984) concluded that if the area in contact remains constant during unloading, then the elastic behaviour can be modeled as that of a blunt punch, thus using Sneddon's (Sneddon,

1965) simpler maximum load solution for a cylindrical punch,

$$W = \frac{4\mu r h}{1-\nu}, \tag{1.2}$$

where $h$ is the maximum depth of penetration of the punch.

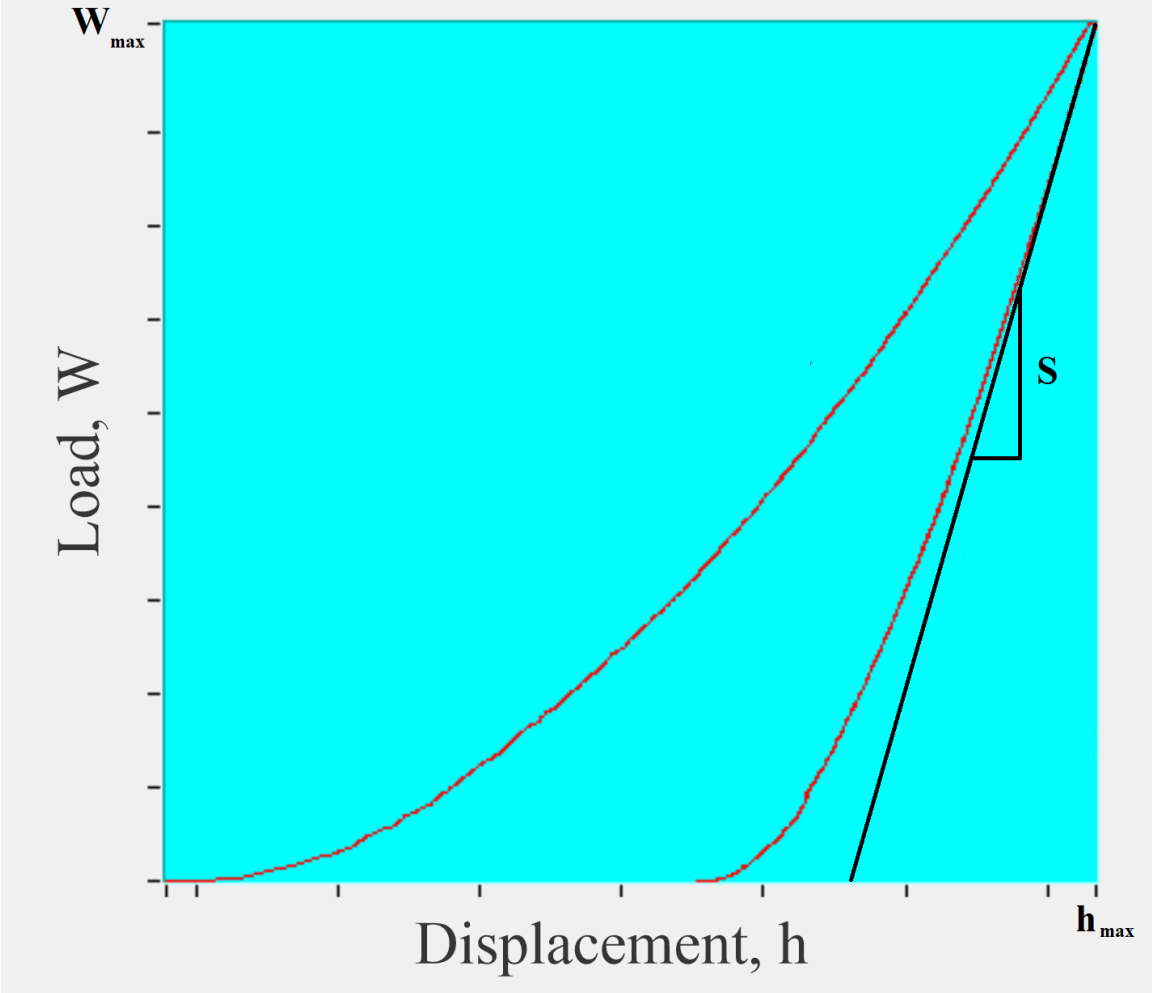


Figure 1.2: $W - h$ load schematic

Assuming that the same condition is present during the initial unloading of a nanoindenter, Oliver and Pharr (Oliver and Pharr, 1992, 2004) used this equation to determine the stiffness, $S$, defined as the slope of the linear portion of the unloading curve (see figure 1.2),

$$S = \frac{dW}{dh}, \tag{1.3}$$

which is the derivative of equation (1.2),

$$\frac{dW}{dh} = \frac{4\mu r}{1-\nu}. \tag{1.4}$$

Now, taking the area of a circle, $A$,

$$A = \pi r^2, \tag{1.5}$$

and solving for $r$,

$$r = \sqrt{\frac{A}{\pi}}, \tag{1.6}$$

and then substituting into equation (1.4),

$$\frac{dW}{dh} = \sqrt{\frac{A}{\pi}}\frac{4\mu}{1-\nu}, \tag{1.7}$$

gives a relationship between the stiffness, $S$, and the projected area of contact, $A$. This relationship can be used to determine the elastic modulus, $E$, starting with the relationship between the shear modulus and elastic modulus,

$$E = 2\mu\left(1+\nu\right). \tag{1.8}$$

This is re-arranged to solve for $\mu$,

$$\mu = \frac{E}{2\,(1+\nu)}, \tag{1.9}$$

and then substituted into equation (1.7),

$$\frac{dW}{dh} = \frac{2E}{1-\nu^2}\sqrt{\frac{A}{\pi}}. \tag{1.10}$$

Now, the portion of equation (1.10) that is the elastic modulus, $E$, over Poisson's ratio, $\nu$,

$$\frac{E}{1-\nu^2}, \tag{1.11}$$

does not account for both the indenter and the testing sample (Timoshenko, 1951). To account for both the indenter and the testing sample, the elastic modulus is recognized as the effective elastic modulus, $E_r$, and is a combination of the elastic modulus and Poisson's ratio of the sample, $E_s$, $\nu_s$, and the elastic modulus and Poisson's ratio of the indenter, $E_i$, $\nu_i$,

$$E_r = \frac{E_s}{1-\nu_s^2} + \frac{E_i}{1-\nu_i^2}. \tag{1.12}$$

Therefore, when $E_r$ is substituted into (1.10) and solved for, the resulting equation is

$$E_r = \frac{dW}{2dh}\sqrt{\frac{\pi}{A}}. \tag{1.13}$$

Now, $A$, the projected area of contact is a function of $h_c$, the depth of contact, which is described in figure 1.3.

As can be seen in figure 1.3, $h$ is the maximum displacement, $h_s$ is the sink-in depth

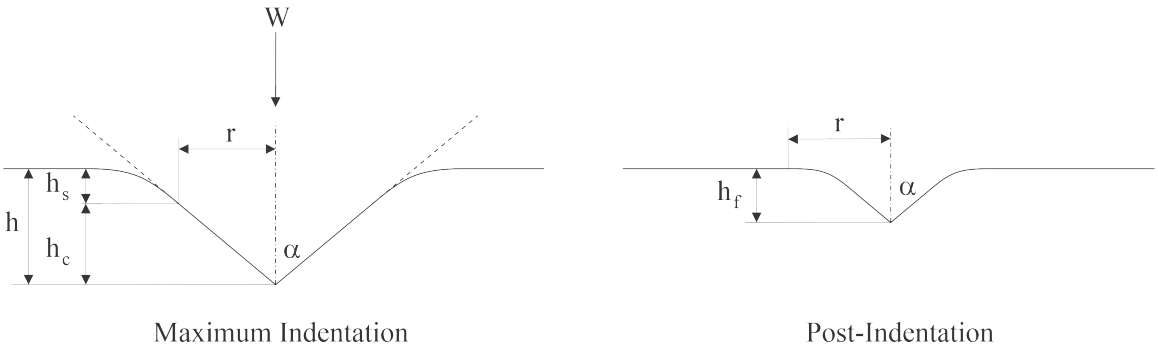


Figure 1.3: Schematic of indentation

(the depth due to elastic deformation from the indenter), $h_f$ is the final depth once the indenter is removed, and $a$ is the radius of the indenter.

Now, to determine $h_c$, begin with Sneddon's (Sneddon, 1965) definition for the vertical displacement of a conical indenter,

$$u_z(\rho, 0) = \frac{2D}{\pi r}\left\{ r \sin^{-1}\left(\frac{r}{\rho}\right) - \rho + \sqrt{\rho^2 - r^2} \right\}. \tag{1.14}$$

In the purely elastic case, at maximum displacement,

$$u_z(r, 0) = h_s, \tag{1.15}$$

where,

$$\rho = r. \tag{1.16}$$

This means that the equation is being applied right at the edge of the indenter. The relationship to the other indentation variables from figure 1.3 can be expressed as

$$D = h - h_f, \tag{1.17}$$

where $h$ is the maximum displacement, and $D$ is the depth of elastic penetration. Substituting equation (1.16) and (1.17) into Sneddon's equation and solving,

$$h_s = \frac{2(h - h_f)}{\pi r}\left\{r\sin^{-1}(1) - r + \sqrt{r^2 - r^2}\right\}, \tag{1.18}$$

$$h_s = \frac{2(h - h_f)}{\pi r} r\left\{\sin^{-1}(1) - 1\right\}, \tag{1.19}$$

$$h_s = \frac{h - h_f}{\pi}(\pi - 2). \tag{1.20}$$

Now, taking Sneddon's (Sneddon, 1965) description of the conical punch load,

$$W = \frac{4\mu h^2 \cot\alpha}{\pi(1 - \eta)}, \tag{1.21}$$

and re-arranging,

$$\frac{W}{h} = \frac{4\mu h \cot\alpha}{\pi(1 - \eta)}, \tag{1.22}$$

to take the derivative,

$$dW = \frac{\mu h dh \cot\alpha}{\pi(1 - \eta)}, \tag{1.23}$$

$$\frac{dP}{dh} = \frac{8\mu h \cot\alpha}{\pi(1 - \eta)}. \tag{1.24}$$

Now, substitute equation (1.23) into the derivative to get

$$\frac{dW}{dh} = \frac{2W}{h}, \tag{1.25}$$

and solving for $h$, which from elastic conditions at maximum displacement is $h - h_f$,

$$h - h_f = \frac{2W}{\frac{dW}{dh}}. \tag{1.26}$$

Now, substituting equation (1.20) into (1.26),

$$h_s = \frac{2W\,(\pi - 2)}{\pi \frac{dW}{dh}} \tag{1.27}$$

However, the relationship between the load and displacement requires the context of the cross-sectional area displacement, $h_c$. From figure 1.3, the displacement relationships are:

$$h = h_s + h_c \tag{1.28}$$

At the maximum displacement where $h = h_{max}$, which results in the maximum load, $W_{max}$, with the stiffness, $S = dW/dh$. Substituting equation (1.27) into (1.28) as solving for $h_c$,

$$h_c = h_{max} - \frac{2W_{max}\,(\pi - 2)}{\pi S}, \tag{1.29}$$

where $h_{max}$, $W_{max}$ and $S$ can all be read from the unloading curve. In the case of the Micro Materials Vantage used for some of the experiments in this thesis, the constant $\epsilon$ is equated to the geometry as follows,

$$\epsilon = \frac{2\,(\pi - 2)}{\pi}. \tag{1.30}$$

When equation (1.30) is substituted into equation (1.29), the simplified equation is

$$h_c = h_{max} - \frac{W_{max}\epsilon}{S}. \tag{1.31}$$

**Non-linearity of Unloading Curve** Since the initial publication of the hardness methodology and calculations, there have been some adjustments made to address the non-linearity of the unloading curve and the approximation of the Berkovich indenter with a cone.

The first issue that is noted by Oliver and Pharr (Oliver and Pharr, 1992) is the non-linearity of the unloading curve, which follows the equation:

$$W = \alpha \left(h - h_f\right)^m \tag{1.32}$$

where the constants $\alpha$ and $m$ are material dependent. This non-linearity is due to the phenomenon where during the unloading there is a curve to the indentation's sides (Stilwell and Tabor, 1961; Tabor, 1951).

Because the portions of the effective elastic modulus and hardness equations that are based on Sneddon (Sneddon, 1965) and Doerner and Nix (Doerner and Nix, 1986) assume a linear unloading curve, finite element analysis was used to determine an "effective indenter shape" to transform the contact geometry into one where the flat punch and linear unloading approach could be used (Bolshakov and Pharr, 1998). The main limitation to choosing an effective indenter shape is that it requires prior knowledge of the pressure that is being applied to the sample, thus it is difficult to

apply to an unknown sample (Pharr and Bolshakov, 2002; Oliver and Pharr, 2004; Fischer-Cripps, 2011).

**Approximation of Berkovich Indenter with Cone** Another issue with the methodology has to do with approximating the Berkovich indenter with a cone, where in order to give the same area-to-depth ratio, the semi-angle is widened from 65.27 degrees to 70.3 degrees.

This was first noted by King (King, 1987), with the solution being the addition of a correction factor, $\beta$, thus the effective elastic modulus becomes

$$E_r = \frac{1}{\beta}\frac{dW}{2dh}\sqrt{\frac{\pi}{A}}, \tag{1.33}$$

where the value for $\beta$ typically ranges from 1.02 to 1.08 (King, 1987; Cheng and Cheng, 1998; Hay *et al.*, 1999).

### Hardness Calculation

The hardness value formula is

$$H = \frac{W_{max}}{A}, \tag{1.34}$$

where $W_{max}$ is the maximum load and the area, $A$, is a function of $h_c$, which was solved for in the previous section.

### Mathematical Assumptions to Method

The mathematics assume an ideal situation where there is no friction between the indenter and the sample. While this may be a small factor, it is an important one

when considering coating the indenter and its corresponding durability. This will be addressed further in chapter 3.

### 1.2.2 Cutting Tool CVD/PVD Coatings

Chemical and Physical Vapour Deposition (CVD and PVD, respectively), are two coating methodologies that are used for the coating of cutting tools or machine tool inserts. Cutting tools and machine tool inserts are sometimes used interchangeably as the tool that cuts away the workpiece, with many machine tools having interchangeable inserts that are easier to replace when worn. PVD and/or CVD coatings are used because, by reducing the wear rate they can extend tool life by a factor of 2 to 3 or, alternatively, enable the cutting speed to be increased by 25 to 50% during the high speed turning of cast iron and steel (Trent and Wright, 2000). Due to more recent finite element model (FEM) studies, it has been shown that a good coating will also reduce the maximum stress below the yield stress of the coating during machining operations (Bouzakis *et al.*, 2012; Attia *et al.*, 2002; Davies *et al.*, 2007; Klocke *et al.*, 2010; Rech *et al.*, 2005). As a note, the McMaster Manufacturing Research Institute does extensive research in cutting tool coatings, and this experience, particularly with some of the earliest and most common coatings such as TiN and TiAlN (Loffler, 1994; Bouzakis *et al.*, 2012), has been leveraged for this study on the coating of diamond.

#### Chemical Vapour Deposition

The first published research on CVD was in 1909 by Pring and Fielding (Pring and Fielding, 1909). The first use for commercial machine-tool coating was in 1969 by Krupp in West Germany. CVD coatings are still favoured in turning, but have a

tendency to fail from cyclic thermal load and forces in milling (Bouzakis *et al.*, 2012).

### Physical Vapour Deposition

The first publication concerning PVD coating was in 1857 by Michael Faraday (Faraday, 1857), but was first applied to machining in 1979 (Bouzakis *et al.*, 2012).

### Research Direction of Cutting Tool Coatings

Research in cutting tool coatings for decades has been focused on coating hardness due to the strong correlation between hardness and tool life (Sproul, 1996). The current area of advancement is the machining of much more difficult to machine alloys, such as Ni-based "super alloys" (Pervaiz *et al.*, 2014; Fox-Rabinovich *et al.*, 2010a,b). Many of these super alloys have poor heat distribution in the cutting zone, which can cause the tool tip to reach temperatures in excess of 1000°C with mechanical loads on the tools of 1-5 GPa (Fox-Rabinovich *et al.*, 2012).

As a result, the industry not only requires hard coatings at room temperature, but also ones at elevated temperatures. Protecting the diamond in a nanoindenter for this application would be advantageous for understanding machine-tool coatings, as measurements could be performed at temperatures closer to the temperature they experience during machining operations.

## 1.3 Hypothesis

Based on the background and the problem statement, the hypothesis to this thesis is that if diamond were protected in some manner, it could be used for an application

such as nanoindentation between the temperatures of 400-750°C.

## 1.4 Thesis Outline

The approach used in this thesis to substantiate the hypothesis is as follows:

1. Chapter 2: Literature Review - This illustrates that this is a unique work, while also showing that the coating decisions were based on previously published work.

2. Chapter 3: Test of Gold Coated Diamond Nanoindenter - This explores the use of a gold coating on the diamond nanoindenter. As the first coating attempt, this study revealed the need for better adhesion to the diamond and provided the motivation for exploring PVD coatings.

3. Chapter 4: Titanium Coatings - This documents the experiments that looked into Ti, TiAl, TiN, and TiAlN PVD coatings on diamond. Research into these types of coatings found that one of the most likely failure mechanisms of titanium-based coatings was oxidation at elevated temperatures, as titanium oxide is a powder and would fail to adhere to the diamond. As the cost of coating diamond nanoindenters is high, this chapter focuses on experiments performed on the flat diamond surface of a single crystal diamond tool which were available from ultra precision machining studies to determine the most oxidation resistant coating. The purpose of these experiments was to assess the adhesion of the coating and study the layer between the coating and the substrate to apply one or more coatings on a nanoindenter for use in nanoindentation measurements.

4. Chapter 5: Titanium Coating Thickness - As titanium was found to be the most oxidation resistant PVD coating, these experiments focus on determining

the optimum thickness for the titanium coating. As described in the nanoindentation measurement theory, it is important to know the geometry of the nanoindenter and for it to remain relatively constant throughout the measurement for the results to be accurate. Results from Chapter 4 indicated that thicker coatings were better in terms of oxidation, but thinner coatings would be better from a nanoindentation measurement perspective. This is because the relationship between the depth and the cross sectional area of the indenter (also known as the diamond area function) would change with any deformation of the coating. A thinner coating would experience a proportionally smaller deformation, and therefore cause fewer inaccuracies. Furthermore, the literature on diamond coating indicated that the TiC that forms on the interface between the diamond and the titanium is the source of the strong adhesion, so a heat treatment was introduced post-coating to ensure that there was a TiC interlayer in all the coatings.

5. Chapter 6: Nanoindentation Measurement with PVD Titanium Coated Nanoindenter - This is the documentation of the final experiment, where a PVD titanium coated nanoindenter performed a nanoindentation measurement at 450°C to corroborate the hypothesis.

6. Chapter 7: Conclusions and Recommendations

# Chapter 2

# Literature Review

## 2.1 Elevated-Temperature Nanoindentation Measurements

Elevated-temperature nanoindentation has been researched since the 1990's (Lucas and Oliver, 1995; Syed Asif and Pethica, 1998) in an attempt to determine the most effective method of performing an elevated temperature measurement. The most recent maximum temperature was 1000°C (Gibson *et al.*, 2017). The general trend for elevated temperature nanoindentation is that the entire indentation is performed inside a vacuum chamber, with heating elements on both the nanoindenter and the sample to control thermal drift. This design in its full conceptualized form was published by Trenkle (Trenkle *et al.*, 2010) for measurements at 500°C.

The typical high-temperature nanoindentation instrument centres around three things:

- High vacuum chamber

- Dual thermocouples for sample and nanoindenter
- cBN nanoindenter

The advantages to this system are that:

- The sample doesn't oxidize; thus, if a specific material nanohardness is required this protects the sample from reacting and generating oxides on the surface.
- Current systems can go up to 1000°C.

The disadvantages to this system are that:

- It is expensive.
- There is an added complexity to the operation.
- The cBN nanoindenter is softer than the diamond one.

As discussed in the problem statement, protecting the diamond to allow for its use at higher temperatures would enable nanoindentation instruments to forego the high vacuum chamber up to at least 750°C, which would lower the expense and complexity, while also allowing for the use of a harder nanoindenter. This review starts by surveying the literature to confirm that there is no record of an attempt at coating an indenter or nanoindenter. As no record was found, the review is broadened to survey indenter and nanoindenter materials, specifically establishing whether there is an indenter material of similar or higher hardness than diamond at temperatures between 400-750°C. As a subsidiary to the review of indenter materials, an analysis is performed based on published research that explores the relationship between the hardness of the indenter in comparison to the hardness of the sample. Once this

review establishes that there were no comparable indenter or nanoindenter materials of similar or higher hardness than diamond at the temperatures of interest, a more general literature survey was performed on the coating of diamond.

## 2.2 Indenter & Nanoindenter Materials and Coatings

A review of the literature about coating a traditional indenter (for example, for Brinell, Rockwell, Vickers, or Knoop hardness tests) or a nanoindenter used for nanoindentation tests, showed that there was no documented study of coating either indenter or nanoindenter, although Dr. Beeke of Micro Materials mentioned that they had looked into this idea but had not developed it (B. D. Beake, personal communication, October 2018). It should also be noted that although diamond is thermodynamically unstable at any temperature (Berman and Simon, 1955), the temperature at which it turns to graphite is unclear in the literature - ranging from 1500°C (Davies and Evans, 1972) to 900°C (Khmelnitsky and Gippius, 2014) to 500-750°C (Howe, 2001) based on diamond orientation and coverage. It is not uncommon to find diamond being used for Vickers and Knoop indentation at 1200°C (Everitt, 1990), despite how it admittedly dulls the indenter. It is therefore not surprising that traditional indentation would have the same issue with needing a harder indenter between the temperatures of 400-750°C, as diamond is still considered suitable.

In both nanoindentation and traditional indentation techniques to date, indenter

materials have all been uniform, uncoated materials. For performing nanoindentation measurements at temperatures above room temperature but below 400°C, the indenter of choice is diamond because of its hardness, low coefficient of friction and general inertness. It has been known since at least 2010 (Trenkle *et al.*, 2010) that a diamond indenter erodes at 500°C; further research by Wheeler (Wheeler *et al.*, 2010a) has reduced the practical application temperature for diamond to 400°C, in addition to demonstrating that performing a nanoindentation test in an inert gas of commercial purity does not help protect the diamond indenter. It should be noted that in both (Wheeler and Michler, 2013) and (Wheeler *et al.*, 2015) it is stated that diamond can be exposed to higher temperatures without oxidizing in high vacuum, while referencing a paper that used a sapphire indenter; to date, there is no published data to support that statement.

Nanoindentation above 400°C was first achieved by using sapphire for an indenter (Korte *et al.*, 2012) before sapphire fell out of favour due to its reactivity and lower hardness in comparison to the more popular indenter material, cBN (Harris *et al.*, 2016). These values are reflected in figure 2.1, where it shows that diamond (Mukhanov *et al.*, 2009) is by far the hardest material even when compared to cBN (Wheeler and Michler, 2013), Sapphire ($Al_2O_3$) (Mukhanov *et al.*, 2009), tungsten carbide (WC) (Lee, 1983), $ReB_2$ (Mukhanov *et al.*, 2009) and $B_4C$ (Mukhanov *et al.*, 2009). For nanoindentation Wheeler (Wheeler and Michler, 2013), in the most recent paper discussing indenter materials, cites $ReB_2$ and $B_4C$ (among other Boron compounds) as potential materials for high temperature nanoindentation. To date there is no published information on these materials as indenter materials, even

though $B_4C$ has been used for the large indentation methods at elevated temperatures (Koester and Moak, 1967). Note as well that the focus is on compounds and elements that make up the tip instead of protecting the diamond to extend its useful temperature.

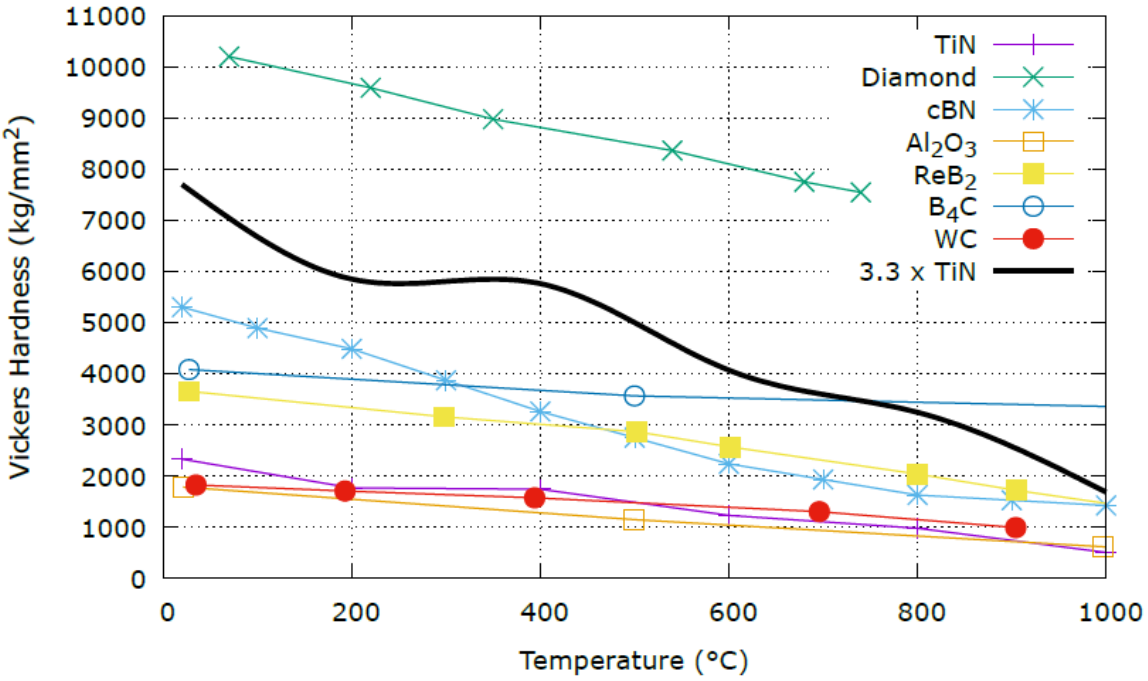


Figure 2.1: Vickers hardness vs. temperature of $Al_2O_3$, $B_4C$, cBN, Diamond, $ReB_2$, TiN, & WC

## 2.3 Hardness of Indenter vs. Hardness of Sample

What is unclear from comparing the different indenter materials is how hard they must be in relation to the sample. To date, there is no documented analysis of the limits of sample hardness, beyond the obvious conclusion that if the sample is harder than the indenter, the indentation is not going to work. It is only recently that the

issue of the elastic deformation of the indenter has begun to be addressed comprehensively (Lo and Bogy, 1999; Galanov and Dub, 2017).

For a general idea of the difference, the following is an adaptation of an analysis performed by Tabor (Tabor, 1948, 1951) for Vickers hardness where the relationship between the yield stress ($Y$) and the yield pressure ($P$) for a Vickers indenter was experimentally determined as:

$$P_{indenter} = 3.3Y \tag{2.1}$$

Now, due to the nature of the Vickers indentation test, the pressure is independent of the load. It is also thought that this relationship takes into account the friction between the indenter and the sample, as the theoretical relationship has the yield stress at 3 times the pressure.

The indenter and the sample both experience yield pressure, due to a balance of forces. As the pressure that the indenter undergoes is effectively the average stress, since it is the load divided by the cross-sectional area of the indenter, the pressure must be less than the yield stress of the indenter $Y_{ind}$:

$$Y_{ind} > P \tag{2.2}$$

which (2.1) can then be substituted into:

$$Y_{ind} > 3.3Y \tag{2.3}$$

Tabor also established experimentally that the relationship between the Vickers hardness $H_v$ and the yield strength was:

$$H_v = 3Y \tag{2.4}$$

Therefore, as there is a direct proportional relationship between the hardness and the yield strength, the same relationship exists between the hardness of the indenter and the sample as it does with the yield strength:

$$H_{v-indenter} > 3.3H_{v-sample} \tag{2.5}$$

Now, recalling figure 2.1, the hardness of a common cutting tool PVD coating, TiN (Quinto *et al.*, 1987), was graphed, in addition to 3.3 times this hardness. As can be seen, there is no indenter material besides diamond that would be able to indent this PVD coating at any temperature, with the exception of $B_4C$ above 800°C. Thus, if diamond could be protected, it would greatly improve the capabilities of nanoindentation instruments.

## 2.4 Coating for Diamond

The following is the review of different coatings considered for the diamond nanoindenter.

### 2.4.1 Gold

Due to the use of gold for dental, biomedical and electrical industries, research shows that the wear properties should be sufficient for nanoindentation (Bikulcius *et al.*, 1994). However, gold is generally electroplated onto copper or steel. There was no literature found on the coating of natural or synthetic diamond with gold; however, there was some research performed on the coating of CVD diamond with gold, whether by electroplating or by sputtering (Glezen *et al.*, 1999; Iacovangelo and Jerabek, 1993). In both cases, a PVD interlayer was used to bond the gold to the diamond.

### 2.4.2 Titanium

The literature review on coating diamond shows that carbide forming elements such as Ti, Cr, W, Zr, and V are effective for this purpose (Naidich *et al.*, 1984; Tadao *et al.*, 1997; Webb, 1999; Egan and Engels, 2004; Greene *et al.*, 2006). Wang et al. (Wang *et al.*, 2003) deposited 1 $\mu$m thick Ti coatings on a single crystal diamond, where they determined through tensile tests on the coating and through dissolving the Ti using a hydrogen flouride solution that the coverage of TiC underneath the Ti coating correlated to an increase in strength of the adherence of the Ti to the diamond. As the temperature range investigated was between 650°C and 800°C, the conclusion that TiC formed at 650°C does not answer the question of when TiC forms at temperatures between 400-650°C. From differential thermal analysis (DTA) of Ti coated diamond grits, Rosa et al. (Rosa *et al.*, 2015) showed that a Ti coating will oxidize at approximately 680°C, in addition to showing that the Ti coating will protect diamond at 1200°C for less than an hour. Zhang and Lu (Zhang and Lu, 2007) coated diamond grits with titanium 3 $\mu$m thick by PVD and uses an impact

test to show that Ti protects diamond. The temperature range explored was between 650°C and 1000°C. As can be seen from the literature, there is no data on oxidation protection between 400-750°C.

### 2.4.3 CVD Diamond Coating

As there is very little literature on the coating of diamond in the temperature ranges of interest, the chemical vapour deposition (CVD) of diamond on a substrate was examined as well. Through this literature, it has been well established that titanium will adhere to the diamond (Fu *et al.*, 2000; Polini *et al.*, 2006; Silva *et al.*, 2002; Yu *et al.*, 2014). It was also noted that the compound TiC will form at the interface at the temperatures at which CVD diamond is deposited (Fu *et al.*, 2000; Peng and Clyne, 1997). Further review into the oxidation protection that a TiC coating would offer found a paper that showed that it does protect diamond for a limited amount of time at 1200°C (das Chagas *et al.*, 2019).

There is no literature on a TiN coating being deposited on diamond. However, some papers discuss TiN being used as an interlayer for diamond CVD coating. In two papers, the TiN was PVD coated onto a substrate (Fu *et al.*, 2000; Polini *et al.*, 2006), and in the third paper, the TiN was laser-arc deposited (Endler *et al.*, 1996). In all the papers, the diamond was deposited on top by CVD. The conclusion from all three papers was that there is poor adhesion between the diamond CVD and the TiN coating. As the method for depositing TiN is to deposit titanium in a nitrogen gas environment, the hypothesis for the poor adhesion is that the nitrogen interferes with the titanium bonding to the diamond.

### 2.4.4 TiC

While researching how to ensure that TiC forms, a paper was found that investigated the diffusion of carbon into titanium and the formation of TiC between the temperatures 450-700°C (Arvieu *et al.*, 2004). It was noted when reviewing that paper that the largest increase in TiC thickness occurred between 450°C and 500°C, where the mean thickness more than doubled to 116 nm (with a standard deviation of 13.1 nm) for the same heat treatment time of 30 minutes.

## 2.5 Literature Review Summary

From the review of the literature, it is clear that there have been no studies that perform the same experiment and analysis of coating a diamond nanoindenter for use in nanoindentation tests from 400-750°C. Additionally, there is limited information on what coatings are ideal for this task and which are the most likely to protect the diamond from wear in such a way that the geometry would remain relatively constant. It must therefore be concluded that this thesis is a unique contribution to the existing literature.

# Chapter 3

# Test of Gold Coated Diamond Nanoindenter

## 3.1 Hypothesis

The hypothesis for this experiment is that gold will protect the diamond indenter.

## 3.2 Experimental Observations

As the first attempt at protecting the diamond indenter, a sputtered gold coating has several appealing characteristics. The equipment and technique are both readily available, which makes it cost effective and easy to perform. The sputtering technique does not damage the indenter in any way, which enables the researcher to immediately coat the indenter instead of coating a different sample and performing other tests on it to confirm its effectiveness.

In terms of material properties at temperatures between 400-750°C, gold is an inert solid, so it does not react with the sample or the diamond on the nanoindenter, nor does it melt. Gold is also known for its ability to be thinned to an almost atomistic level, which has a twofold advantage for this application. First, it is presumed that any deformation of the gold during the indentation would simply result in a thinner coating, which would maintain its role as a chemical/oxidation protector for the diamond underneath while the diamond retains its hardness (just like how the hardness of teeth is retained with gold fillings that keep the teeth together). Second, the mathematics of the nanoindentation measurement require that the geometry of the nanoindenter remain relatively constant throughout the indentation. For an already thin coating, further thinning would have a nominal effect on the results.

In addition to the assumption about how the gold will perform during nanoindentation, another assumption about this method is that the metal holding the diamond in the nanoindenter has enough surface roughness that if the gold does not bond to the diamond (something that is expected), it would at least friction fit to the holder. It is also assumed that if there is any friction between the nanoindenter and the sample, it would be insufficient to tear the gold away from the diamond.

## 3.3 Experiment Criteria

The criteria for this experiment is that the gold covers the diamond of the nanoindenter post-indentation.

## 3.4 Design of Experiment

Several attempts were made to adhere the gold to the surface of a nanoindentation indenter. Initial attempts with gold sheet that was press fit onto the indenter were unsuccessful, revealing that the assumption about the gold adhering to the metal holding the diamond was incorrect. However, these initial experiments provided good experience for a more comprehensive set of experiments. Two Berkovich indenters were prepared to be used for measuring a silicon glass calibration sample on a nanoindentation instrument (Micro Materials NanoTest Platform 3). The following methodology was used:

1. Sputter the gold onto the indenter to approximately 1.0 $\mu$m thick.
2. To ensure coverage of the indenter, inspect the surface using SEM and EDS.
3. Perform nanoindentation. In this case, the nanoindentation was performed on the silicon glass calibration sample, indenting to a maximum load of 500 mN. One indenter was used to perform a measurement at room temperature, while the other indenter was used to perform a measurement at 150°C. This was to see the effects of increasing the temperature and whether it would noticeably impact the results.
4. Measure the indenters with SEM and EDS to determine whether the gold was still covering the indenters.

## 3.5 Results

The initial SEM/EDS of the indenter can be seen in figure 3.1, where the gold thoroughly covers the indenter. The results of two tests performed on indenters at room

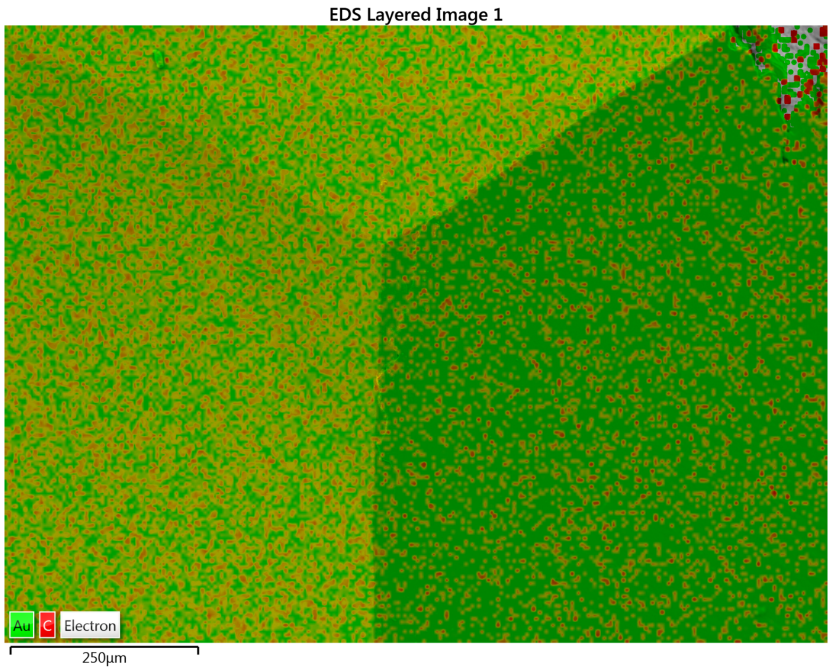


Figure 3.1: EDS of gold coated Berkovich indenter

temperature and 150°C can be see in figures 3.2 and 3.3, with the gold in yellow and the carbon of the diamond underneath indicated in red.

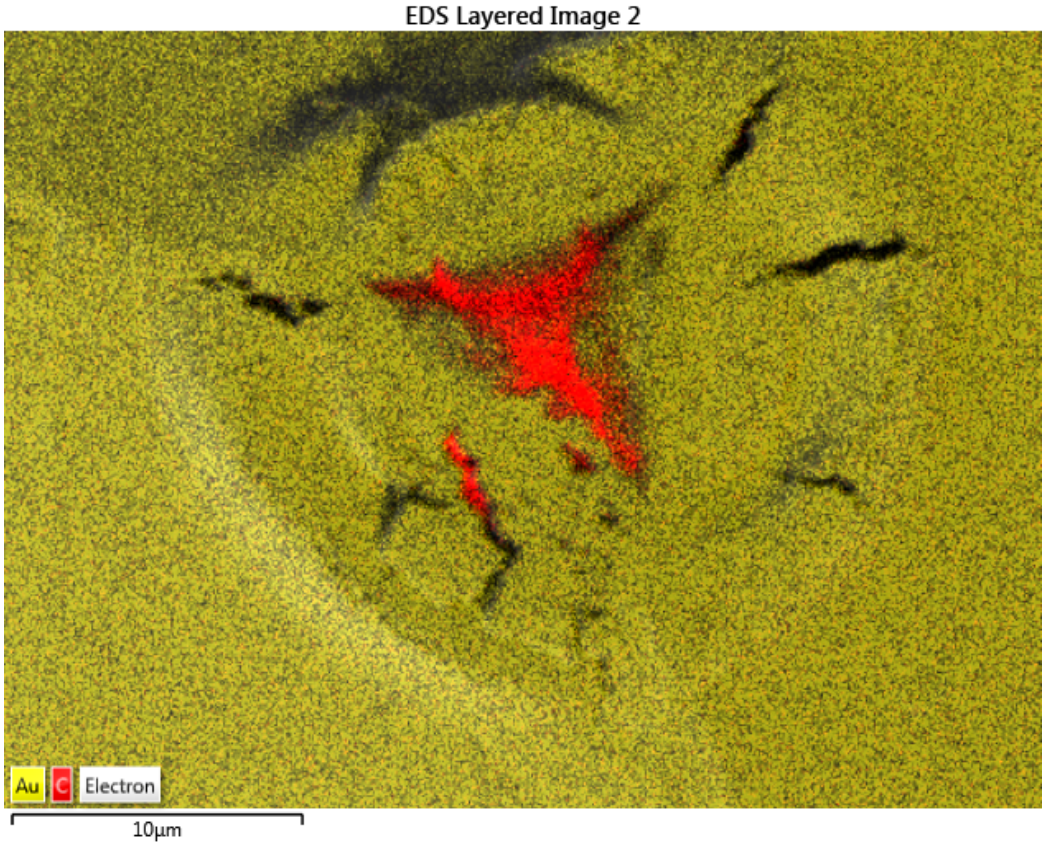


Figure 3.2: Auger SEM and EDS overlay of gold coated Berkovich indenter post room temperature indentation

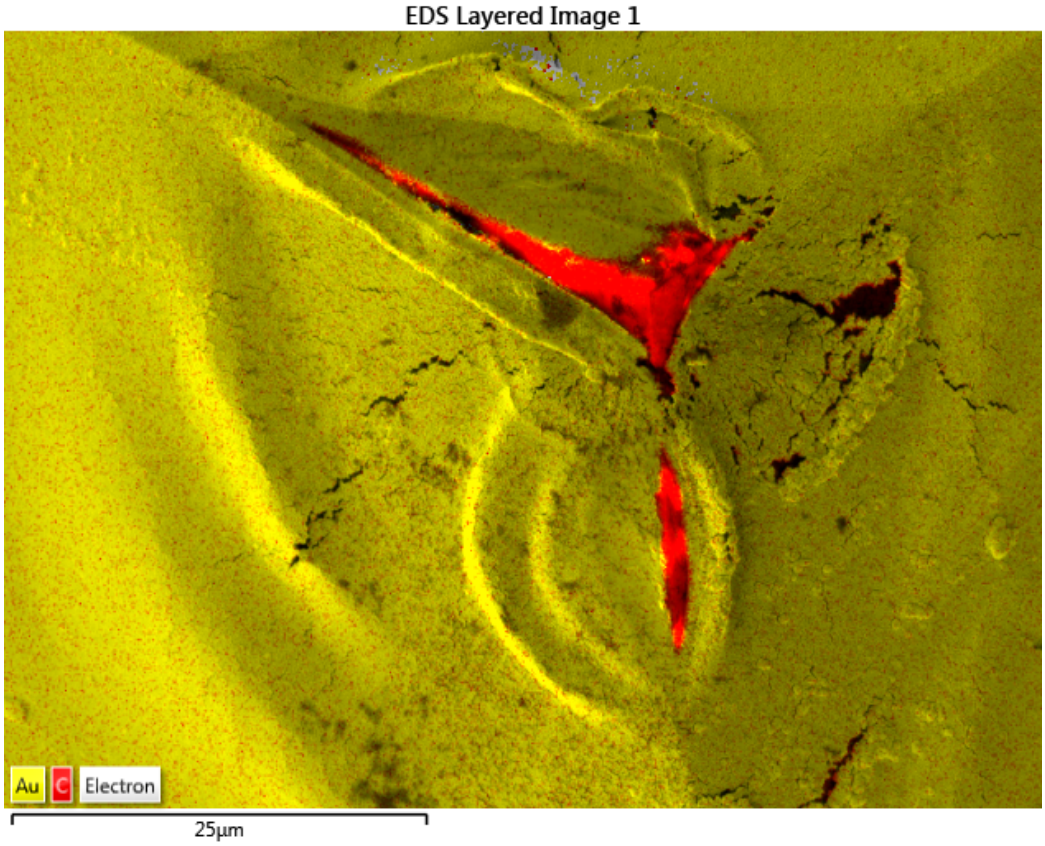


Figure 3.3: Auger SEM and EDS overlay of gold coated Berkovich indenter post 150°C indentation

## 3.6 Analysis

Figures 3.2 and 3.3 show that the gold was torn off at the tip of the indenter due to friction between the nanoindenter and the sample. For a full discussion on friction in indentation and nanoindentation, see appendix A. These results demonstrate that in order for a coating to be effective, it will need to be able to adhere to the diamond of the nanoindenter.

## 3.7 Conclusion

For nanoindentation with a Berkovich indenter, the results of coating it with gold show that there is friction in between the indenter and the sample high enough to tear the gold from the indenter tip. Two ways to address this are to look into whether using a spherical indenter would reduce the friction enough to protect the indenter, or to find a coating that would bond better to the diamond and therefore be more resistant to the effects of friction forces.

# Chapter 4

# Study of Titanium-based Coatings

## 4.1 Hypothesis

Titanium-based coatings as deposited by physical vapour deposition (PVD) can protect diamond at temperatures between 400-750°C.

## 4.2 Experiment Criteria

There was a two stage criteria used to examine the coatings under investigation. The first stage involved visually examining the SEM images to determine the integrity of the coating, where failure was defined as being able to visually identify the diamond substrate in the area that should be covered with the coating. Should the coating pass the first stage, the second stage statistically evaluated the atomic percent of the elements measured by EDS at several points across the coating surface. The depth of penetration of the EDS measurement is typically between 1 to 7 $\mu$m, and is based on the atomic properties and density of the elements and the beam energy

being used. For example, using the Kanaya-Okayama formula (Kanaya and Okayama, 1972) to approximate the maximum depth of penetration, the depth of penetration into pure titanium is 1.7 $\mu$m, and the depth of penetration into pure aluminium is 2.6 $\mu$m. Based on these numbers, it is expected that the EDS would penetrate through all the coatings and slightly into the diamond substrate. The results of the EDS measurements of all the coatings were then compared, with the best coating being the one with the lowest concentration of oxygen - i.e., indicating the coating least effected by oxidation.

## 4.3 Design of Experiment

The literature review showed that titanium reacts with the carbon in the diamond, which creates a strong bond between them. Thus, the coatings that were considered were metallic titanium coatings, Ti and TiAl, and ceramic titanium coatings, TiN and TiAlN. Additional elements were incorporated into the coatings based on experience in cutting tool coatings. Aluminium was included because it is common knowledge in cutting tool coatings that aluminium generates oxides at high temperatures which can be protective. The decision for using the nitrides in contradiction to the findings in literature is related to the appeal of the increased hardness and durability seen in its use as a cutting tool coating. It is inferred from the literature that this reaction between titanium and diamond, in addition to creating a strong bond, would also result in potential damage to the indenter during removal if the titanium layer adhered to the sample and pulled diamond with it upon retraction. The number of titanium-based coatings considered for PVD coating of the diamond indenter was limited by the cost of the target materials as they are cost prohibitive and can have long lead

times.

Aside from the wear experienced during indentation, the other concern with these materials for use as coatings was related to their own oxidation potential. The oxidation reactions for aluminium and titanium are as follows:

$$4\,Al + 3\,O_2 \longrightarrow 2\,Al_2O_3$$

$$Ti + O_2 \longrightarrow TiO_2$$

With respect to both metals, the 5-10 nm thick layer of oxide that forms on the surface of the metal at room temperature is considered protective. This is no longer the case when more of the coating is consumed in the reaction, as the oxide is a powder and would flake off under the wear experienced during nanoindentation. Therefore, this experiment considers an increase in oxygen under similar conditions to what would be seen when using the nanoindenter at elevated temperatures as a degradation to the coating.

### 4.3.1 Substrate Examination

To confirm the quality of the diamond substrate samples, the samples were measured with an Alicona Infinite Focus microscope, which visually looked at the physical state of the diamonds and the angles of the different faces in preparation for coating. The diamond samples were also examined in a SEM, a JEOL 6610LV, and a subset were inspected by an X-ray diffractor (XRD), a Bruker D8 DISCOVER with DAVINCI.DESIGN diffractometer using a Cobalt source.

### 4.3.2 Sample Preparation

A total of 12 samples were chosen to be PVD coated using an arc ion plating AIP-S20 PVD Hybrid coater (Kobelco, Japan). The 0.5-0.6 $\mu$m thick coatings were coated for 15 minutes, and the 1-1.5 $\mu$m thick coatings for 30 minutes. The pressure was 2.7 Pa in argon if the coating was metallic or in nitrogen if it was ceramic. The bias voltage was 50 V, the arc current 150 A, and the table rotation speed 5 rpm. There were 4 different sets of 2 for the metallic coatings, with each set coated as follows:

- Ti coating with a thickness of 0.5-0.6 $\mu$m
- Ti coating with a thickness of 1-1.5 $\mu$m
- TiAl 40:60 coating with a thickness of 1-1.5 $\mu$m
- TiAl 50:50 coating with a thickness of 1-1.5 $\mu$m

There were 2 different sets of 2 for the ceramic coatings, with each set coated as follows:

- TiN coating with a thickness of 1-1.5 $\mu$m
- TiAlN 50:50 coating with a thickness of 1-1.5 $\mu$m

The Ti coating was chosen to be the baseline, so its thickness was varied to study the effect of thickness on oxidation protection.

### 4.3.3 Experimental Procedure

#### Round 1

For the first set of experiments on the Ti and TiAl coatings, an initial methodology was applied that was modified for subsequent experiments to address the challenges

encountered. The methodology employed for this first round is as follows.

Once the samples were coated, they were then re-examined by XRD and SEM, before being statically oxidized in a furnace. The temperature in the furnace was raised at a rate of 1.6°C/min until it reached the holding temperature where it was maintained for 1 hour. Once an hour had passed, the furnace was turned off to allow the sample to be air cooled down to room temperature. After oxidation, the samples were examined again by SEM/EDS and XRD. The static oxidation was performed at 3 temperatures: 425°C, 500°C, and 575°C, in that sequence.

The refinements performed for subsequent experiments were as follows:

- Initial analysis indicated that very little happened to the coating at 425°C. The response to this initial finding was to increase the 3 oxidation temperatures in the second round to 500°C, 575°C, and 650°C. Comparison of the two sets of experiments found this to be an incorrect assumption, as shown in Appendix B, but as there was more interest in the higher set of temperatures, they continued to be used.

- The samples were small (approximately 0.5 cm x 0.5 cm) with a crystalline material structure, which is a challenge for the XRD technique. XRD measurements were therefore not taken in the second round due to their limited effectiveness.

- The glue that held the samples to a larger metal stud started to liquify at 500°C, and may have bubbled over onto the coated surface of the sample. Thus, there was contamination in some of the 500°C and several of the 575°C measurements.

For the second round, a high temperature cement was applied around the sides of the diamond in such a way as to reduce the chance that this would happen.

As a result of these modifications, the second round of experiments on the same coatings had much better measurement quality and therefore became the main focus of further study.

**Round 2**

The subsequent experiments on all the coatings listed in section 4.3.2 were performed in the following manner. Once the samples were coated, they were then re-examined by SEM, before being statically oxidized. This was done by placing them in a furnace and raising the temperature at a rate of 1.6°C/min until the hold temperature was reached, at which it was held for 1 hour. After the hour was complete, the furnace was shut off and the sample allowed to air cool down to room temperature. After the oxidation, they were again examined by SEM/EDS. The static oxidation was performed at 3 different hold temperatures: 500°C, 575°C, and 650°C. The flow chart of the methodology can be seen in figure 4.1.

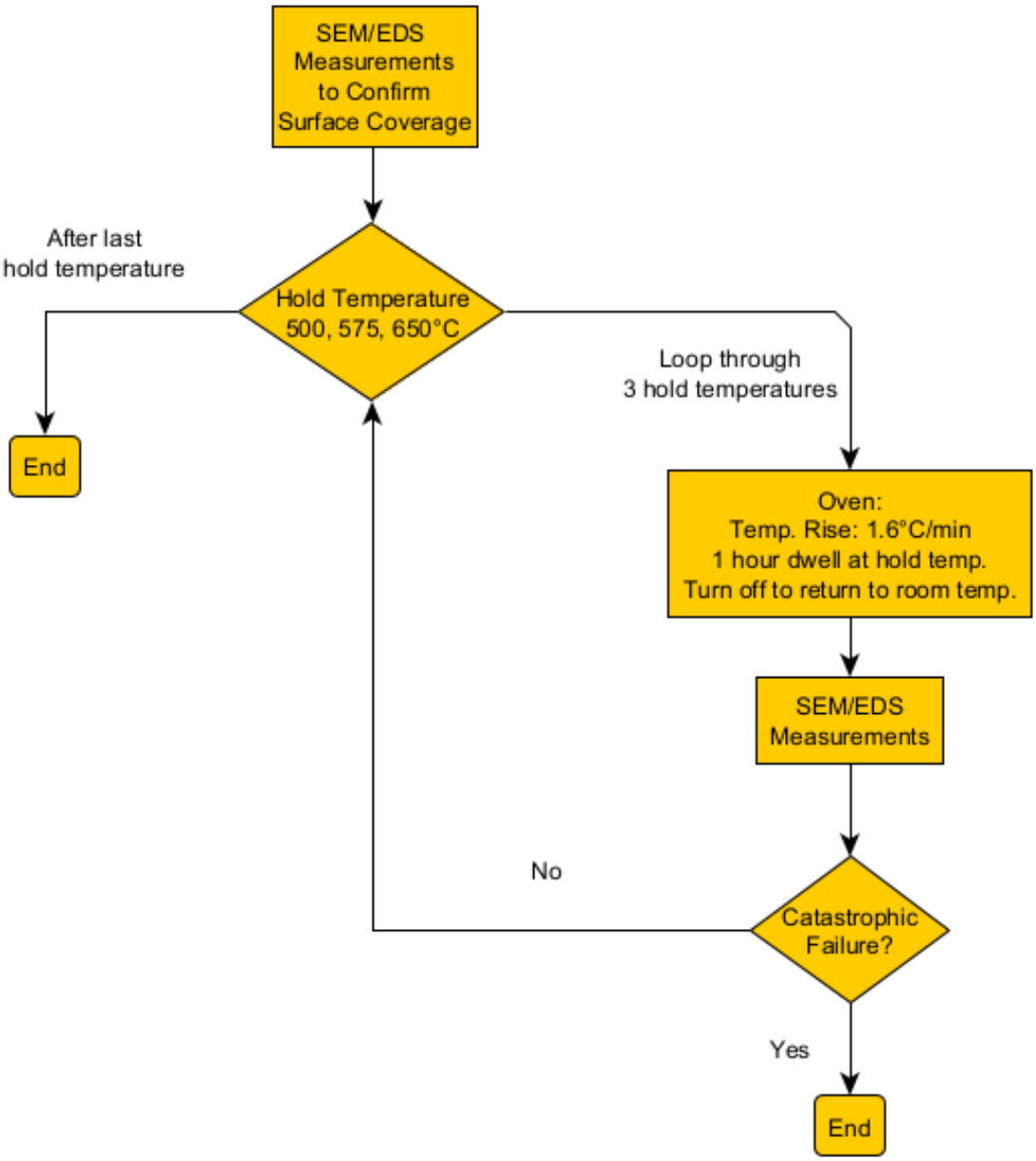


Figure 4.1: Study of Ti-based Coatings Methodology

## 4.4 Results

These are the results of the second round of experiments performed at 500°C, 575°C, and 650°C, where the SEM and EDS point analysis were transferred to a database and analyzed. The bar graphs show the site number on the x-axis, and the atomic percent on the y-axis. The SEM pictures have the location of the EDS site locations, which correspond to the site numbers on the x-axis of the graph. Before graphing, the data was filtered, excluding all elements except for Ti, Al, O, and C. If the graph does not have one of those 4 elements, then it was not found in the EDS element analysis. The bar graph is stacked, so if there are only members of the elements of interest detected, the atomic percent will add up to 100%.

### 4.4.1 Metallic Titanium Coatings

#### Ti Coating with 0.5-0.6 $\mu$m Thickness

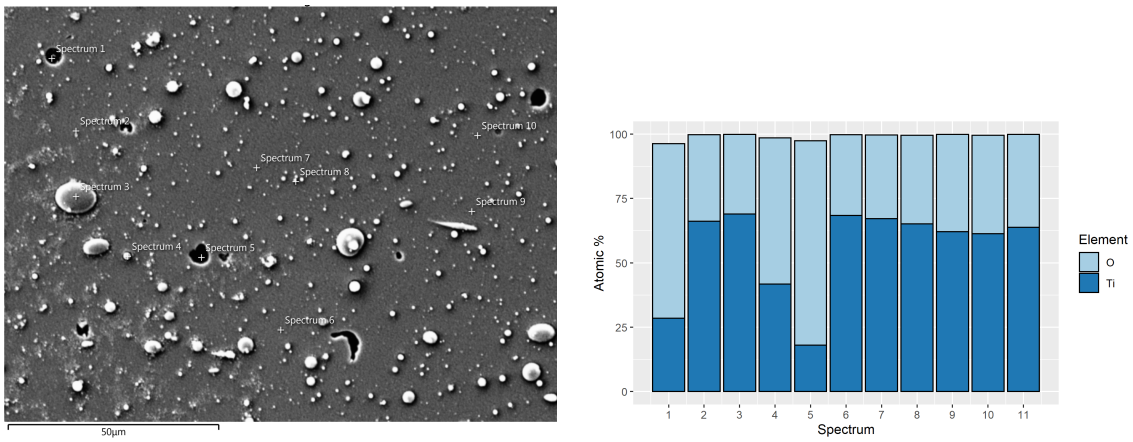


(a) EDS site locations (b) Atomic percent at spectrum locations

Figure 4.2: Ti coating 0.5 - 0.6 $\mu$m thick at 500°C SEM/EDS site analysis

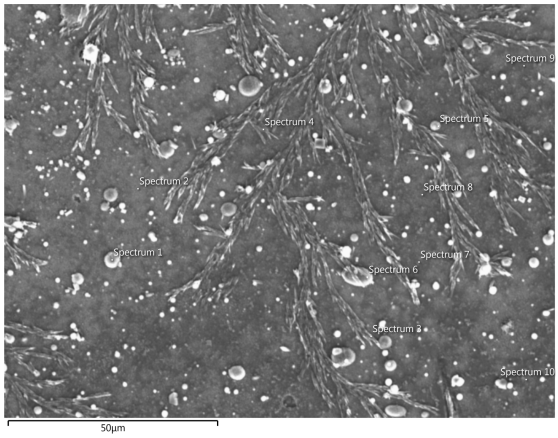


(a) EDS site locations

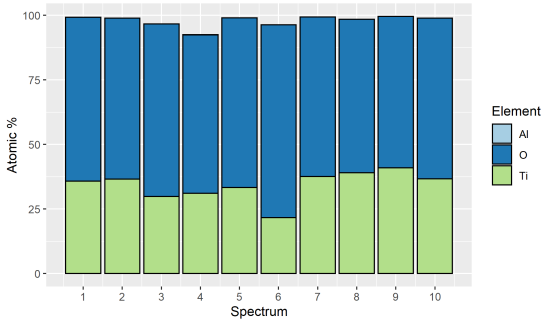


(b) Atomic percent at spectrum locations

Figure 4.3: Ti coating 0.5 - 0.6 $\mu$m thick at 575°C SEM/EDS site analysis

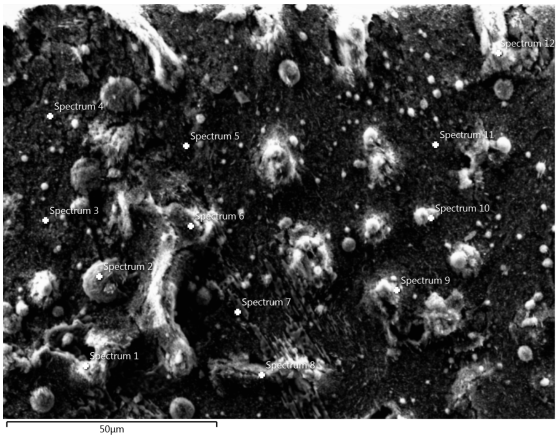


(a) EDS site locations

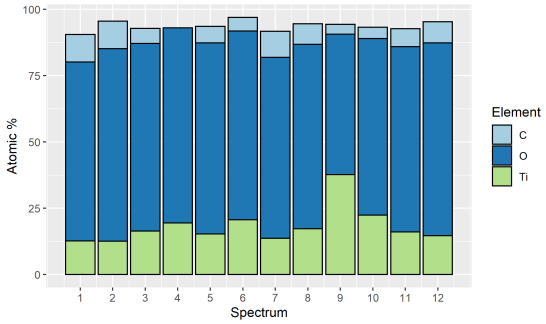


(b) Atomic percent at spectrum locations

Figure 4.4: Ti coating 0.5 - 0.6 $\mu$m thick at 650°C SEM/EDS site analysis

### Ti Coating with 1.0-1.5 $\mu$m Thickness


(a) EDS site locations

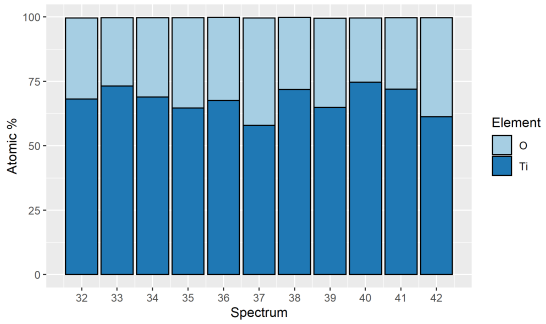


(b) Atomic percent at spectrum locations

Figure 4.5: Ti coating 1.0 - 1.5 $\mu$m thick at 500°C SEM/EDS site analysis

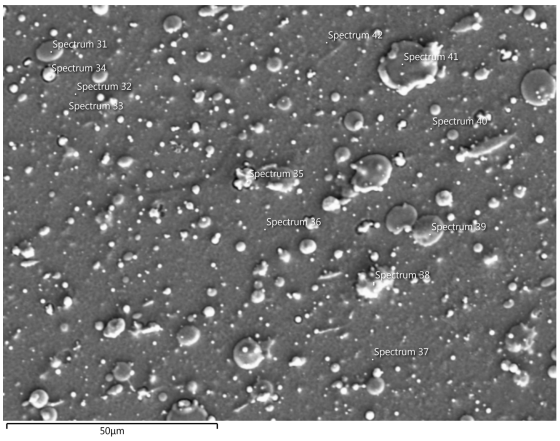


(a) EDS site locations

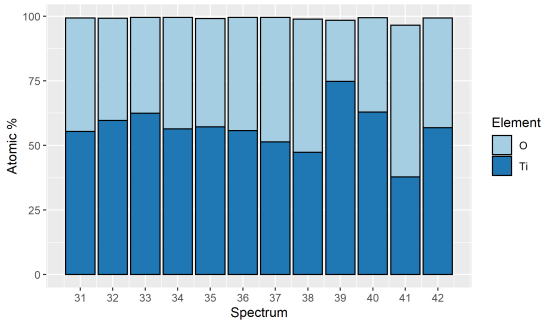


(b) Atomic percent at spectrum locations

Figure 4.6: Ti coating 1.0 - 1.5 $\mu$m thick at 575°C SEM/EDS site analysis

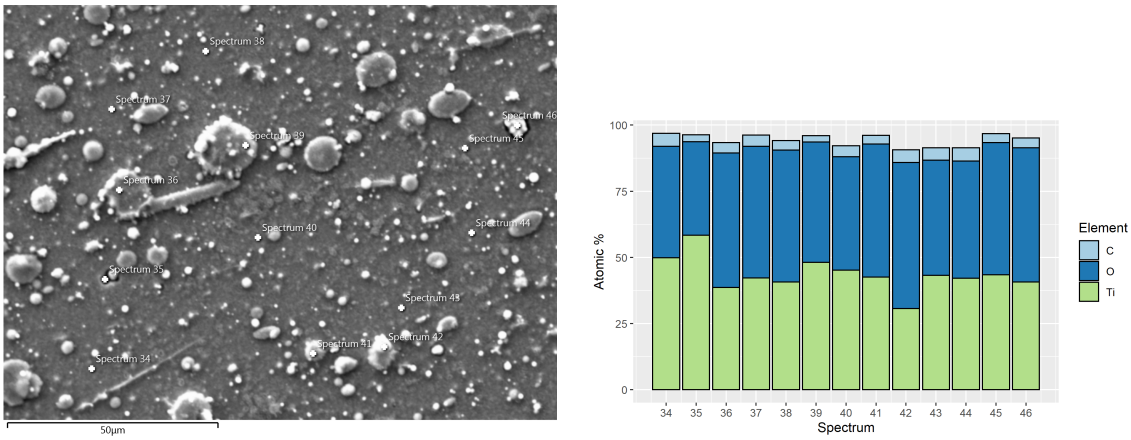


(a) EDS site locations (b) Atomic percent at spectrum locations

Figure 4.7: Ti coating 1.0 - 1.5 $\mu$m thick at 650°C SEM/EDS site analysis

### TiAl 50:50 Coating with 1.0-1.5 $\mu$m Thickness

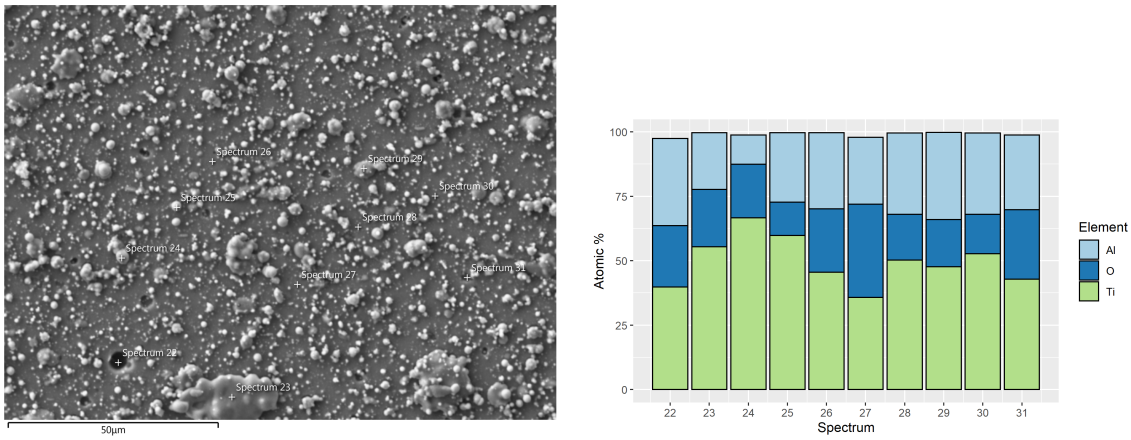


(a) EDS site locations (b) Atomic percent at spectrum locations

Figure 4.8: TiAl 50:50 coating 1.0 - 1.5 $\mu$m thick at 500°C SEM/EDS site analysis

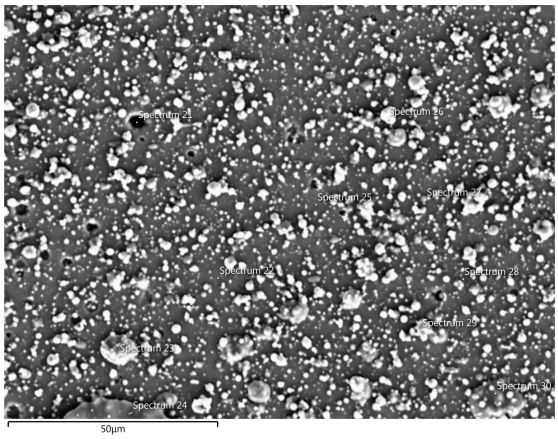


(a) EDS site locations

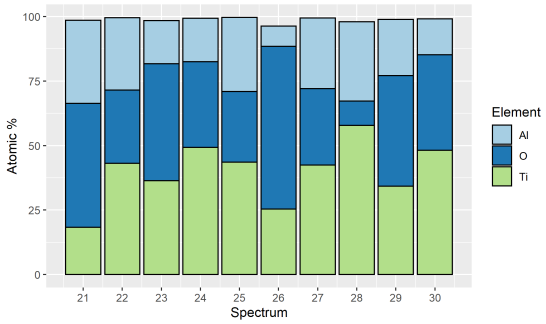


(b) Atomic percent at spectrum locations

Figure 4.9: TiAl 50:50 coating 1.0 - 1.5 $\mu$m thick at 575°C SEM/EDS site analysis

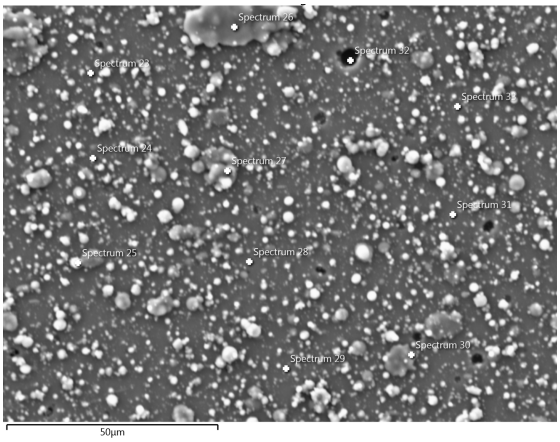


(a) EDS site locations

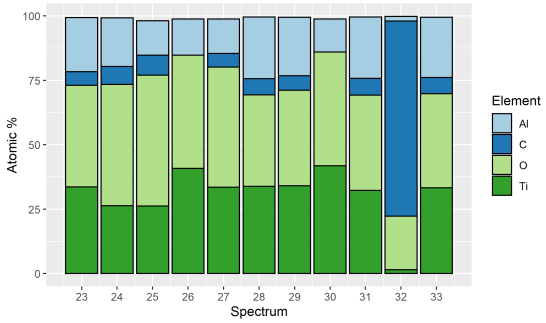


(b) Atomic percent at spectrum locations

Figure 4.10: TiAl 50:50 coating 1.0 - 1.5 $\mu$m thick at 650°C SEM/EDS site analysis

### TiAl 40:60 Coating with 1.0-1.5 $\mu$m Thickness

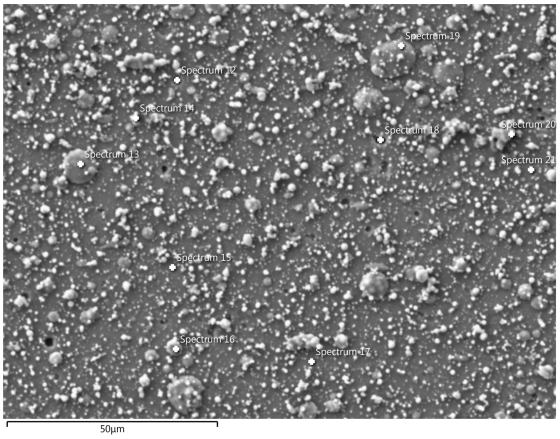


(a) EDS site locations

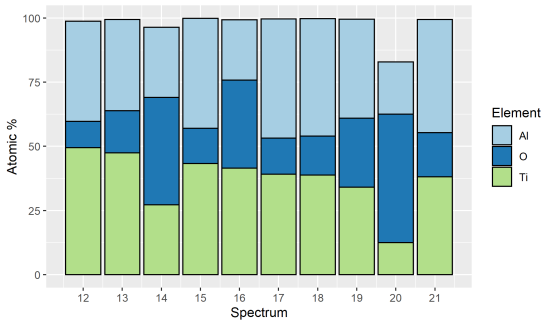


(b) Atomic percent at spectrum locations

Figure 4.11: TiAl 40:60 coating 1.0 - 1.5 $\mu$m thick at 500°C SEM/EDS site analysis

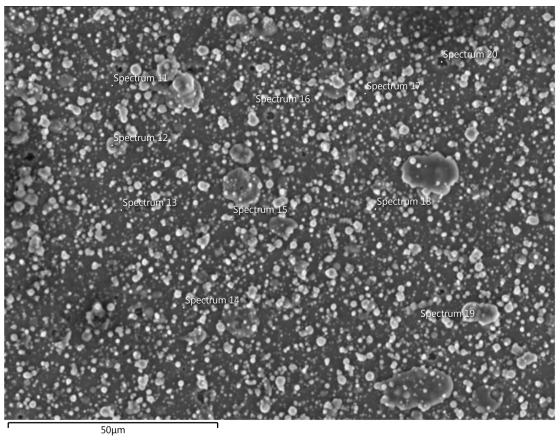


(a) EDS site locations

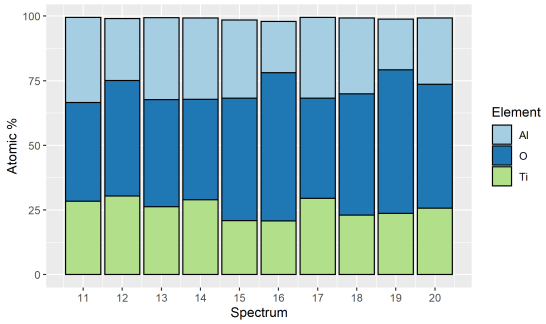


(b) Atomic percent at spectrum locations

Figure 4.12: TiAl 40:60 coating 1.0 - 1.5 $\mu$m thick at 575°C SEM/EDS site analysis

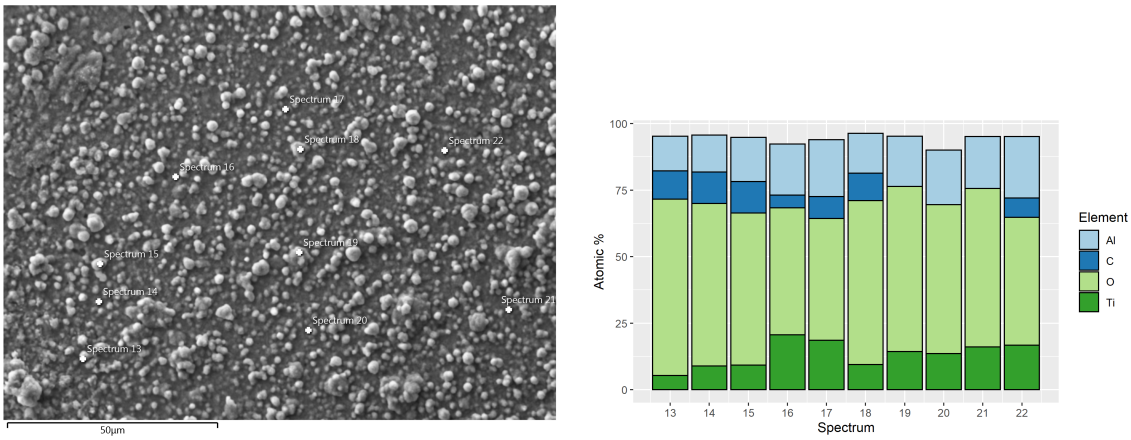


(a) EDS site locations (b) Atomic percent at spectrum locations

Figure 4.13: TiAl 40:60 coating 1.0 - 1.5 $\mu$m thick at 650°C SEM/EDS site analysis

### Discussion of Metallic Titanium Coatings

**Topographical Analysis** For all of the metallic titanium coatings, it was observed in the SEM images that there was a variety of topography on the surface, from white protrusions to black holes or bubbles. To determine if the topography reflected concentrations of certain elements, or in the case of the bubbles, a porosity of the coating, the data from EDS site locations was graphed to see if there were observable differences in the features. These graphs are in Appendix C, and show that there is no statistical reason to evaluate the different features separately.

**EDS Maps** EDS Maps of the entire surface of the sample were taken to determine the consistency of the coating and detect if any part of the coating was coming off. These are documented in Appendix D, where it shows a consistent, uniform coverage of the elements throughout the oxidation experiments and post analysis.

**Ti 0.5 - 0.6 $\mu$m Thick Coating** For this coating, there are signs of contamination at 575°C (figure 4.3a), seen in the feature that looks like a branch with leaves on it. This contamination explains the visual difference between figure 4.4a and figure 4.7a, which should be similar. This also shows up in the bar graph at 650°C, where the largest atomic percent outside of titanium, oxygen, and carbon is silver (a component of the epoxy used to adhere the diamond to the stud). As can be seen from the filtered graph in figure 4.4b, the amount is small. Another observation from the bar graphs is that the atomic percent of the elements is fairly consistent across the surface, with a general trend of titanium decreasing and oxygen and carbon increasing, a phenomenon expected as the titanium coating oxidises.

**Ti 1.0 - 1.5 $\mu$m Thick Coating** For this coating, the SEM images reveal a consistent surface that shows very few changes after oxidation experiments from 500-650°C. The bar graphs reflect this, with consistent values for the EDS locations.

**TiAl 50:50 1.0 - 1.5 $\mu$m Thick Coating** The SEM images of this coating show that it has a lot more protrusions on the surface than the pure titanium coatings. They also show that there are no noticeable changes between temperatures. The bar graphs do show some variation of the atomic percent of titanium, with oxygen and aluminium being the beneficiaries of a lower titanium value. The bubbles may be a long term protection concern for the diamond, since, as the bar graph in figure 4.10 from the final oxidation experiment at 650°C shows, the hole picked at spectrum 32 exhibits signs of failure with very little titanium left. However, small bubbles are much different than the coating flaking off in catastrophic failure, and it may only be a matter of refining the PVD coating technique for this particular coating. Thus,

this coating is analysed in general, not specifically in regards to spectrum 32.

**TiAl 40:60 1.0 - 1.5 $\mu$m Thick Coating** When comparing the protrusions seen in the SEM images of the TiAl 50:50 coating to those of the TiAl 40:60 coating, the number of small protrusions increases in the latter, which was taken to indicate that they are a feature of the aluminium. There is no noticeable difference between the SEM images of the temperatures, and no signs of a catastrophic failure of the coating. At 500°C, figure 4.11 shows a general consistency in the coating except for at spectrum 20, which appears to have some contamination in the selected protrusion. This is not reflective of the surface in general, and the bar graphs at 575°C and 650°C reflect that. By 650°C, the atomic percent of titanium is quite low, which will be discussed in more detail in the analysis.

### 4.4.2 Ceramic Titanium Coatings

#### TiN Coating with 1.0-1.5 $\mu$m Thickness

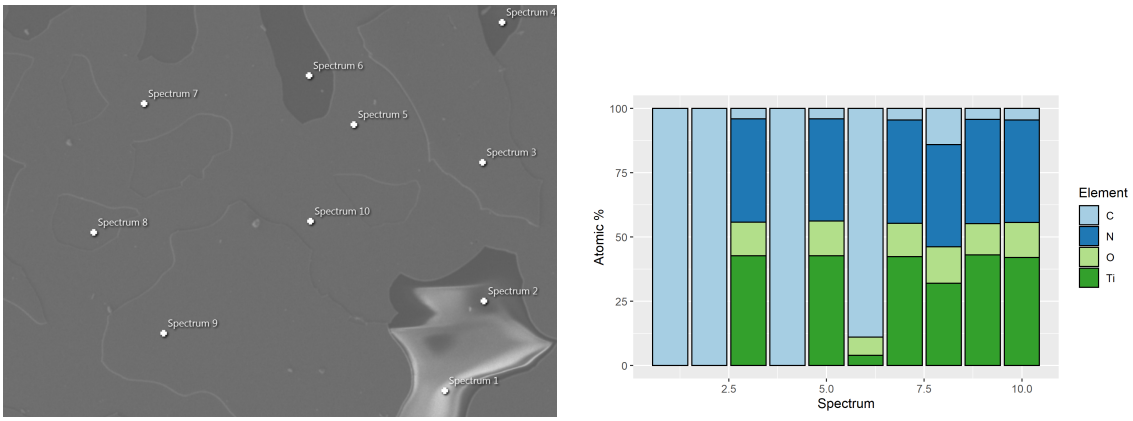


(a) EDS site locations (b) Atomic percent at spectrum locations

Figure 4.14: TiN coating 1.0 - 1.5 $\mu$m thick at 500°C SEM/EDS site analysis

### TiAlN 50:50 Coating with 1.0-1.5 $\mu$m Thickness

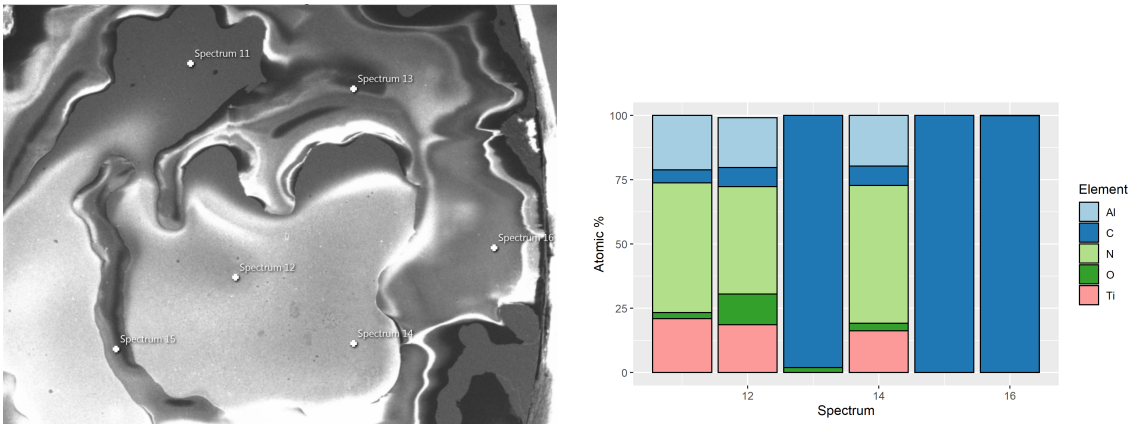


(a) EDS site locations (b) Atomic percent at spectrum locations

Figure 4.15: TiAlN coating 1.0 - 1.5 $\mu$m thick at 500°C SEM/EDS site analysis

### Discussion of Ceramic Titanium Coatings

As can be seen in the SEM images of the TiN and TiAlN coatings, figures 4.14a and 4.15a, both failed catastrophically, as per the experiment criteria. The uniformly gray part of the image that looks like puzzle pieces is the coating, while the diamond substrate has a much broader range of white to gray, which gives it a glossy look. Confirmation of this failure can be seen in the bar graphs, figures 4.14b and 4.15b, where the spectrum locations for the EDS analysis that are located on the diamond substrate are recorded at 100% carbon.

## 4.5 Analysis

The SEM and EDS measurements of elements were put into R, a statistical analysis program, where they were analysed.

### 4.5.1 Metallic Titanium Coatings

#### Element Analysis

The elements of interest are titanium (Ti), oxygen (O), and carbon (C) for all coatings, and aluminium (Al) for the TiAl coatings. The atomic percent of these elements were graphed by temperature for each coating, where the line is a linear regression with grey confidence intervals. It was found that the carbon did not appear until 650°C, hence its exclusion from the figures. To determine the best coating for oxidation protection, the graph to focus on is the oxygen atomic percent one. The ideal coating should have the flattest slope and the narrowest confidence intervals. In both cases, that is the pure titanium coating with a thickness of 1.0-1.5 $\mu$m. The corresponding titanium atomic percent graph reflects this, with the lowest decrease in titanium. The titanium 0.5-0.6 $\mu$m thickness has a higher oxygen atomic percent in general, while also having a higher rate of increase and thicker confidence intervals.

However, the titanium 0.5-0.6 $\mu$m thickness coating also had issues with contamination, and these results do not clarify if that had an impact on the overall trend.

For the aluminium coatings, if the thin aluminium oxide layer that forms at room temperature helped to prevent further oxidation, then there should be a lower increase in oxygen atomic percent in comparison to the coatings without Al. The reverse of this happened, with the pure titanium coating showing itself to be much more robust against oxidation. Therefore, it can be concluded that it is more important to have a higher concentration of an element that will bond with the diamond substrate for oxidation protection than to have an element known for oxidation protection.

If oxidation protection is the only criteria, making titanium an interlayer and then applying a coating on top may have better results.

### 4.5.2 Ceramic Titanium Coatings

As can be seen from the results, large portions of the TiN and TiAlN 50:50 coating flaked off of the diamond substrate after oxidation at 500°C. This is a catastrophic failure, so the coatings are not considered suitable for protecting the diamond from oxidation. As such, the oxidation tests were not continued since the coatings failed for both samples.

For the TiN coating, these results are similar to those reported in the literature, as noted in section 2.4.3. In comparison to the TiN sample, the TiAlN 50:50 sample had more exposed diamond substrate, indicating that the aluminium was detrimental to the coating adhering to the diamond.

Furthermore, these results show that the hypothesis from the literature that the nitrogen gas environment used to deposit PVD nitride coatings interferes with the bonding of the titanium to the diamond surface is still valid.

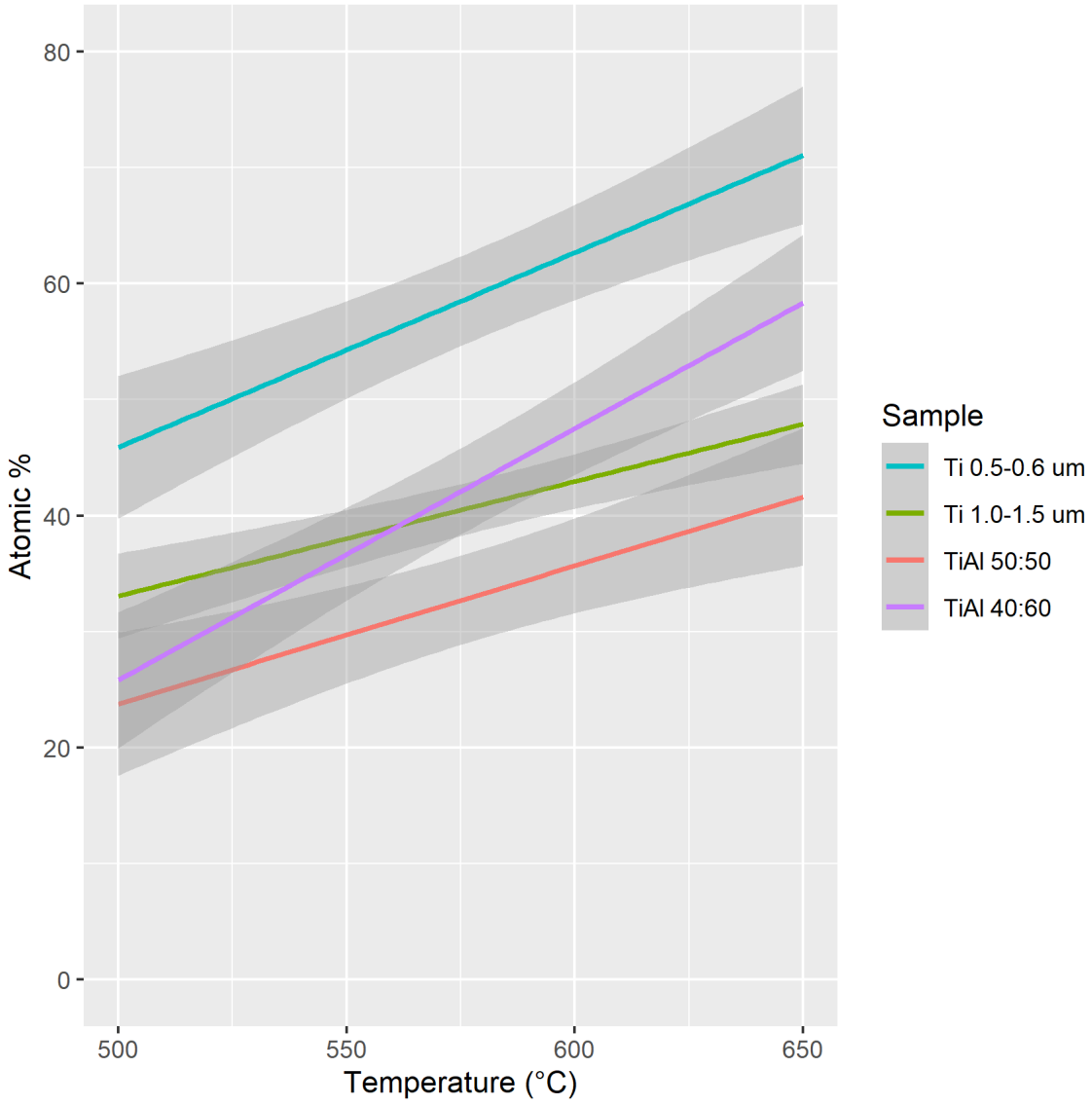


Figure 4.16: Comparison of oxygen atomic percent

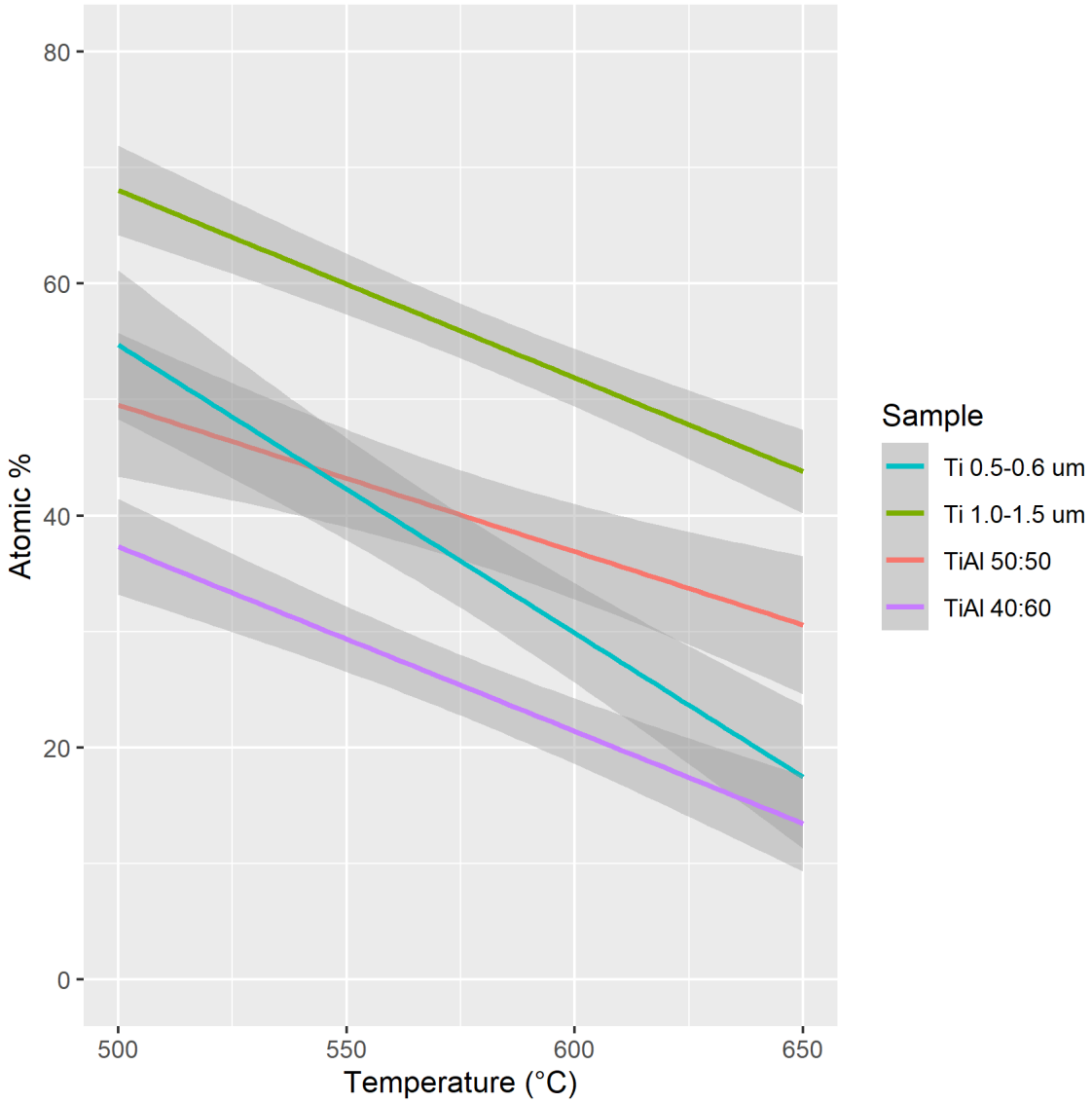


Figure 4.17: Comparison of titanium atomic percent

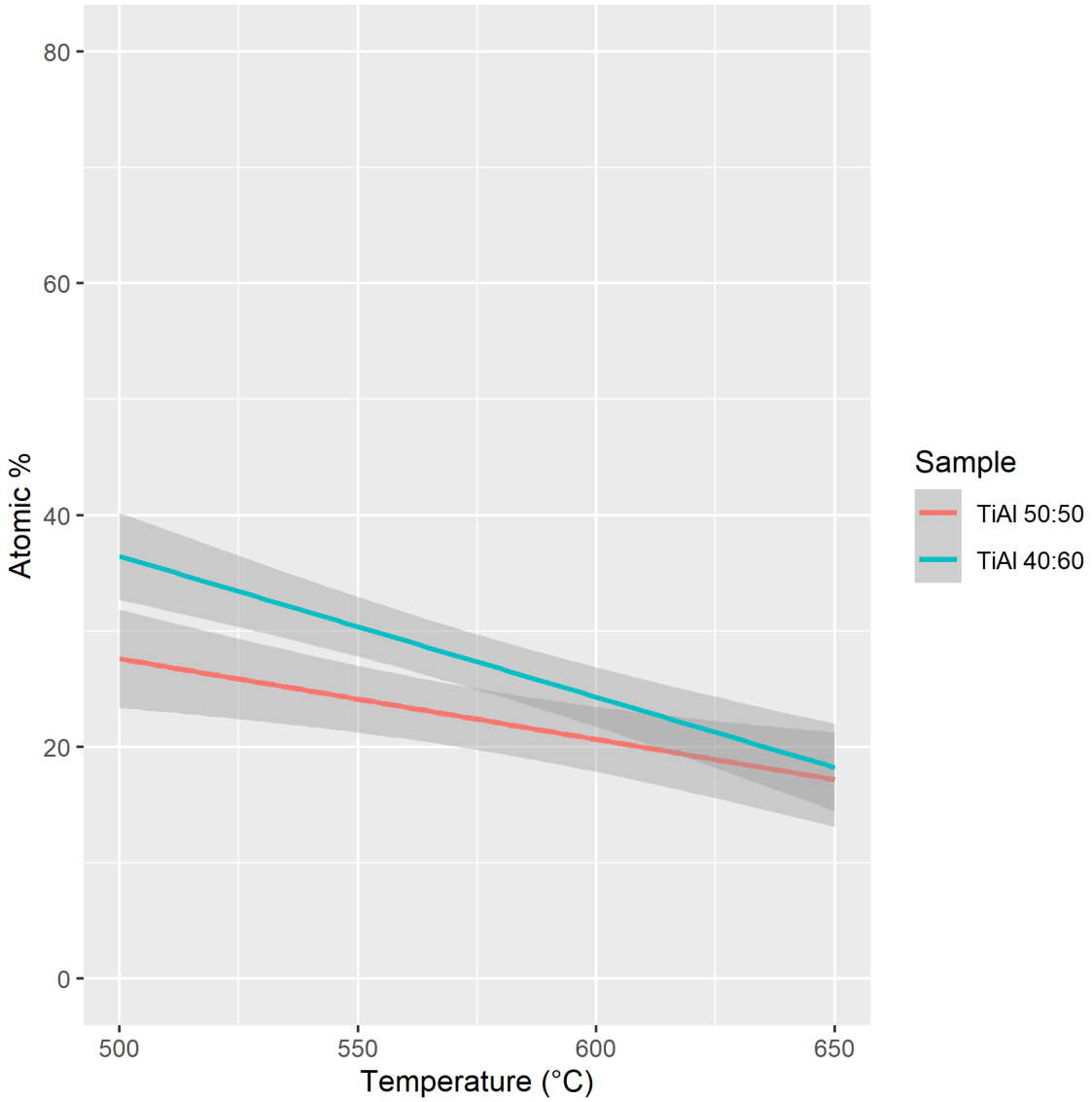


Figure 4.18: Comparison of aluminium atomic percent

## 4.6 Conclusion

The conclusion to this analysis is as follows:

- In comparison to the gold coating, the metallic titanium coatings were much more robust.
- Of the 6 different coatings, the pure titanium coating at a thickness of 1.0-1.5 $\mu$m was the superior coating based on a higher level of adhesion which led to higher titanium retention on the surface and, therefore, better protection of the diamond substrate.
- The presence of aluminium did not improve the protection of the surface during oxidation, so the TiAl metallic coatings were deemed inferior.
- The ceramic titanium coatings performed as badly, if not worse, than what was found in the literature review, and both failed catastrophically.
- As there was some contamination in the 0.5-0.6 $\mu$m thick pure titanium coating, the results are inconclusive.

# Chapter 5

# Study of Titanium Coating Thickness

## 5.1 Hypothesis

The hypothesis remains similar to the one in Chapter 4 in that a titanium coating can protect diamond when operating in temperatures between 400-750°C. It is also hypothesized that the coating thickness has an impact on oxidation protection, hence this experiment.

## 5.2 Experimental Observations

Of the coatings evaluated in chapter 4, titanium was the best coating. However, the ideal thickness of the coating was not explored thoroughly. From a nanoindentation measurement perspective, a thinner coating would be more ideal as there is less of a

likelihood that there would be significant geometric changes if there were any deformation in the coating during a measurement. However, from the results in chapter 4, it was the thicker coating that performed better, so this investigation will have smaller thickness increments than what was performed previously.

As per the literature review, it is critical to this study to ensure that the titanium and the diamond have bonded. As such, an added aspect of these experiments was ensuring the formation of TiC at the interface between the titanium and diamond by changing the methodology to include a post-coating heat treatment.

## 5.3 Experiment Criteria

There was a two stage criteria used to examine the coatings. The first stage visually examined the SEM images to determine the integrity of the coating, where failure was defined as being able to visually identify the diamond substrate. Should the coating pass the first stage, the second stage statistically evaluated the atomic percent of the elements measured by EDS at several points across the coating surface. The results of all the coatings were then compared, with the best coating being the one with the slowest increase in oxygen - i.e., the coating least effected by oxidation.

## 5.4 Design of Experiment

### 5.4.1 Substrate Examination

No changes were made to the substrate examination step.

### 5.4.2 Sample Preparation

There were 6 samples chosen to be PVD coated using an arc ion plating AIP-S20 PVD Hybrid coater (Kobelco, Japan). The coating times were 7.5 minutes, 15 minutes, and 30 minutes for the 0.25 $\mu$m, 0.50 $\mu$m, and 1.00 $\mu$m thick coatings, respectively. There were 6 different sets of 2, with each set coated as follows:

- Ti coating with a thickness of 0.25 $\mu$m
- Ti coating with a thickness of 0.50 $\mu$m
- Ti coating with a thickness of 1.00 $\mu$m

To ensure that the TiC compound formed, all samples were held at 500°C for 30 minutes after the coating (note that the coating was performed at 500°C).

### 5.4.3 Experimental Procedure

In addition to the static oxidation experiment with SEM/EDS examinations performed 3 times at 3 different temperatures (500°C, 575°C, and 650°C), the set that was not oxidized was examined by XRD for a 12 hour scan to verify the existence of the TiC layer. The optimum coating thickness sample (as determined by the analysis of the SEM/EDS examination of the static oxidation) had a Zeiss NVision 40 focused ion beam (FIB) mill through the coating to the substrate, after which it was examined by a ThermoFisher Scientific Talos 200X STEM with EELS and HAADF microscopy. This methodology can be seen graphically in figure 5.1.

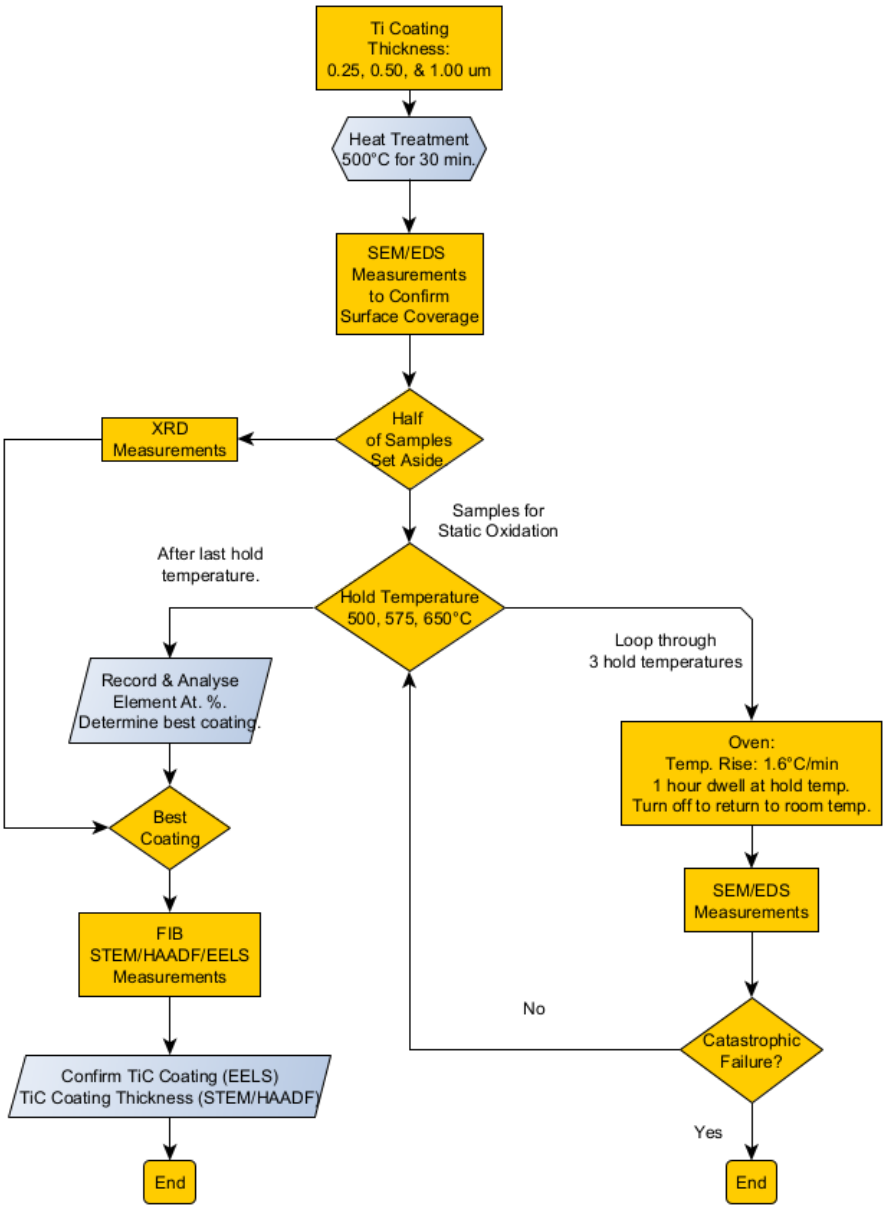


Figure 5.1: Study of Coatings Thickness Methodology

## 5.5 Results

### 5.5.1 Static Oxidation

These are the results of the experiments performed at 500°C, 575°C, and 650°C, where the SEM and EDS point analysis were transferred to a database and analysed. The bar graphs show the site number on the x-axis, and the atomic percent on the y-axis. The SEM pictures note the positions of the EDS site locations, which correspond to the site numbers on the x-axis of the graph. Before graphing, the data was filtered, excluding all elements except for Ti, O, and C. If the graph does not have one of those 3 elements, then it was not found in the EDS element analysis. The bar graph is stacked, thus if there are only members of the elements of interest detected, the atomic percent will add up to 100%.

#### Ti Coating with 0.25 $\mu$m Thickness

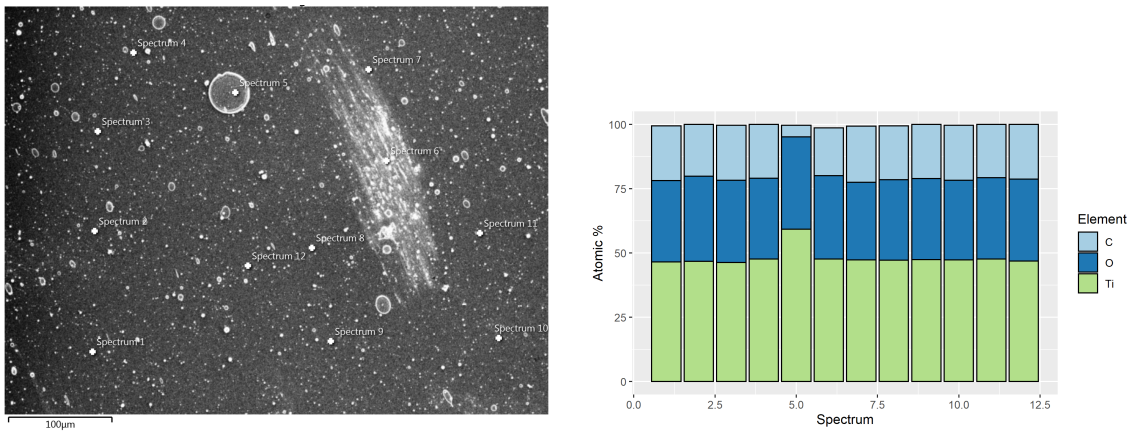


(a) EDS site locations (b) Atomic percent at spectrum locations

Figure 5.2: Ti coating 0.25 $\mu$m thick at 500°C SEM/EDS site analysis

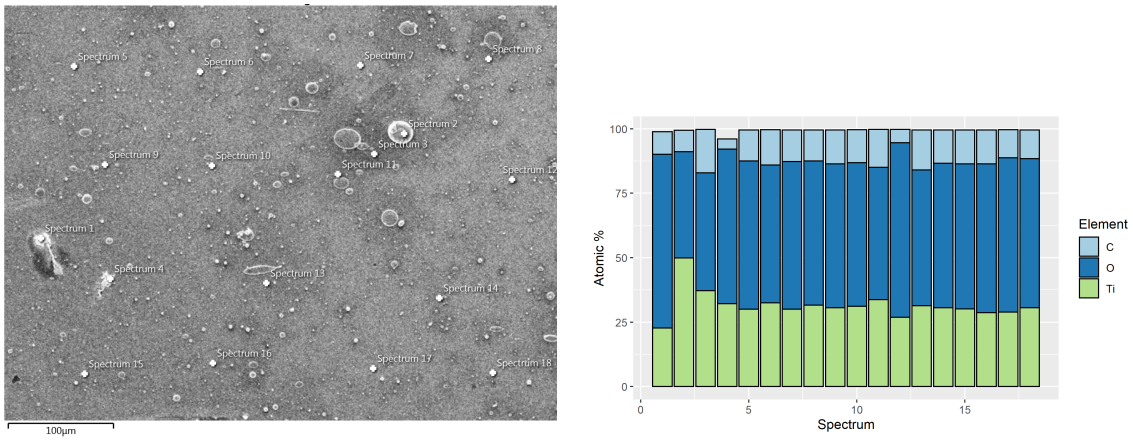


(a) EDS site locations (b) Atomic percent at spectrum locations

Figure 5.3: Ti coating 0.25 $\mu$m thick at 575°C SEM/EDS site analysis

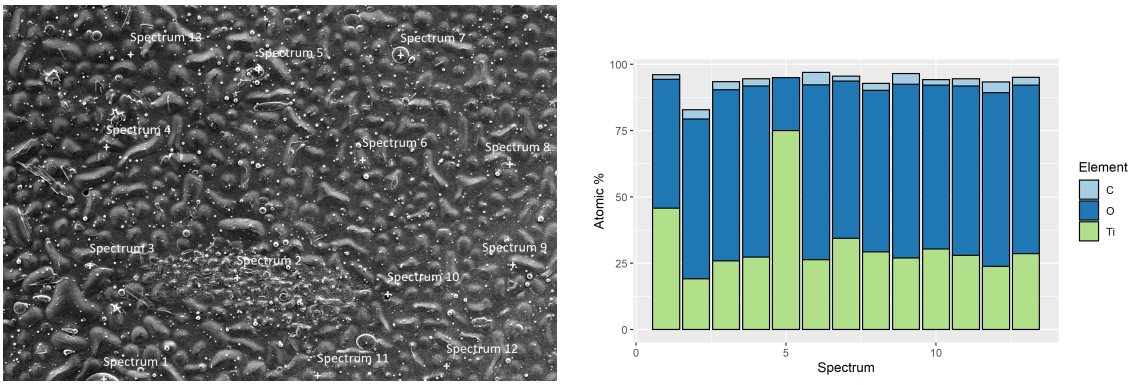


(a) EDS site locations (b) Atomic percent at spectrum locations

Figure 5.4: Ti coating 0.25 $\mu$m thick at 650°C SEM/EDS site analysis

### Ti Coating with 0.50 $\mu$m Thickness

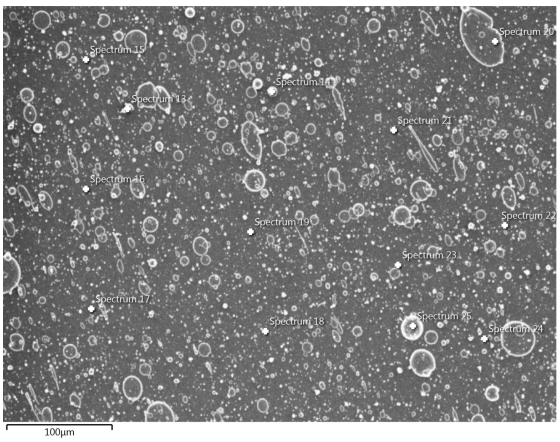


(a) EDS site locations

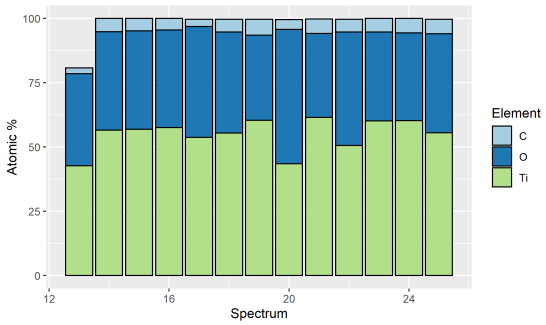


(b) Atomic percent at spectrum locations

Figure 5.5: Ti coating 0.5 $\mu$m thick at 500°C SEM/EDS site analysis

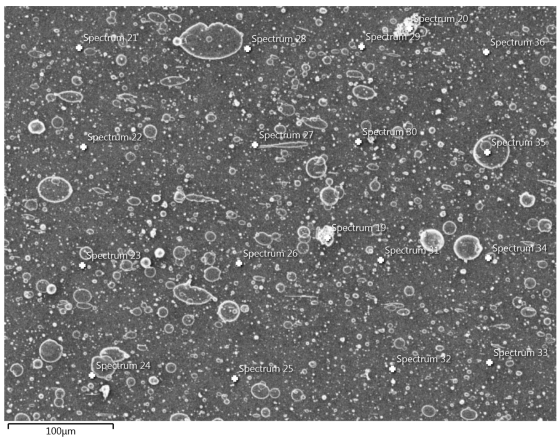


(a) EDS site locations

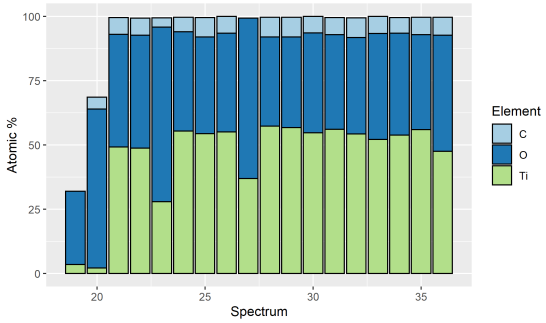


(b) Atomic percent at spectrum locations

Figure 5.6: Ti coating 0.5 $\mu$m thick at 575°C SEM/EDS site analysis

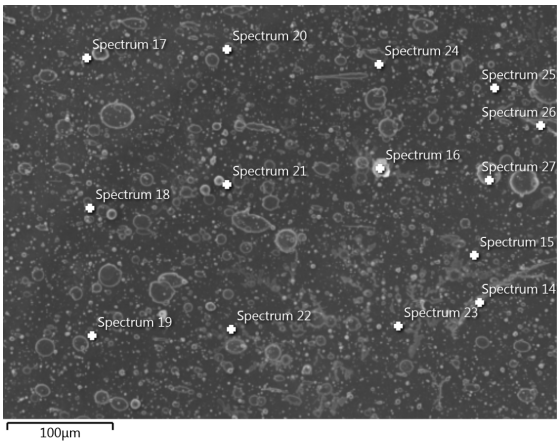


(a) EDS site locations

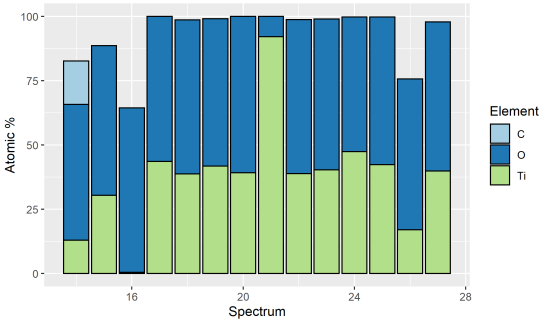


(b) Atomic percent at spectrum locations

Figure 5.7: Ti coating 0.5 $\mu$m thick at 650°C SEM/EDS site analysis

### Ti Coating with 1.00 $\mu$m Thickness

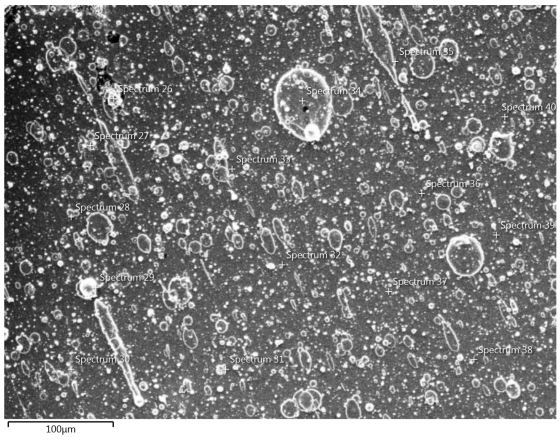


(a) EDS site locations

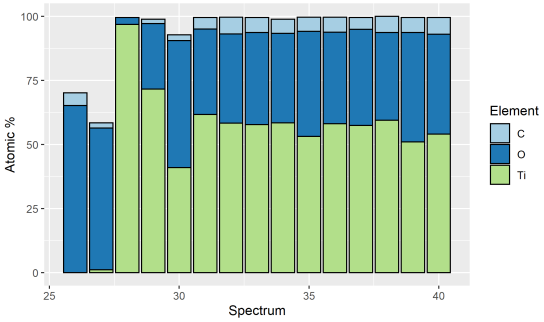


(b) Atomic percent at spectrum locations

Figure 5.8: Ti coating 1.0 $\mu$m thick at 500°C SEM/EDS site analysis

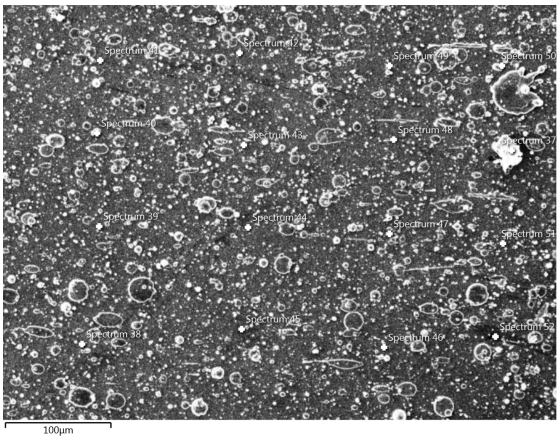


(a) EDS site locations

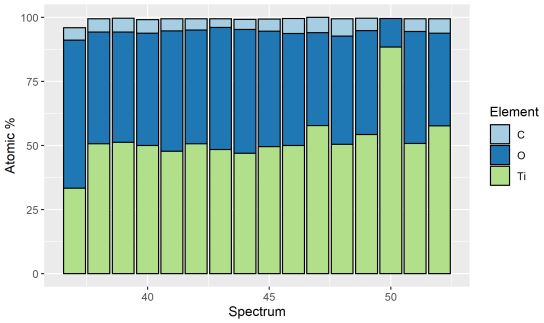


(b) Atomic percent at spectrum locations

Figure 5.9: Ti coating 1.0 $\mu$m thick at 575°C SEM/EDS site analysis

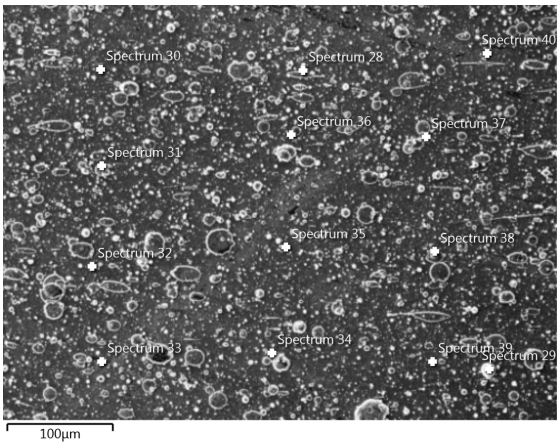


(a) EDS site locations

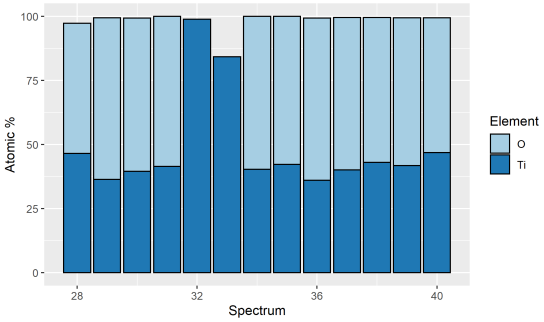


(b) Atomic percent at spectrum locations

Figure 5.10: Ti coating 1.0 $\mu$m thick at 650°C SEM/EDS site analysis

**Discussion of SEM/EDS**

The SEM images all show a consistency between temperatures except for the 0.25 $\mu$m thick coating at 650°C, which has a different appearance. In all cases, however, the coating was still on the diamond substrate with no signs of peeling. In terms of the bar graphs, there do appear to be some drops of contamination in the two thicker coatings, as can be seen from some of the spectrum locations having a cumulative atomic percent that is noticeably below 100%. EDS maps were also performed and showed consistent coatings for all temperatures and samples.

### 5.5.2 Cross Section Scan

These are the results of a cross section scan of a 0.5 $\mu$m thick PVD titanium coating on diamond. The cross section was generated by using a FIB to machine into the sample, which also was used to scan some images as presented in one of the following sections. The cross section is then scanned with STEM using EELS to evaluate the structure of the diamond.

### FIB of 0.5 $\mu$m Thick Ti Coating of Diamond

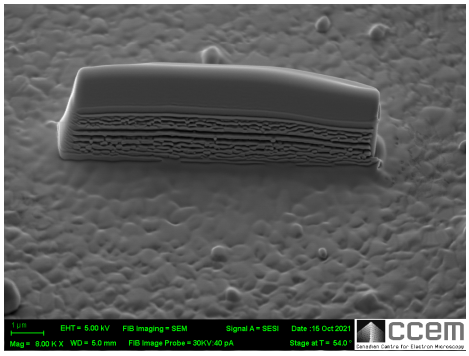

Figure 5.11: FIB coupon of Ti coating 0.5 $\mu$m thick

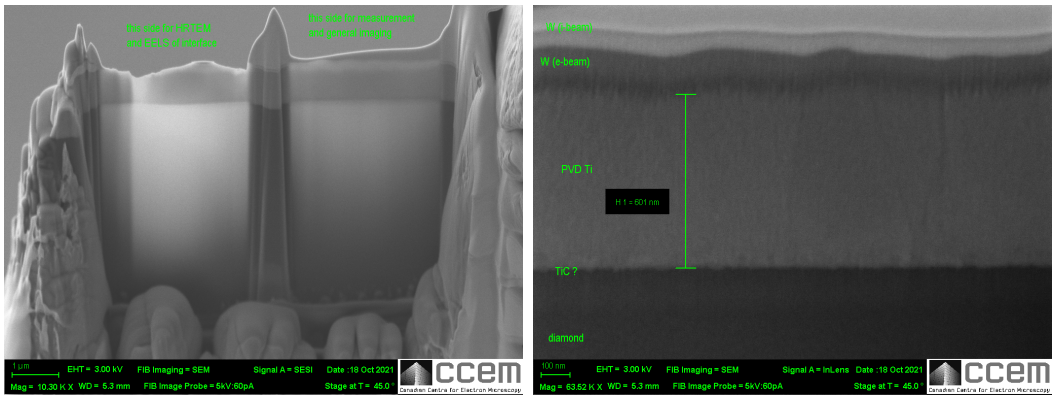


(a) Cross section (b) Cross section close-up

Figure 5.12: FIB cross section of coupon of Ti coating 0.5 $\mu$m thick

### HAADF/STEM Scan

Before interrogating the sample with EELS, the left cut of the sample, as shown in figure 5.13, was examined with STEM and HAADF.

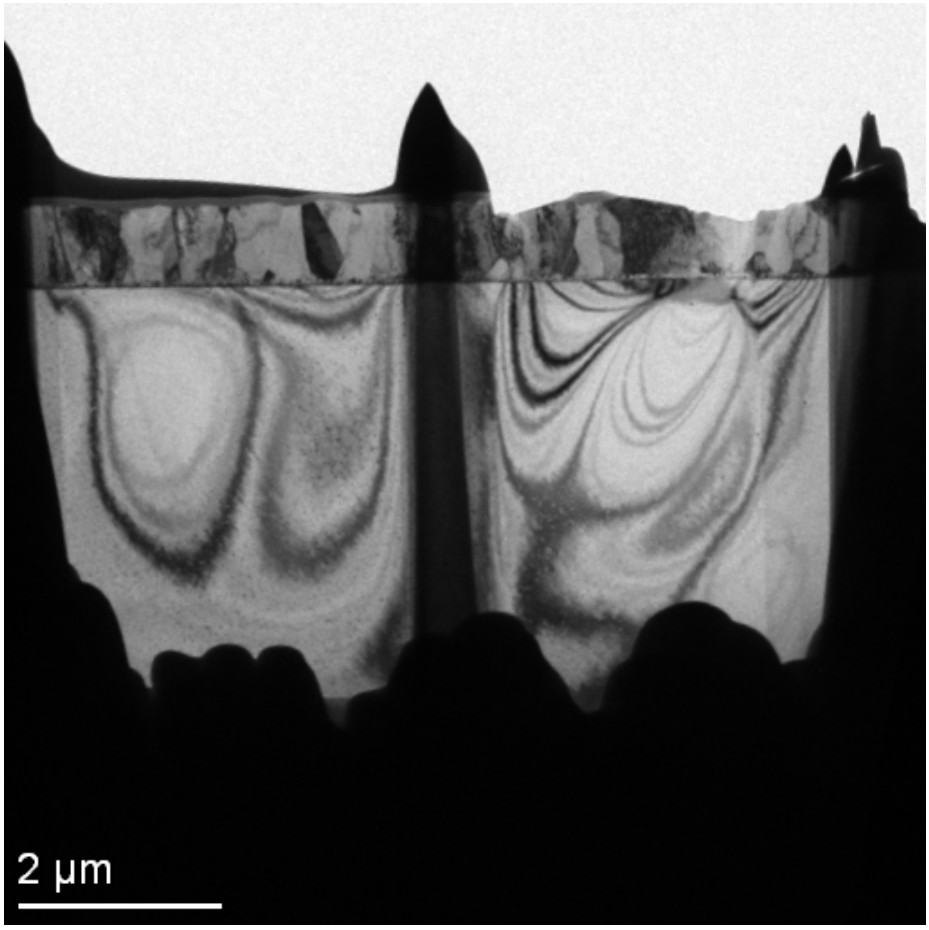


Figure 5.13: STEM scan of FIB cross section of Ti coating 0.5 $\mu$m thick

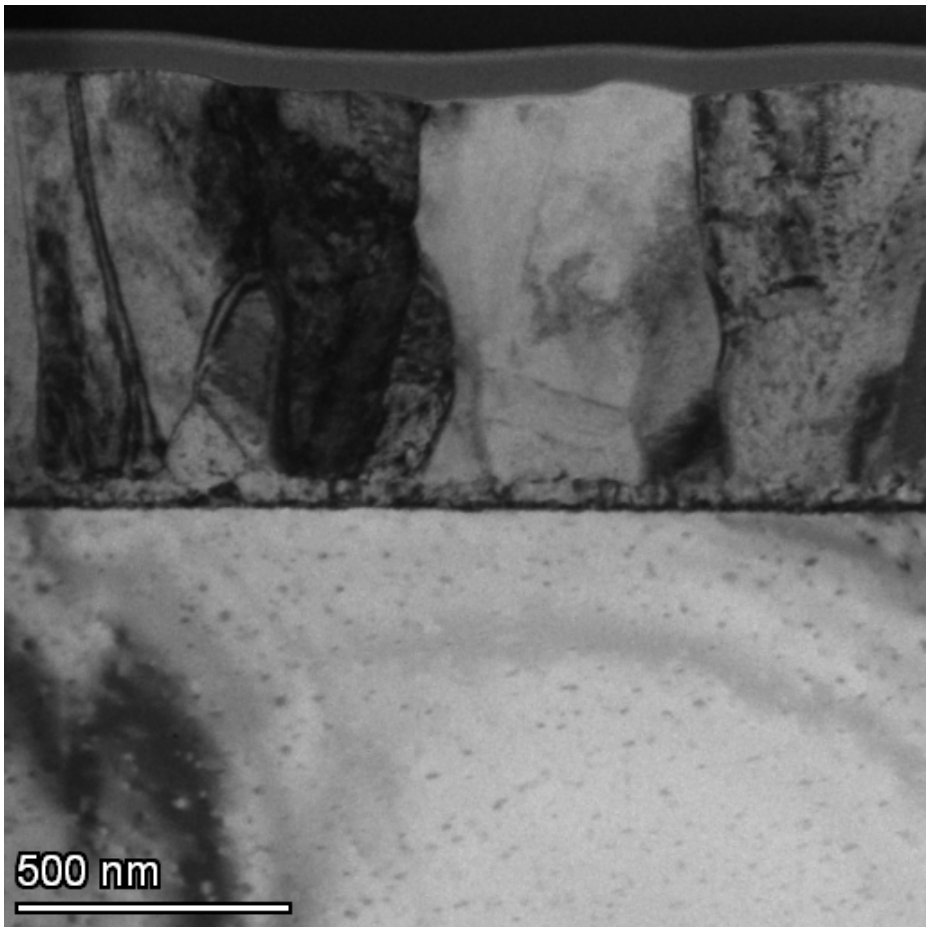


Figure 5.14: STEM scan 500 nm scale of Ti coating 0.5 $\mu$m thick

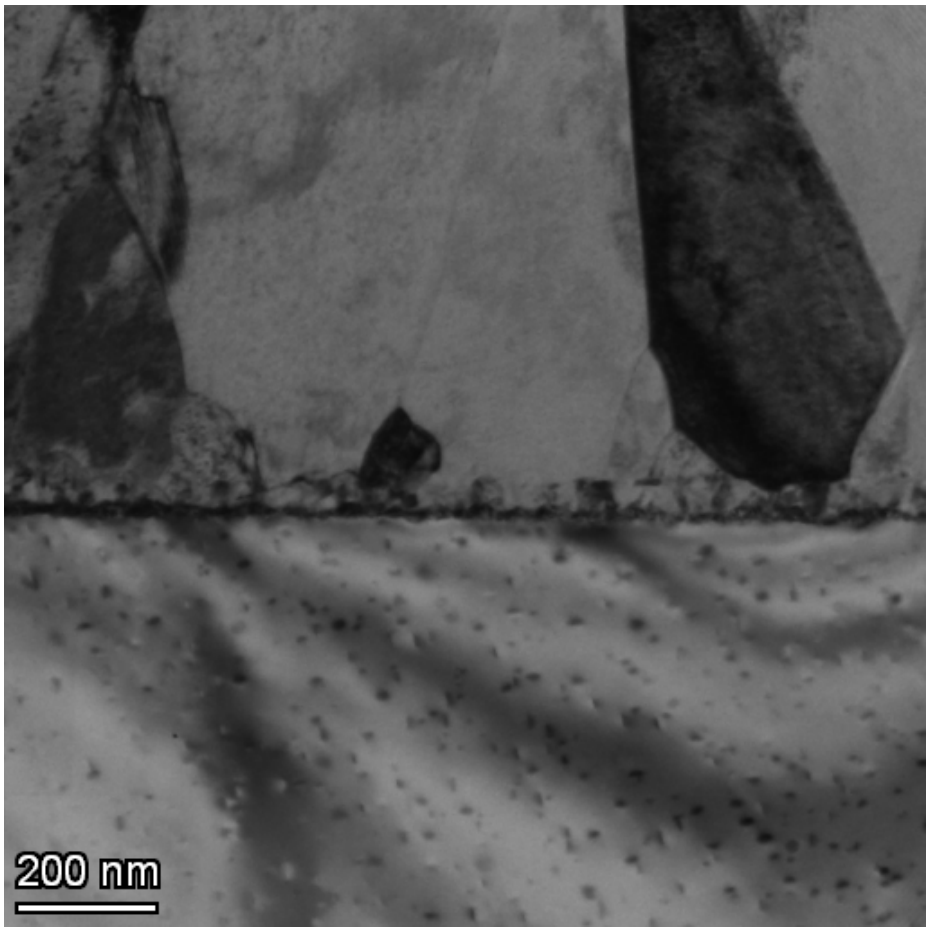


Figure 5.15: STEM scan 200 nm scale of Ti coating 0.5 $\mu$m thick

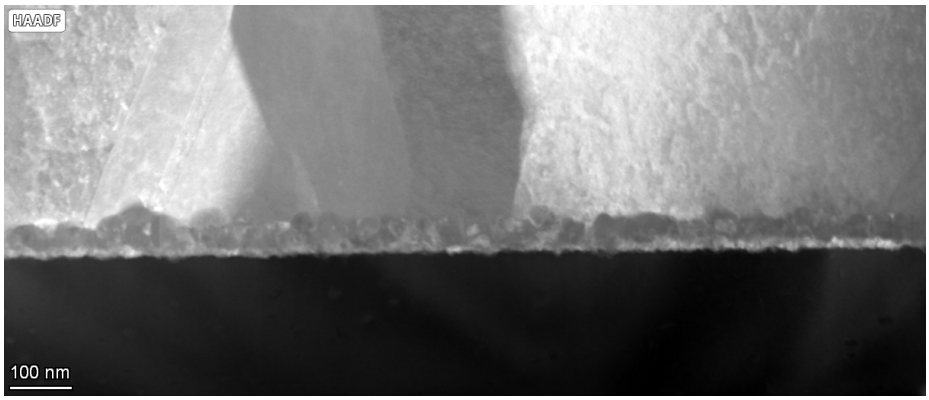


Figure 5.16: STEM scan 100 nm scale of Ti coating 0.5 $\mu$m thick

**STEM/EELS Scan**

These are the STEM HAADF/EELS results from 4 different locations.

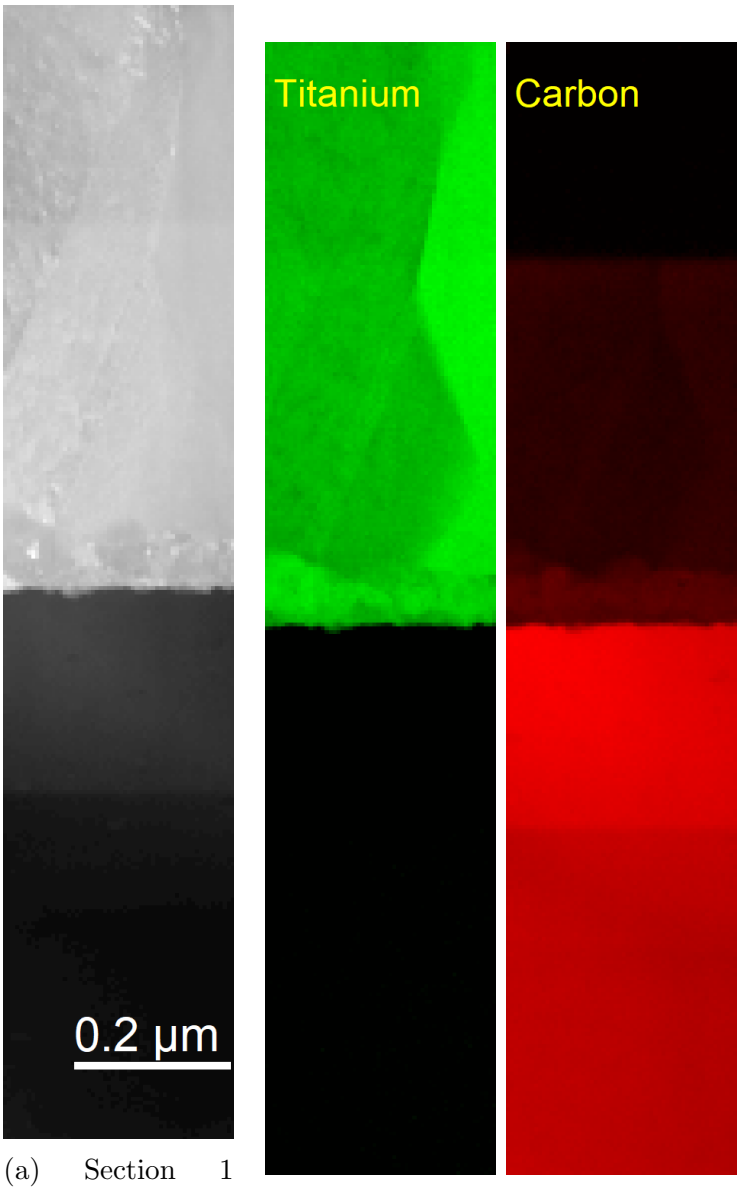


(a) Section 1 STEM Scan of HAADF cross section

(b) Section 1 STEM Scan with EELS Ti L signal

(c) Section 1 STEM Scan with EELS C K signal

Figure 5.17: Section 1 STEM/HAADF cross section of Ti coating 0.5 $\mu$m thick

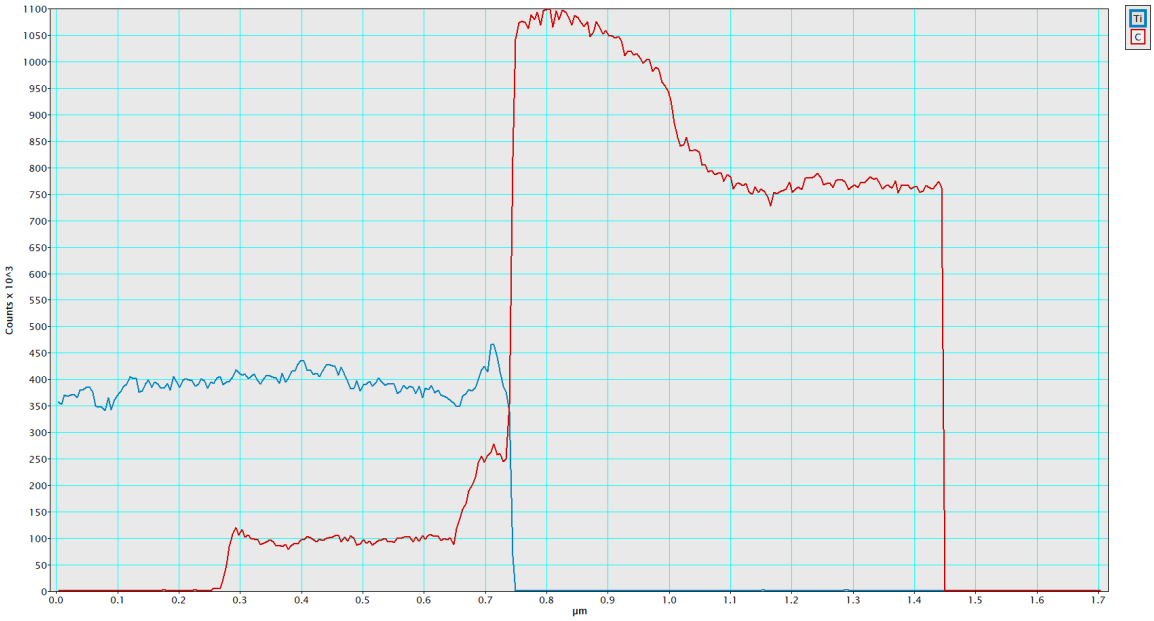


Figure 5.18: Section 1 HAADF cross section line scan of Ti coating 0.5 $\mu$m thick

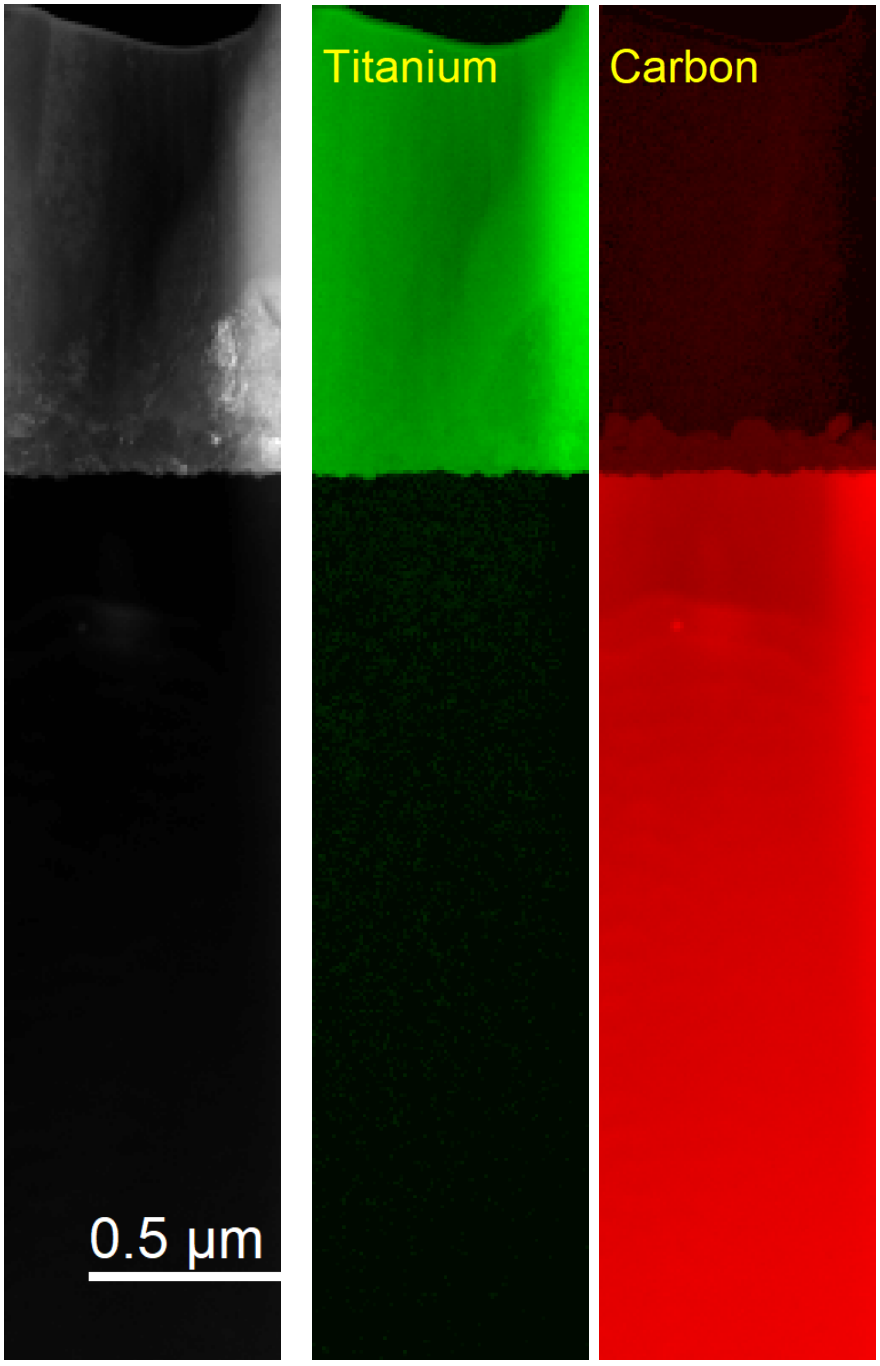


(a) Section 2 STEM scan of HAADF cross section

(b) Section 2 STEM Scan with EELS Ti L signal

(c) Section 2 STEM Scan with EELS C K signal

Figure 5.19: Section 2 STEM/HAADF cross section of Ti coating 0.5 $\mu$m thick

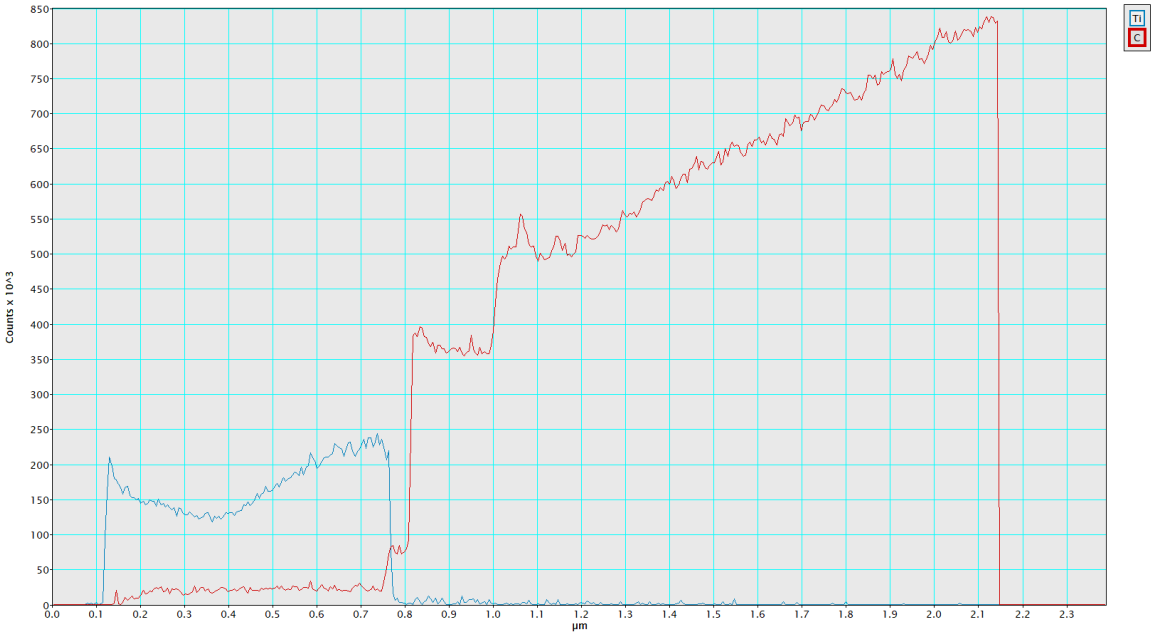


Figure 5.20: Section 2 HAADF cross section line scan of Ti coating 0.5 $\mu$m thick

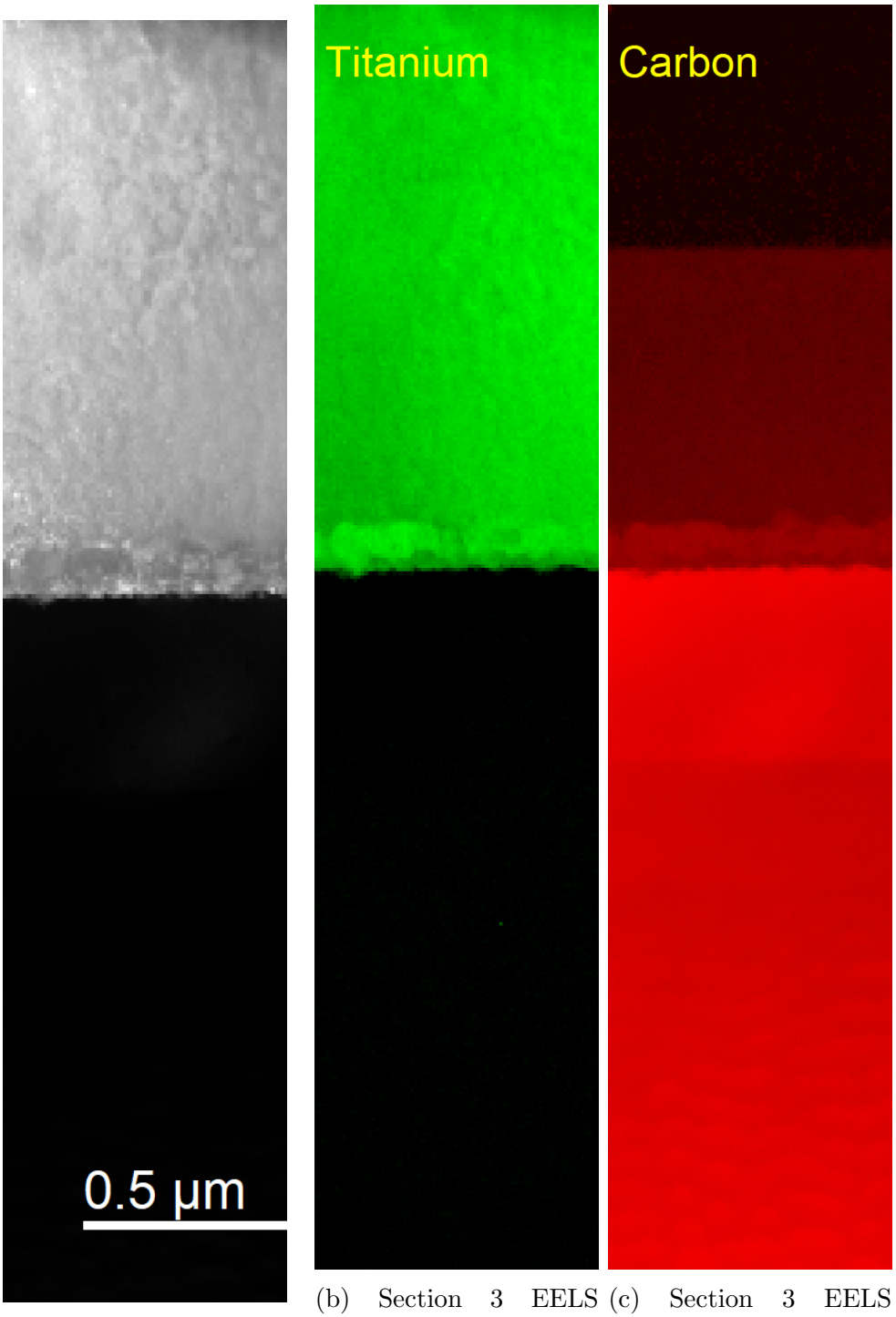


(a) Section 3 STEM scan of HAADF cross section

(b) Section 3 EELS STEM Scan with Ti L signal

(c) Section 3 EELS STEM Scan with C K signal

Figure 5.21: Section 3 STEM/HAADF cross section of Ti coating 0.5 $\mu$m thick

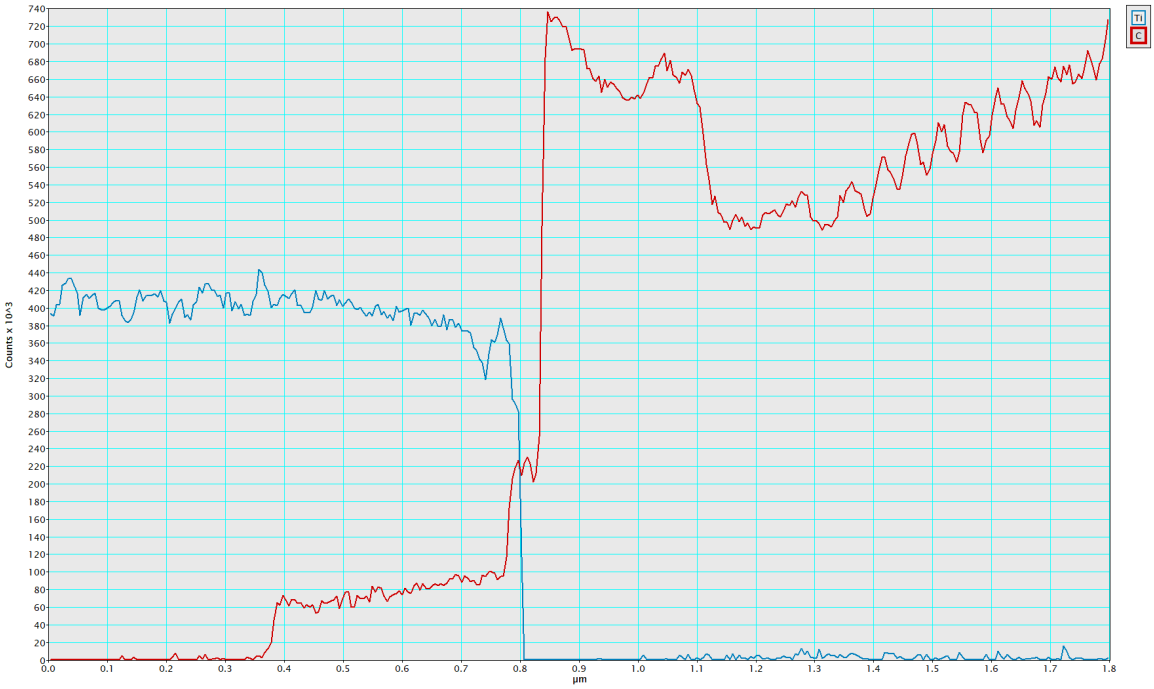


Figure 5.22: Section 3 HAADF cross section line scan of Ti coating 0.5 $\mu$m thick

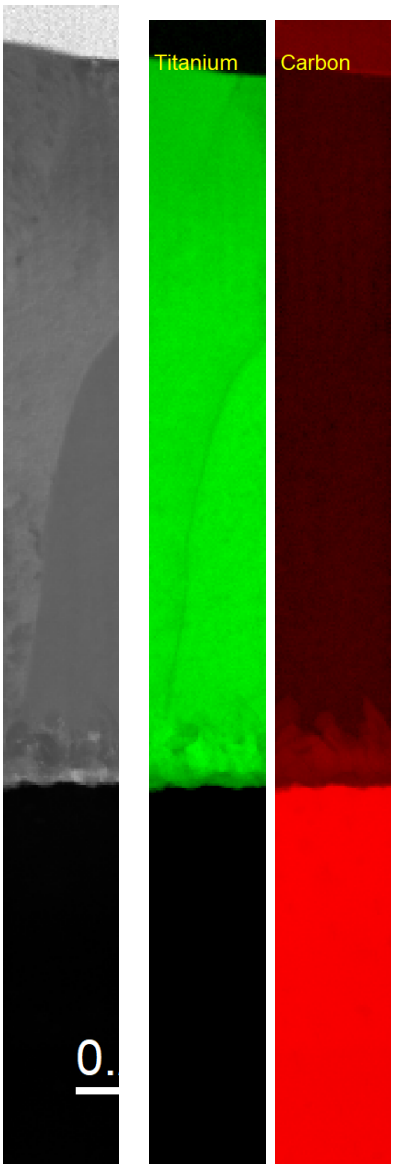


(a) Section 4 STEM scan of HAADF cross section

(b) Section 4 STEM Scan with EELS Ti L signal

(c) Section STEM Scan with 4 EELS C K signal

Figure 5.23: Section 4 STEM/HAADF cross section of Ti coating 0.5 $\mu$m thick

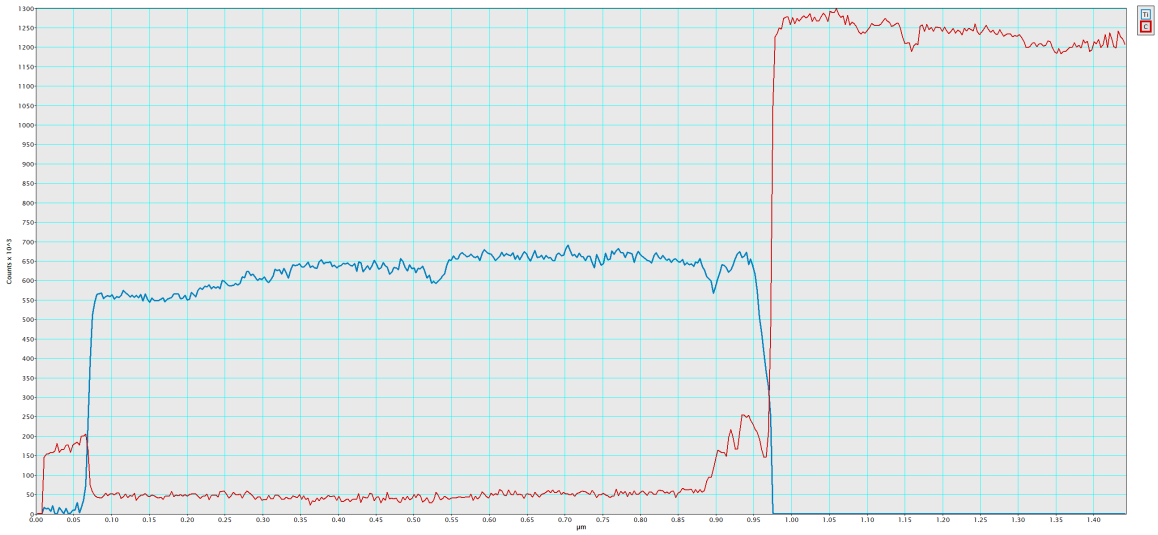


Figure 5.24: Section 4 HAADF cross section line scan of Ti coating 0.5 $\mu$m thick

### EELS Spectrum Scan

For section 1, an EELS analysis of the spectra was performed to determine the status of the elements. Through this, the different carbons can be identified and determined.

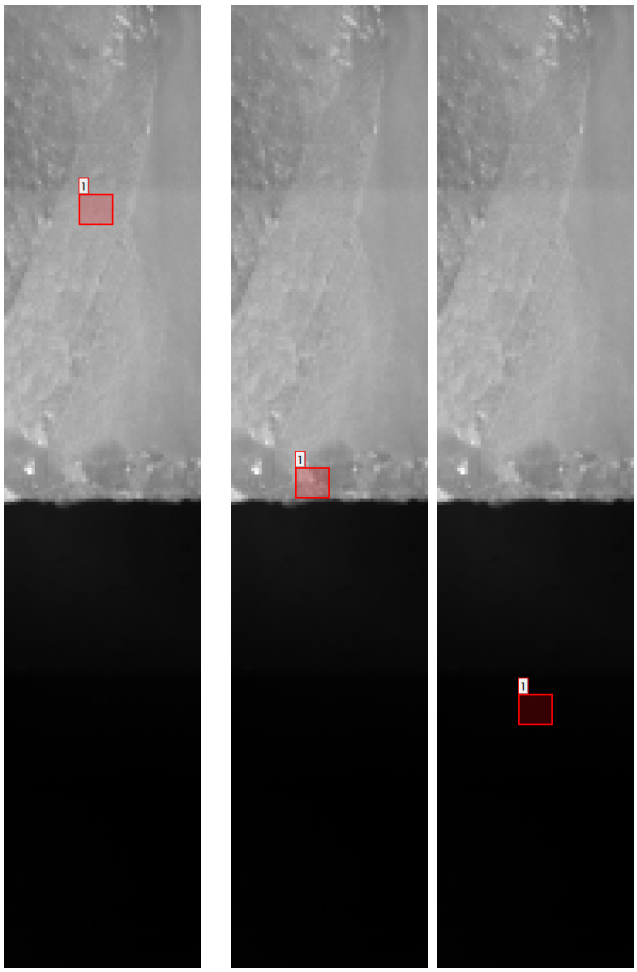

(a) Position 1 (b) Position 2 (c) Position 3

Figure 5.25: Section 1 STEM scan of EELS spectra locations, Ti coating 0.5 $\mu$m thick

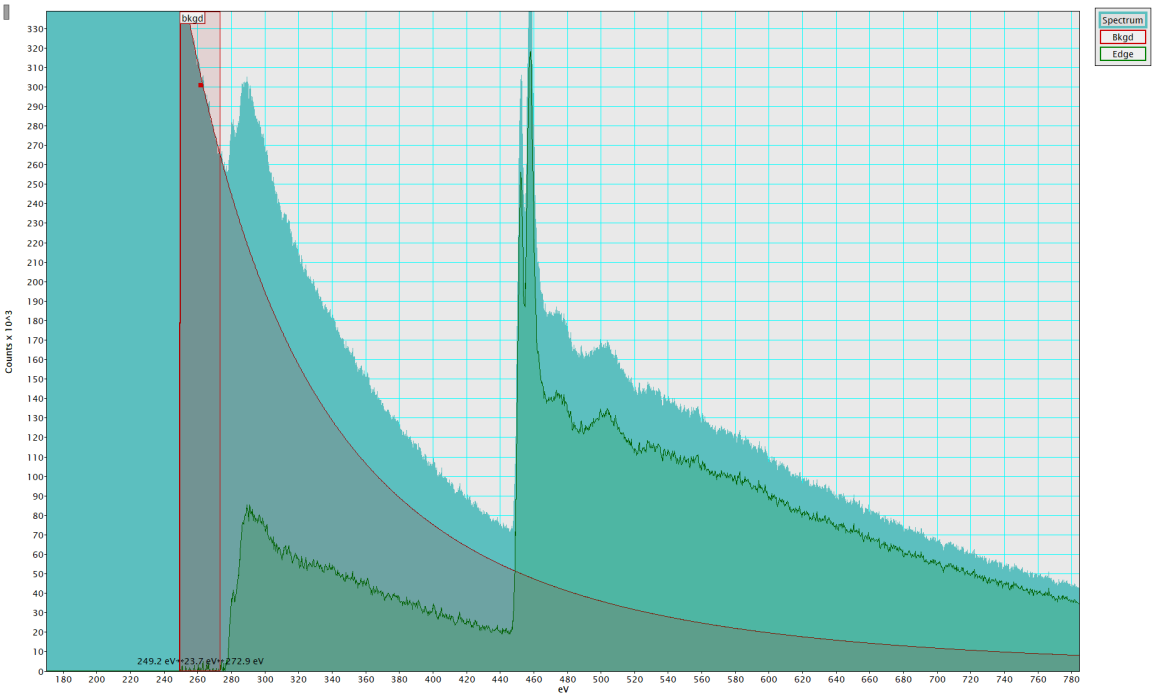


Figure 5.26: Section 1 EELS spectra position 1 of Ti coating 0.5 $\mu$m thick

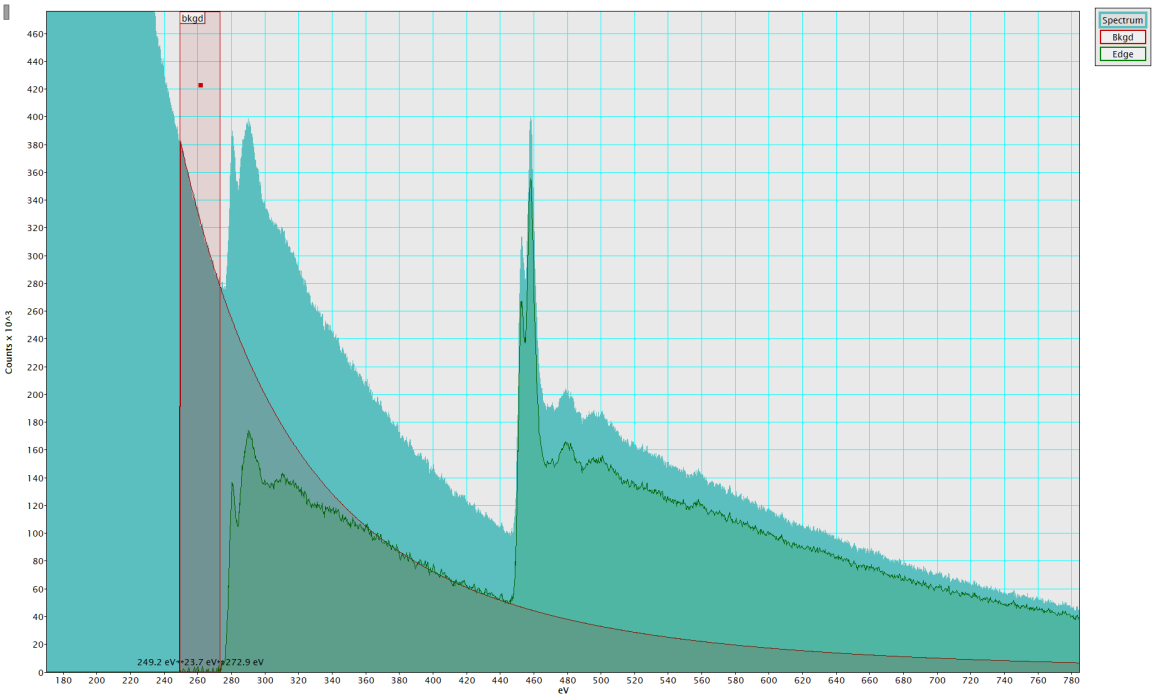


Figure 5.27: Section 1 EELS spectra position 2 of Ti coating 0.5 $\mu$m thick

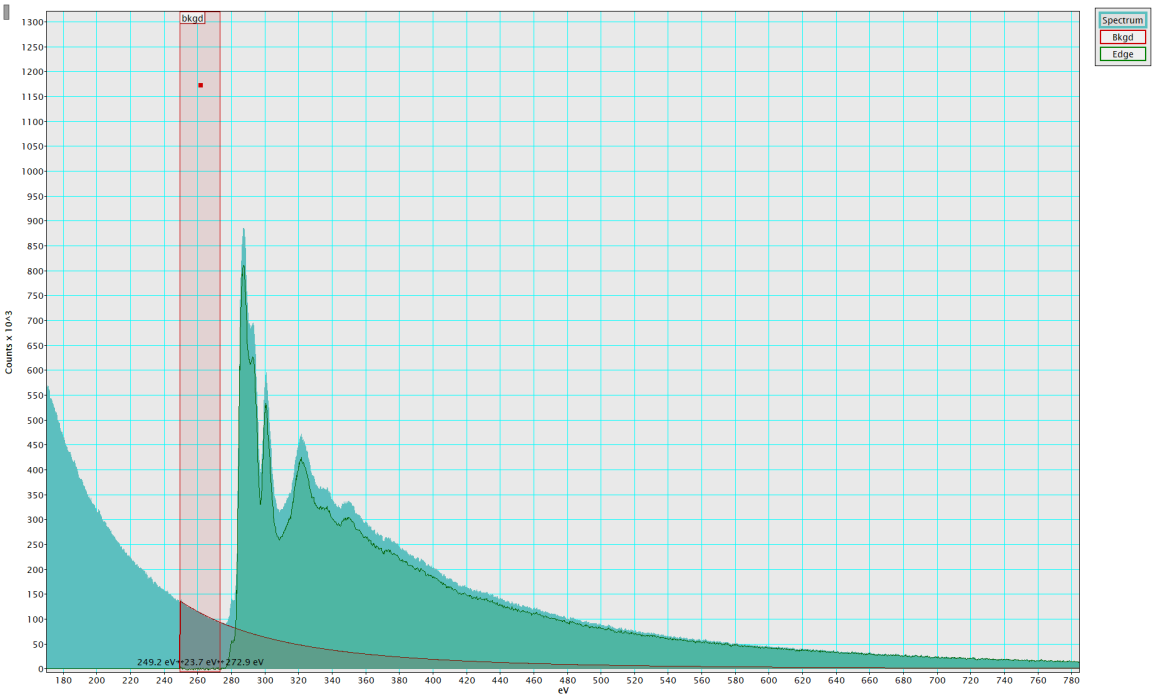


Figure 5.28: Section 1 EELS spectra position 3 of Ti coating 0.5 $\mu$m thick

### STEM/EELS Discussion

The FIB images in figures 5.11 through 5.12b show how the cross section was cut, what was analysed, and, in the case of figure 5.12b, the approximate thickness, which is reasonably close to the calculated 0.50 $\mu$m coating thickness.

Before interrogating the sample with EELS, STEM and HAADF were used to visually examine the cross section. As seen in figures 5.14, 5.15, and 5.16, the diamond was a large single crystal, with a small grain polycrystalline structure between the diamond and the large grain polycrystalline structure of the titanium PVD coating. Four sections were selected for an EELS scan, with the results and the corresponding HAADF images in figures 5.17, 5.19, 5.21, and 5.23. The carbon images show gradients of red, with the solid red being the diamond substrate, red with some black being the TiC layer, and less red and more black being the amorphous carbon. The titanium in green indicates that the titanium does not precipitate into the carbon, and also exhibits a consistent colour. The line scans in figures 5.18, 5.20, 5.22, and 5.24 are a quantification of the titanium and carbon across the coating. The general trend to the line scans is that the titanium coating has a fairly consistent count number, with a decline as it meets the carbon of the diamond. Where the carbon is diamond, it has high count values with some variation, and then has a sharp decline to lower count levels that stay relatively constant over the same span while the titanium counts are decreasing. The carbon then has another sharp decline to another steady lower count level that overlaps with the titanium coating.

The EELS spectrum imaging scan was performed on section 1, with the three positions scanned noted in figure 5.25: position 1 is in the titanium PVD coating, position 2 is on the polycrystalline material at the interface between the diamond and the titanium, and position 3 is in the diamond. For position 1, the corresponding EELS spectrum scan in figure 5.26 confirms the titanium and that there is also amorphous carbon. For position 2, from Urbonaite et al. (Urbonaite *et al.*, 2007), the spectrum confirms that it is titanium carbide, while for position 3, Barros et al. (De Barros *et al.*, 2002) confirms that the carbon profile matches diamond. When this is correlated back to the line graphs, it confirms that, for carbon, the area of highest count is diamond and that the first step down is TiC and the second step down is amorphous carbon in the titanium coating. An approximate thickness of the coating can also be determined, and is presented in table 5.1, where the thickness ranges from 0.04 to 0.09 $\mu$m.

Table 5.1: TiC Thickness

| **Section** | **TiC Thickness ($\mu$m)** |
|---|---|
| 1 | 0.09 |
| 2 | 0.04 |
| 3 | 0.04 |
| 4 | 0.09 |

### 5.5.3 XRD

#### XRD Results

These are the results of the 12 hour XRD scan. The long scan time was used to attempt to overcome the limitations of the XRD technique when applied to small samples and relatively small concentrations of compounds.

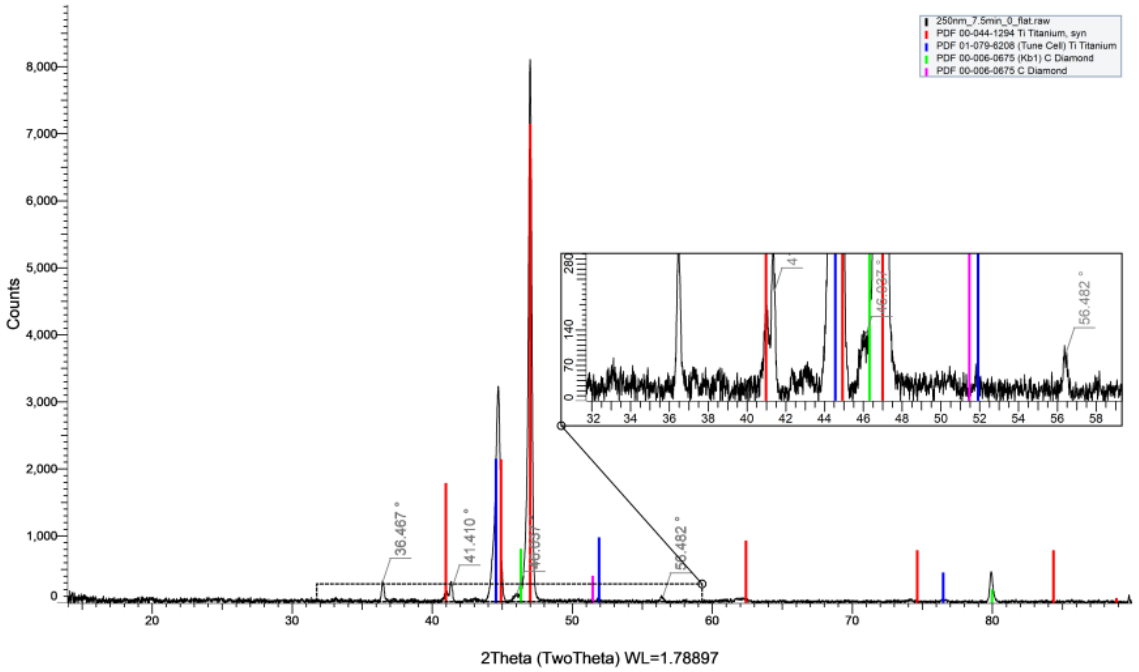


Figure 5.29: XRD results of 0.25 $\mu$m thick Ti coating

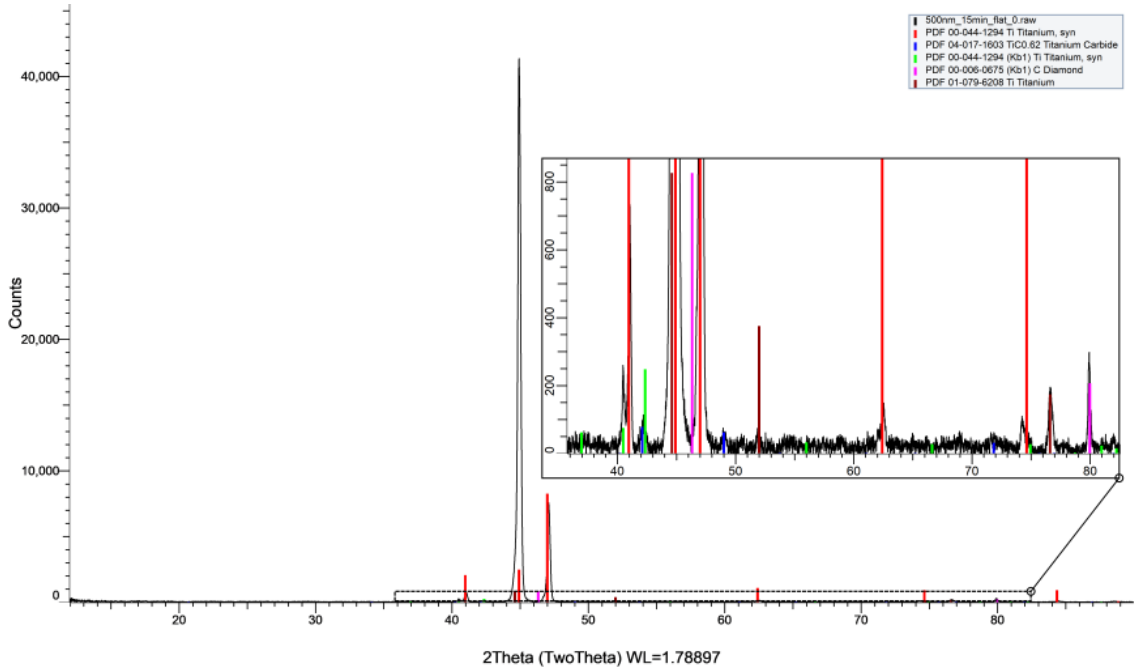


Figure 5.30: XRD results of 0.50 $\mu$m thick Ti coating

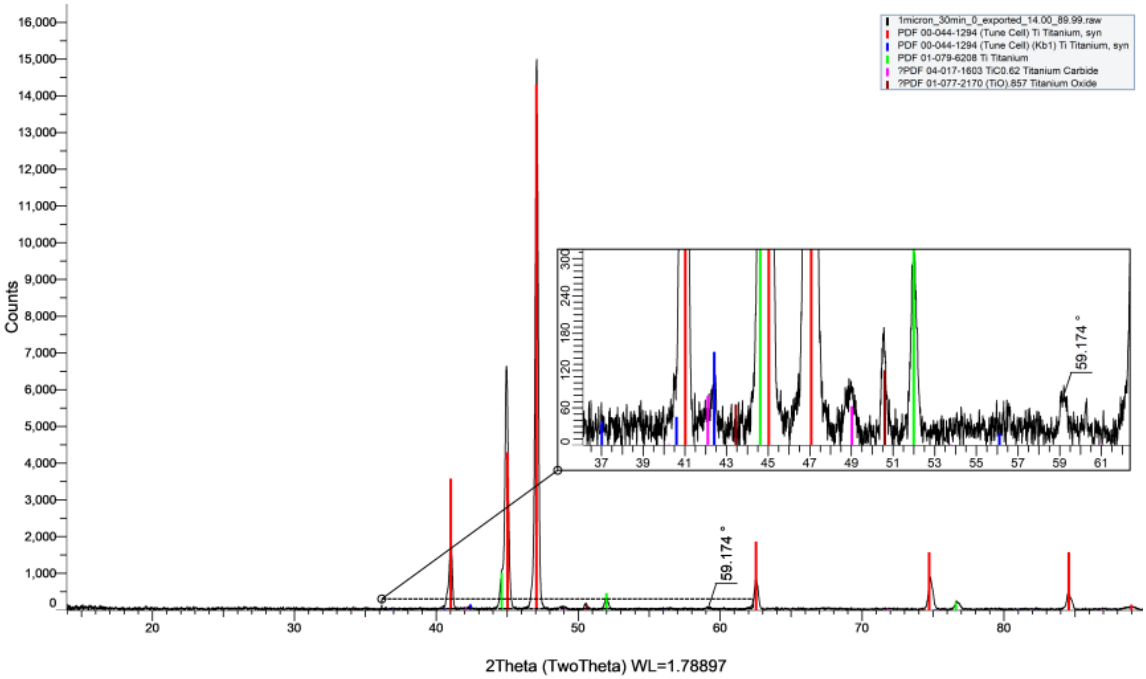


Figure 5.31: XRD results of 1.00 $\mu$m thick Ti coating

### XRD Discussion

As noted earlier, XRD had not been successful at detecting all the compounds in the samples. This is again the case here, with a confident confirmation of TiC occurring only in the 0.5 $\mu$m thick sample.

## 5.6 Analysis

The SEM and EDS measurements of elements were analysed using R, the statistical computing and graphics software. The elements of interest were titanium (Ti), oxygen (O), and carbon (C) for all coating thicknesses. The atomic percent of these elements were graphed by temperature for all of the coatings. In the case of carbon, the EDS did not penetrate past the oxides on the surface for the 0.5$\mu$m and 1.0$\mu$m thick coatings, hence its disappearance at 650°C.

As evident when examining the oxygen increase in figure 5.33, all three of the coating thicknesses started with the same oxygen atomic percent, but the thinnest coating, 0.25 $\mu$m, picked up the oxygen the fastest, making it the least desirable coating. Of the other two coatings, 0.50 $\mu$m and 1.0 $\mu$m thick, there was very little difference between the two. As stated earlier, it is more desirable for the coating to be thinner due to nanoindentation geometric constraints, which is why the 0.5 $\mu$m thick coating was considered the better coating.

As seen in the STEM/EELS cross section scan of a sample, the heat treatment was effective at forming a TiC layer. The variation of the TiC thickness seen in table 5.1

cannot be associated to the crystal orientation of the diamond, as the HAADF/STEM scans show that it was a single crystal. Therefore, the orientation of the titanium crystals in the PVD coating must be the driver for the variation in thickness. The results were interpreted to indicate that carbon will continue to precipitate into the titanium coating thus continuing to grow the TiC layer. If a 30 minute heat treatment at 500°C forms a TiC layer up to 0.09 $\mu$m thick, it is conceivable that the entire titanium coating for the 0.25 $\mu$m thick sample was TiC after three oxidation experiments. This would account for the difference in appearance of that coating at 650°C and would therefore imply that TiC is less resistant to oxidation than titanium alone, explaining why the thicker coating was better.

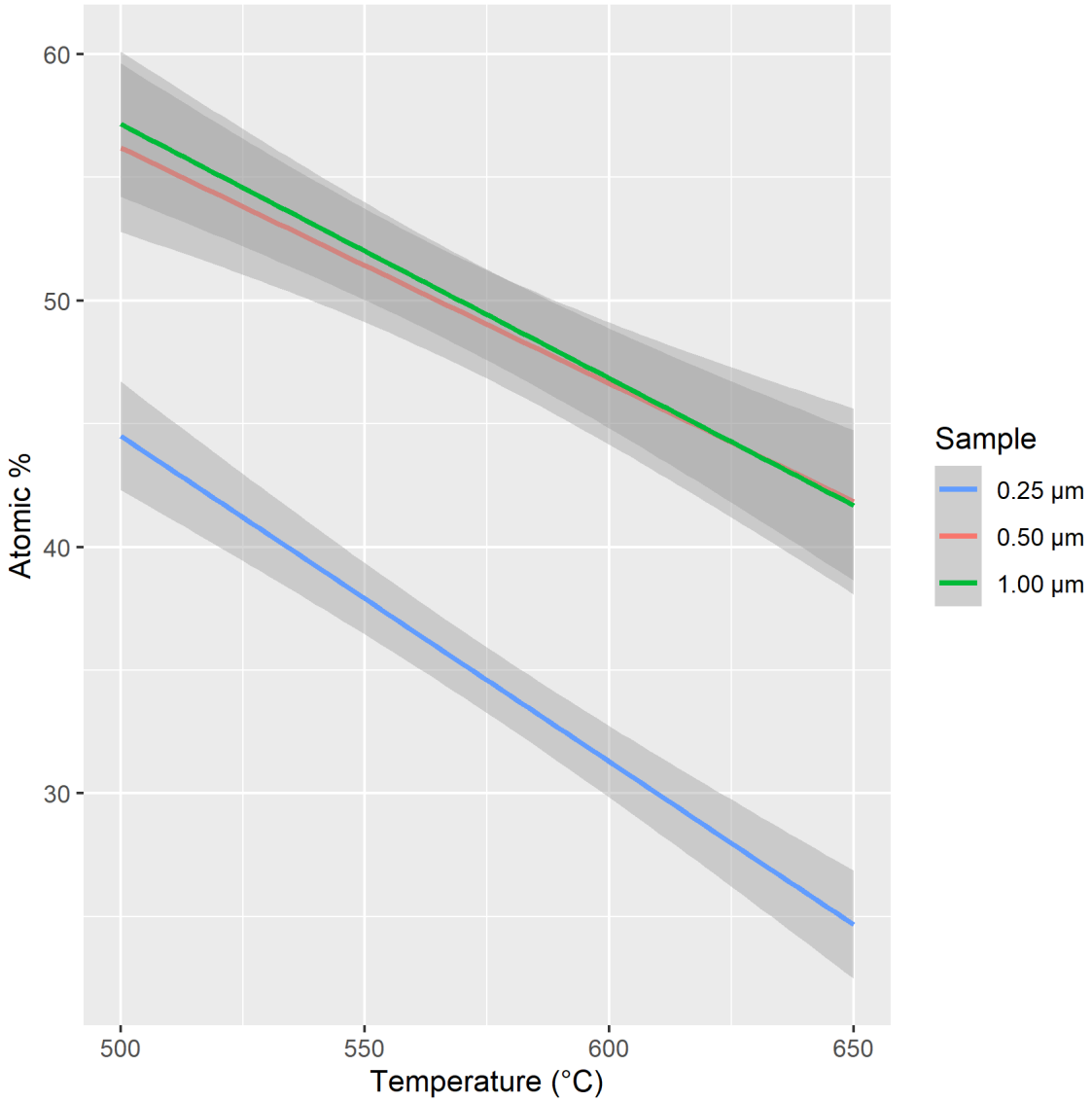


Figure 5.32: Comparison of titanium atomic percent

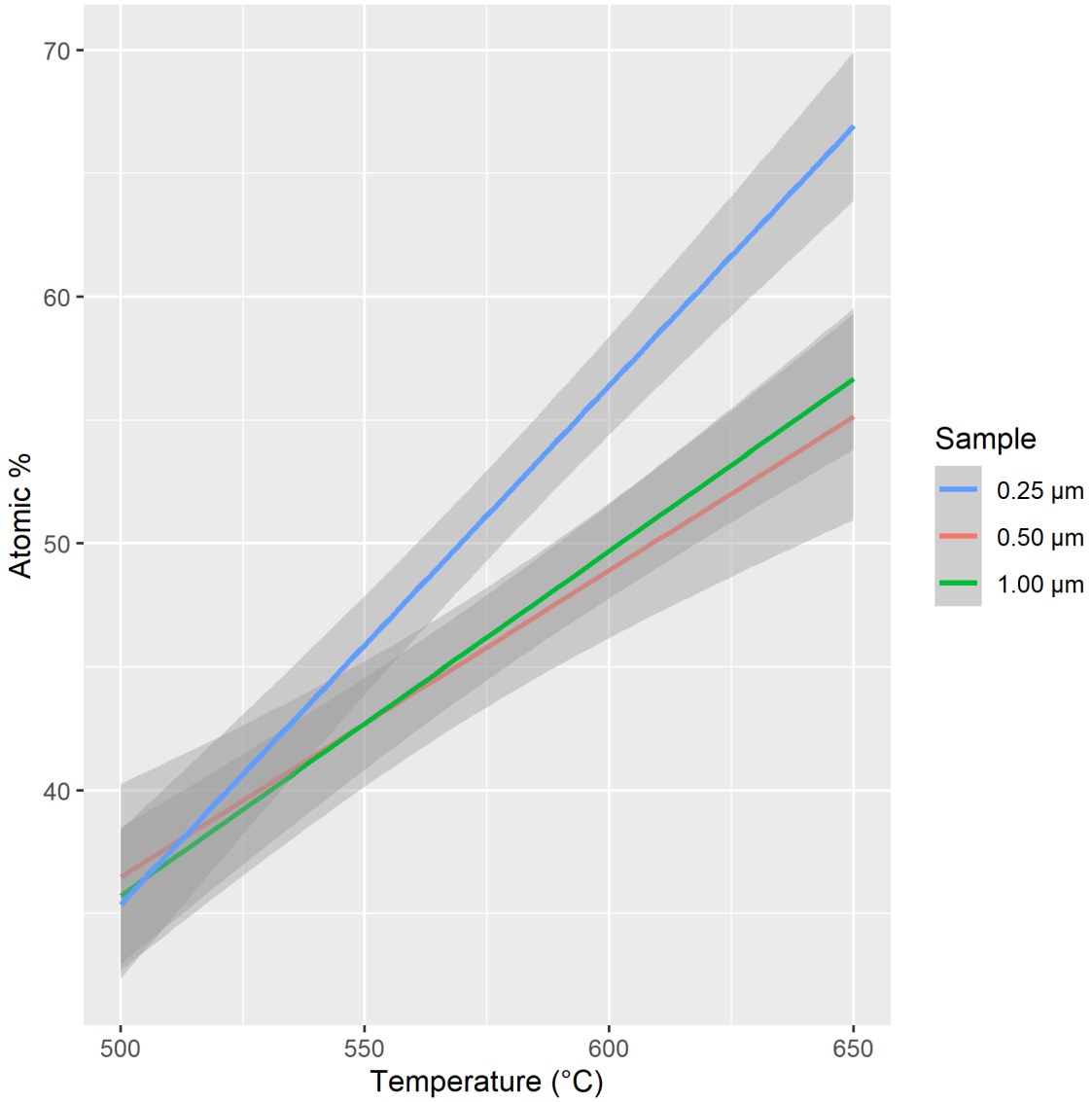


Figure 5.33: Comparison of oxygen atomic percent

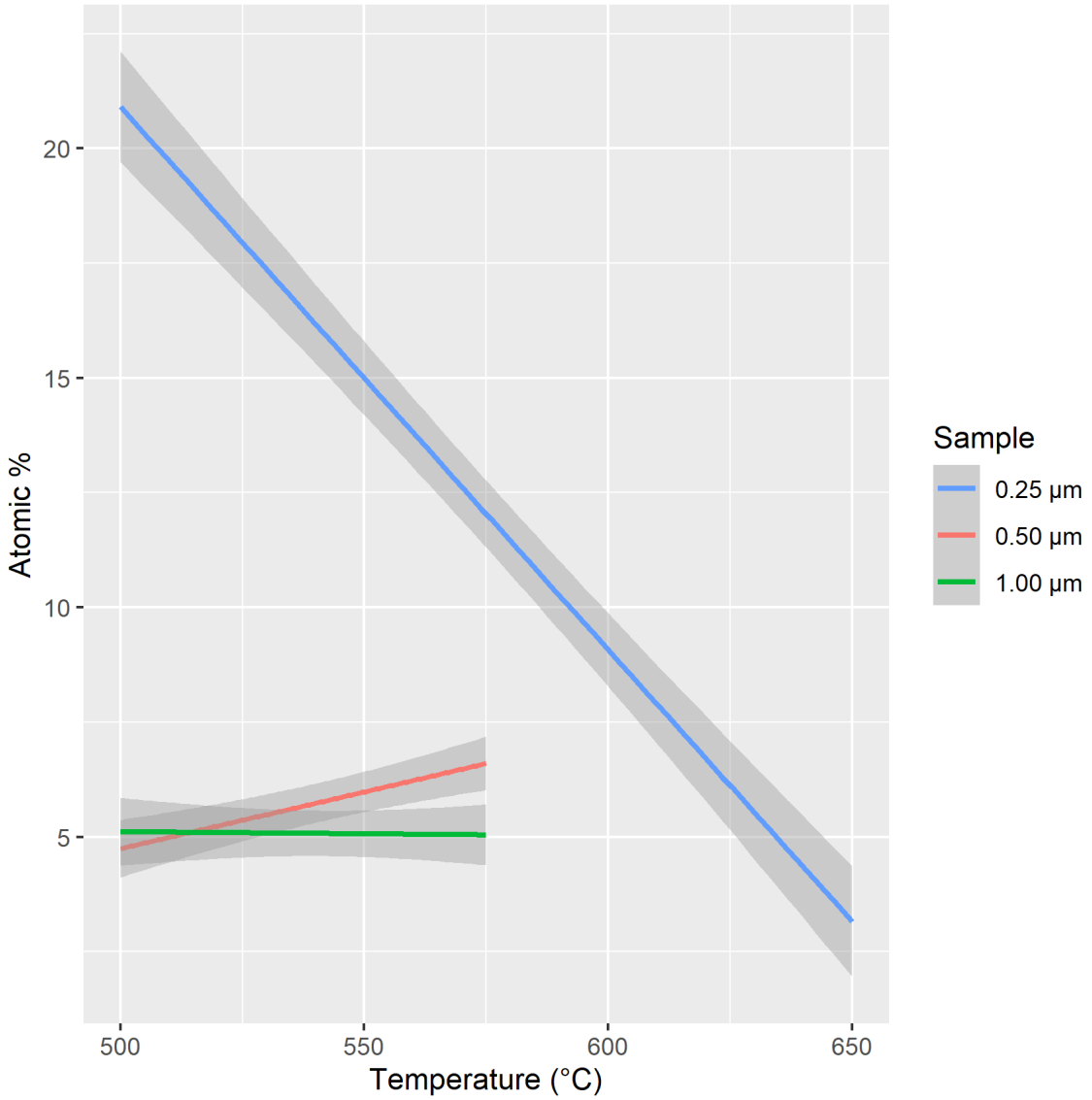


Figure 5.34: Comparison of carbon atomic percent

## 5.7 Conclusion

From the results and the analysis, the following can be concluded:

- The best coating thickness balances competing requirements. As per the static oxidation results a 0.5 $\mu$m or thicker coating was recommended. It is likely that a thicker coating would correspond to greater longevity with respect to oxidation. However, the geometric requirements for nanoindentation favour a thinner coating; thus, for this application, the 0.5 $\mu$m thick coating was deemed to be the optimal one for this application.

- The HAADF and EELS scans confirmed that TiC does form at the interface between the diamond and the titanium, and that while not perfectly uniform in its thickness, there is no location along the examined interface where TiC is absent.

# Chapter 6

# Test of a Titanium Coated Diamond Nanoindenter

## 6.1 Hypothesis

The hypothesis to this thesis is that if diamond were protected from oxidation, it could be used for an application such as nanoindentation between the temperatures of 400-750°C. This was the final test for the pure titanium coating to confirm whether it will work in this application.

## 6.2 Experimental Criteria

To confirm that the titanium coating is effective:

- The coating must adhere to the diamond indenter at elevated temperatures during a measurement.

- The indenter must be shown to be able to be used to perform measurements. This can be shown by calibrating the coated indenter.

Thus, the experimental criteria are as follows:

- Has the coating stayed on the tip after an indentation cycle at high temperature? Some wear is acceptable, but the diamond must be protected by the titanium coating. To determine whether this is the case, the tip is "visually" examined by SEM and also examined by generating an EDS map. If there is noticeable wear in the SEM image, the EDS map would confirm whether any titanium is still present at that location or if it is all carbon.

- The coated indenter needs to show that it can be calibrated, and that the calibration results are reasonably accurate and comparable to the same indenter in its uncoated form. It should be noted that the coating on the indenter is expected to make the indenter more blunt, thus increasing the minimum nanoindentation load.

## 6.3 Design of Experiment

### 6.3.1 Sample Preparation

As the indenters used for these experiments were used, or worn, the indenter was "visually" examined by SEM and an EDS map. This was performed to confirm that the surface was not contaminated. Due to the results of the inquiry, there were no features that required EDS point examination.

### 6.3.2 PVD Coating

The indenter was coated by PVD for 15 minutes with pure titanium, which yielded an approximate thickness of 0.5 $\mu$m (since the indenter is a pyramidal Berkovich tip, the coating could not be as consistently uniform as with a flat sample). The temperature was then held for 30 minutes at 500°C to cause a TiC interface layer to form.

### 6.3.3 Experiment

The experiments were performed on a Micro Materials Vantage nanoindentation system.

#### Elevated Temperature Adhesion

The maximum measurement temperature used was limited to 450°C, as the modifications required to test the diamond indenter did not allow for the use of some of the heat shielding typically used for elevated temperature measurements. There was no change in the typical rise of temperature of 1.6°C/min until the measurement temperature was reached. The sample used was the silicon glass used to calibrate the device for measurements. The indentation load was 20 mN, with a load time of 10 seconds, a dwell of 5 seconds, and an unloading time of 10 seconds. The heating was then turned off, allowing the nanoindenter and sample to air cool to room temperature. The nanoindenter tip was then examined using SEM and EDS maps. The experiment was then performed a second time to increase confidence in the results. This methodology is illustrated in figure 6.1a.

### Diamond Area Function (DAF) Calibration

The diamond area function is the relationship between the depth of contact, $h_c$, and the cross-sectional area of the nanoindenter tip. This relationship is established through a calibration process of indenting a known sample several times over a range of loads. The measured results (load, depth) are used to calculate the diamond area function, $A(h_c)$, which is then used to calculate the hardness, $H$. The slope, $S$, is calculated and is used with the diamond area function to calculate the effective elastic modulus, $E_r$. When using fused silica as the calibration sample, the diamond area function is then optimized such that the calculated values, hardness and effective elastic modulus, are between 8.8 - 9.4 GPa and 69-72 GPa, respectively.

For this experiment, the indenter was first calibrated and then examined by microscope to show the pre-coated shape. Once coated, the indenter was again examined by microscope to visually confirm the coating on the indenter. Some preliminary measurements were then performed and the indenter examined again by microscope to confirm that the coating was adhering. Based on these results, the calibration was performed again on the coated indenter.

For the calibration of the uncoated indenter, there were 4 sets of 10 measurements performed:

- 10 measurements with loads uniformly incremented between 0.5 mN and 5 mN.
- 10 measurements with loads uniformly incremented between 5 mN and 50 mN.
- 10 measurements with loads uniformly incremented between 50 mN and 200

mN.

- 10 measurements with loads uniformly incremented between 200 mN and 500 mN.

Previous experimental work with the worn indenter indicated that the indenter would be usable, but dull for nanoindentation measurements. A dull indenter makes it difficult to get accurate measurements at very low loads. Due to the further blunting effect from applying the coating, only 2 sets of 10 measurements were performed at the higher load levels for the coated indenter:

- 10 measurements with loads uniformly incremented between 50 mN and 200 mN.
- 10 measurements with loads uniformly incremented between 200 mN and 500 mN.

The DAF calibration was performed manually using equations (1.31), (1.34) and (1.33) for the slope, hardness and effective elastic modulus. The maximum load, $W_{max}$, the depth, $h$, and the depth of contact, $h_c$, are output from the Micro Materials nanoindentation system, while the correction factor, $\beta$, is a used determined scaling input. The area function used is one of the most common diamond area funtions,

$$A\left(h_c\right) = C_0 + C_1 \times h_c + C_2 \times h_c^2, \tag{6.1}$$

where $C$ are the coefficients being solved for. The coefficients are then tweaked within the recommended ranges as stated in table 6.1. Note that for coefficient $C_1$ these are general recommended values - for a very sharp indenter the coefficient can be below

Table 6.1: Diamond Area Function Coefficient Ranges

| **Coefficient** | **Range** |
|---|---|
| $C_0$ | 0 |
| $C_1$ | 800-2500 |
| $C_2$ | 23-26 |

800, and for a very blunt indenter the coefficient can be above 2500. While the correction factor, $\beta$, is typically between 1.02 and 1.08, there does not appear to be a physical correlation to that range. Thus, in order to calibrate, the hardness points are optimized over the load range of interest between 8.8 and 9.4 GPa, and the effective elastic modulus points are optimized to be between 69 to 72 GPa.

The reasons for performing the calibration manually are due to limitations of the Micro Materials software, in that it is unable to combine multiple sets of measurements, in addition to it being difficult to determine what measurements are outliers. Furthermore, there is a more recent equation (Oliver and Pharr, 2004) that is recommended for the calculation of the DAF,

$$A\left(h_c\right) = \sum_{n=0}^{8} C_n \left(h_c\right)^{2-n}, \tag{6.2}$$

but is not available as an option in the Micro Materials software being used. This methodology is illustrated in figure 6.1b.

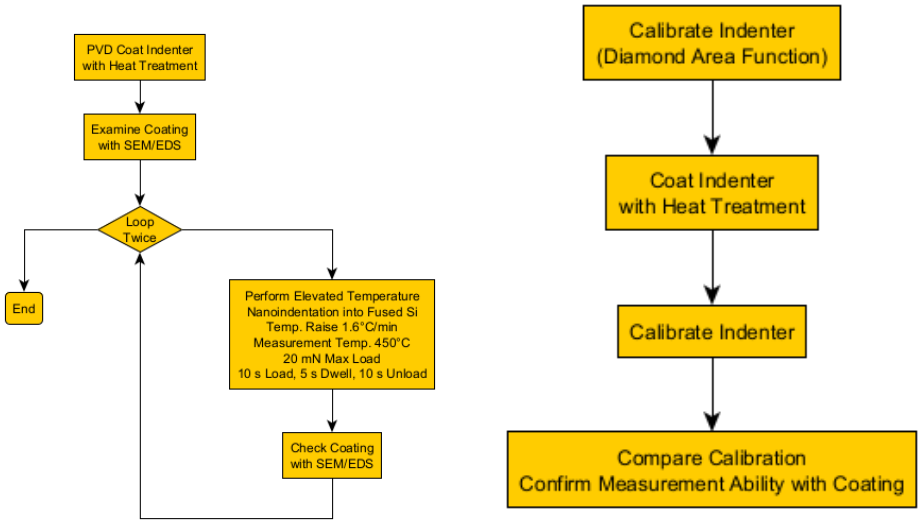


(a) Nanoindentation Test - Nanoindentation Methodology

(b) Nanoindentation Test - Diamond Area Function Methodology

Figure 6.1: Nanoindentation Test Methodology

## 6.4 Results

### 6.4.1 Elevated Temperature Adhesion

#### SEM Images and EDS Maps

These are the SEM images and EDS maps from the two rounds of nanoindentation measurements.

#### Round 1

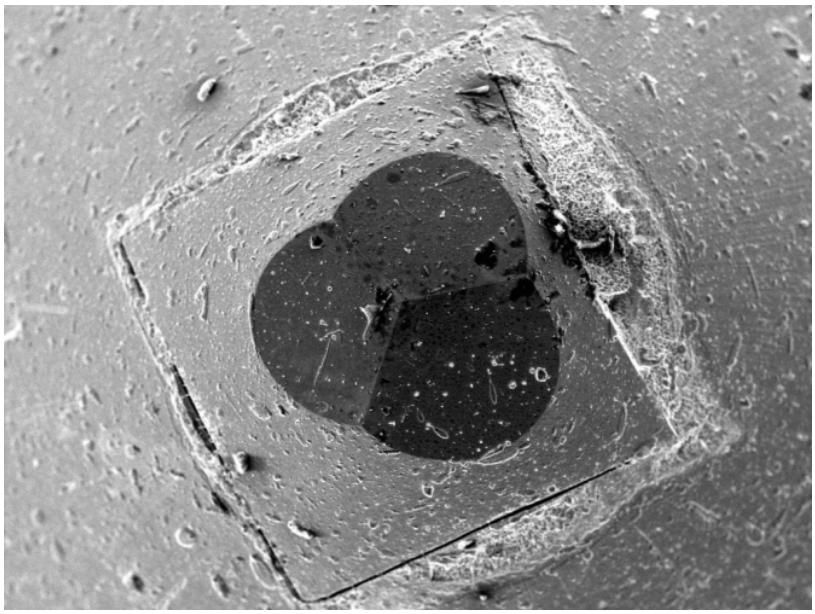

(a) SEM image of nanoindenter

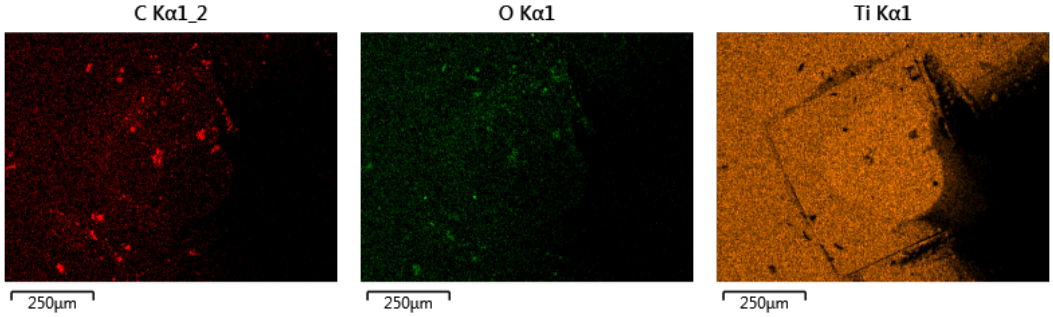


(b) EDS carbon map of nanoindenter (c) EDS oxygen map of nanoindenter (d) EDS titanium map of nanoindenter

Figure 6.2: SEM and EDS maps of first nanoindentation

**Round 2**

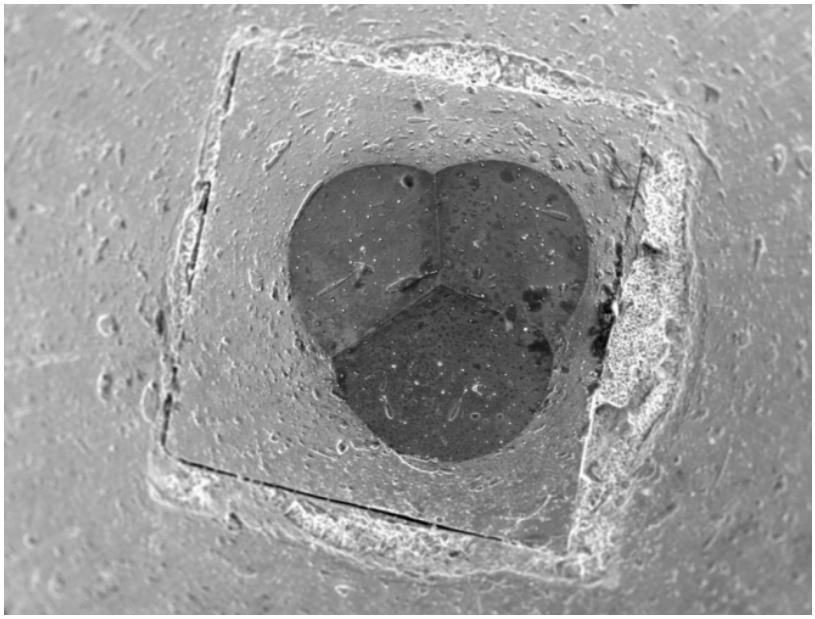

(a) SEM image of nanoindenter

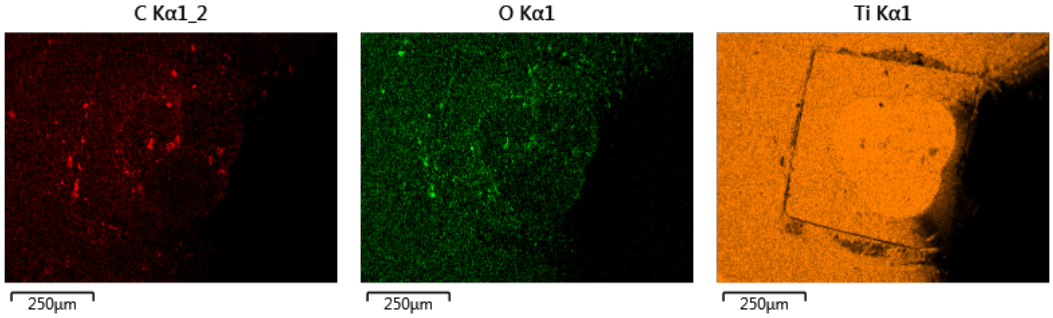


(b) EDS carbon map of nanoindenter (c) EDS oxygen map of nanoindenter (d) EDS titanium map of nanoindenter

Figure 6.3: SEM and EDS maps of second nanoindentation

### Discussion of Elevated Temperature Adhesion Results

The images shown are the top-down orientation of the Berkovich pyramid indenter with the tip in the centre. The portion of the ndenter that is diamond in comparison

to the metal holder can be determined visually, as the diamond is within the square while everything outside the square is the metal holder. Based on the images, further work in this area should use high temperature glue or cement to affix the diamond to the holder, as some of the features at the edges of the square look like the bubbling of glue seen on the other diamond samples post oxidation test.

It is difficult to determine visually if there was any wear between the first and second nanoindention test. The EDS maps show the diamond completely covered by titanium, with a small percentage of carbon, which is what occurs when the electrons from the SEM penetrate through the coating to the substrate. Further confirmation that the diamond is completely covered is that there are no locations observed without titanium.

### 6.4.2 Diamond Area Function Calibration

#### Loading-Unloading Curves

These are the loading curves from the diamond area function calibration.

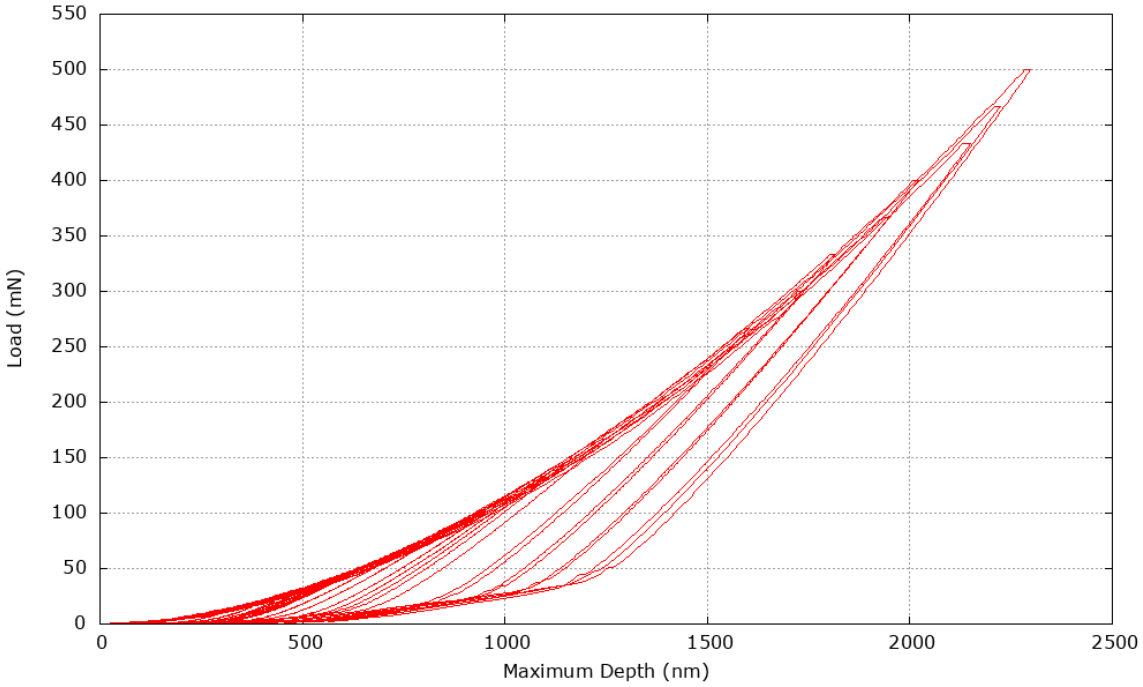


Figure 6.4: Load vs. depth for uncoated indenter

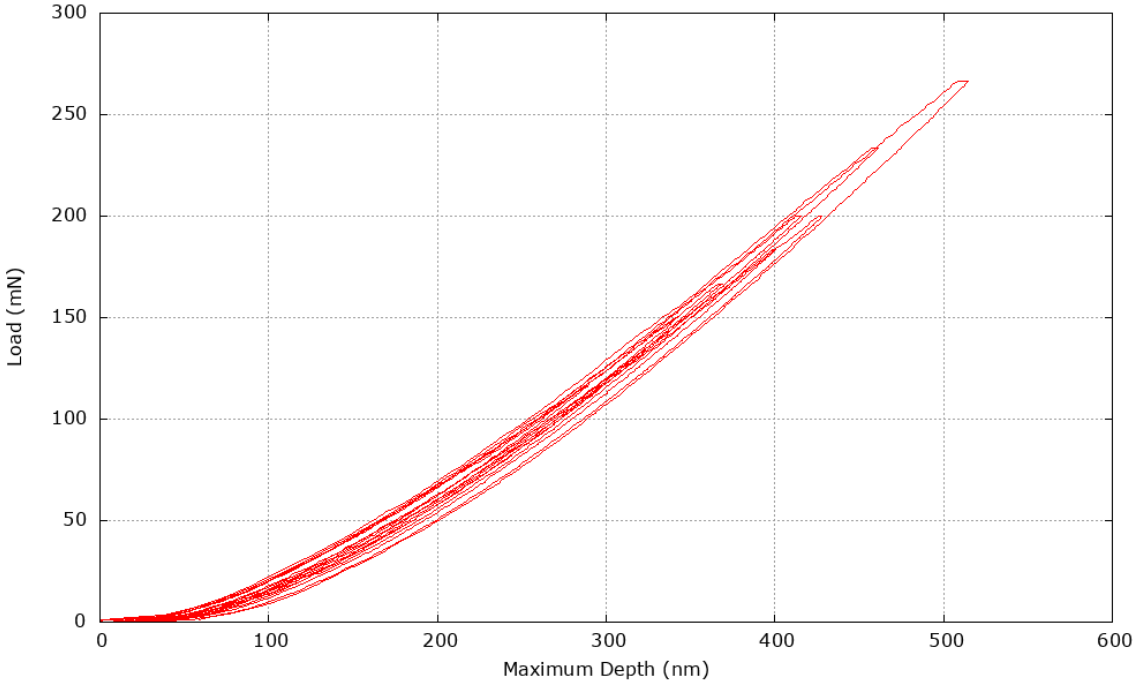


Figure 6.5: Load vs. depth for coated indenter

### Indenter Tip Inspection

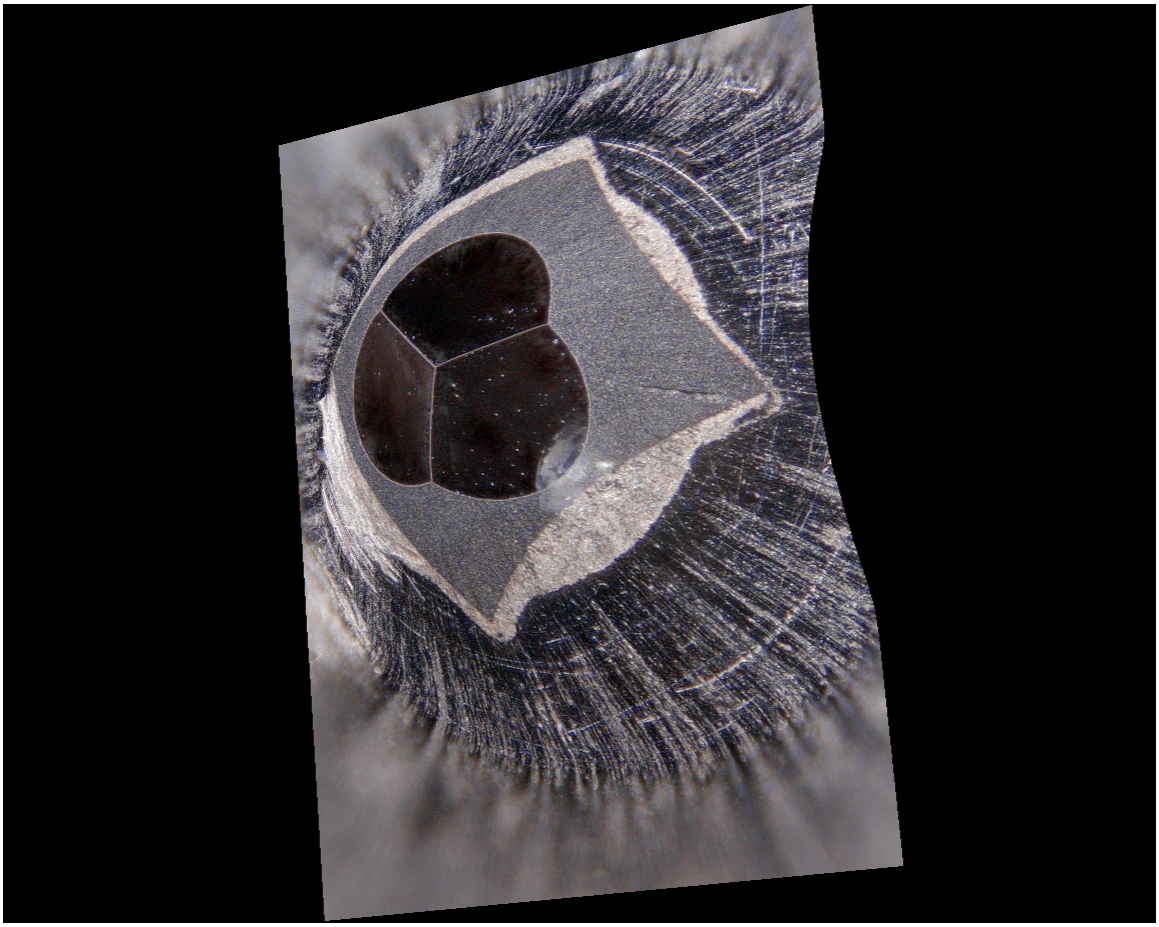

Figure 6.6: Microscope image of uncoated indenter

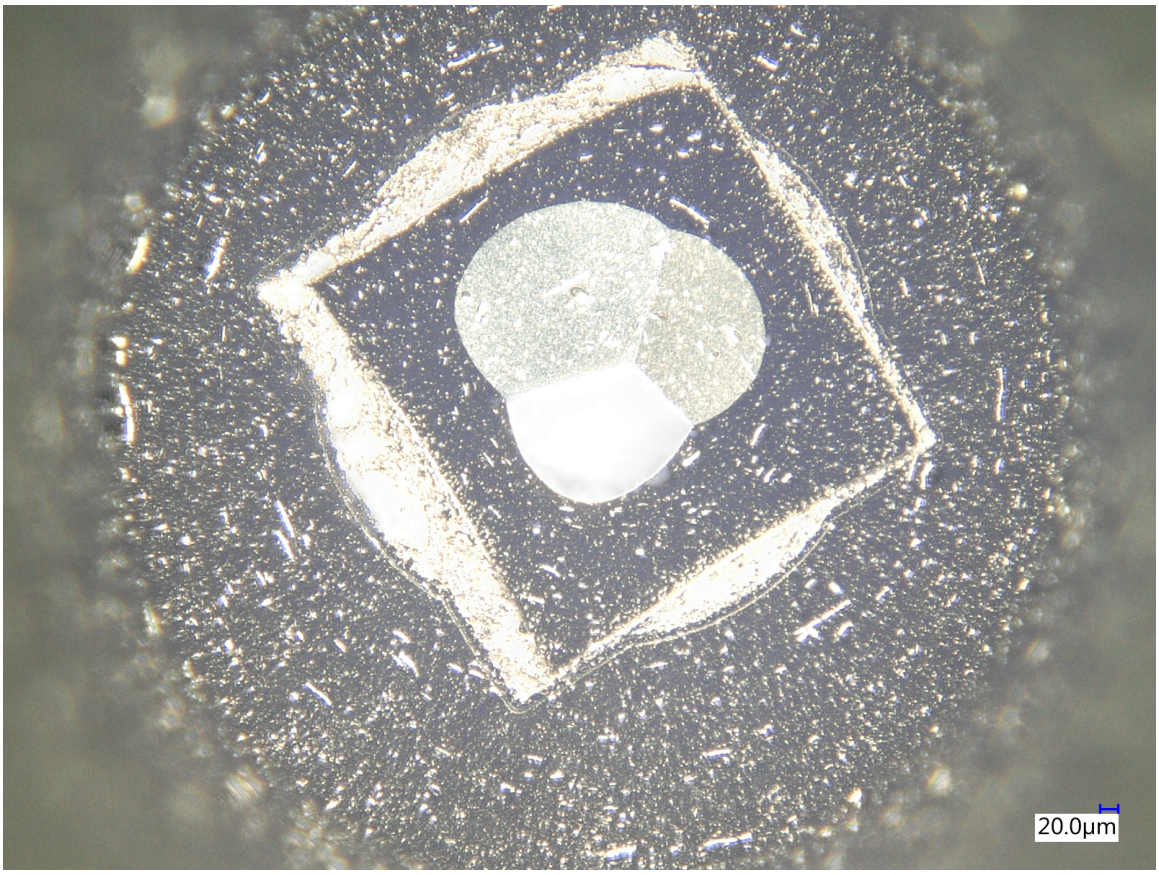


Figure 6.7: Microscope image of coated indenter pre-nanoindentation measurement

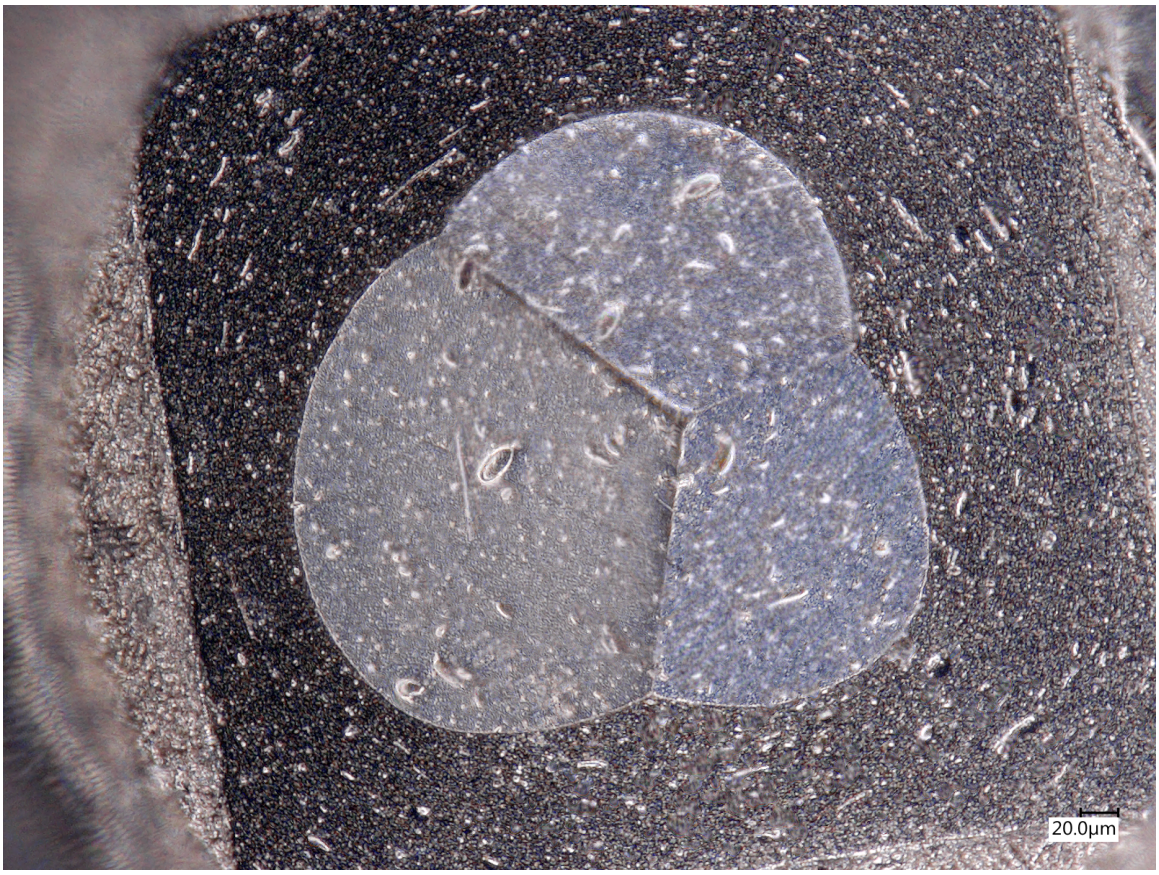


Figure 6.8: Microscope image of coated indenter post-nanoindentation measurement

**Discussion of Diamond Area Function (DAF) Calibration**

The load vs. depth graphs are shown in figures 6.4 and 6.5. These results are filtered, which means that measurements that did not match the consistency seen in these figures were removed. Two of the more common reasons for a failed measurement are the nanoindentation system not finding the surface, or excess noise to the indentation (typically from a combination of a blunt indenter and a low load, causing it to pick up surface roughness). More discussion of these outliers takes place in section 6.5.2.

Figure 6.4 shows a more typical set of measurements for a fused silica sample, where due to the plastic deformation of the sample there is a difference between the loading and loading curves. Figure 6.5 has loading and unloading curves nearly on top of each other, which would indicate that the coated indenter is much more blunt and does not appear to plastically deform the surface. This is also reflected when the depth of penetration is compared across the same load amount. For example, a load of 250 mN would result in a penetration depth of over 1500 nm in the uncoated indenter, or less than 500 nm for the coated indenter.

The microscope image of the indenter, shown in figure 6.6, shows a clean indenter tip with straight, sharp edges on the Berkovich pyramid.

The coated diamond microscope image in figure 6.7 shows the indenter immediately after being coated. In comparison to the uncoated image in figure 6.6, the black of the diamond is now the light gray of the titanium coating, indicating that the diamond is completely coated. The microscope image (figure 6.8) of the indenter after

performing some nanoindentation tests shows that the tip is still covered (no black of the diamond peaking out), with no significant signs of wear.

## 6.5 Analysis

### 6.5.1 Elevated Temperature Adhesion

From the SEM image and EDS maps in figure 6.3, the experimental criteria for the adhesion test has been met - i.e., the coating adheres to the diamond at elevated temperatures.

### 6.5.2 Diamond Area Function Calibration

For the calibration, one of the items compared was how many outliers each data set had (i.e., the uncoated data set and the coated data set). If one had more outliers than the other, there would be a need for further investigation as to why. In this case, the number of outliers were proportionally the same by population size of the data set.

For the uncoated data set, the bluntness of the worn indenter was revealed in the poor results at low loads. For the coated indenter, the nanoindentation system was having trouble finding the surface of the sample, resulting in several measurements having an offset before the load started to increase. Should that portion be removed, the loading-unloading curves would fall on top of the other curves shown in figure 6.5. However, there is no precedent in literature for this sort of post-processing of results, thus the measurements were discarded.

The range of the appropriate indentation load is 45-500 mN for the uncoated indenter, and 115-500 mN for the coated indenter, confirming the reduction in range at lower loads due to the blunting of the indenter with the coating.

Over the appropriate range, the effective elastic modulus and hardness are tabulated in table 6.2. As can be seen from table 6.2, the results are comparable, with

Table 6.2: DAF Calibration Results - Effective Elastic Modulus and Hardness

| **Coating Status** | $E_r$ **(GPa)** | | **Hardness (GPa)** | |
|---|---|---|---|---|
| | $\mu$ | $\sigma$ | $\mu$ | $\sigma$ |
| Uncoated | 70.4 | 3.25 | 9.04 | 0.30 |
| Coated | 70.7 | 1.47 | 9.03 | 0.80 |

the only differences being in the standard deviation - there is more variation in the effective elastic modulus of the uncoated indenter, while there is more variation in the hardness for the coated indenter. In both cases the standard deviation is fairly low and acceptable for performing measurements.

## 6.6 Conclusion

From this set of experiments, it has been shown that the titanium coating can withstand an elevated temperature measurement, and also that the thickness of the coating does not impede the ability to calibrate the indenter for use in measurements. It is also shown through the DAF calibration and the analysis of the DAF calibration measurements that the uncoated and coated indenter measurements compare reasonably well to each other in their appropriate load ranges.

Therefore, the hypothesis that diamond can be protected by a coating at the temperatures of 400-750°C has been substantiated by these results.

# Chapter 7

# Conclusion

The conclusion to this work is that a titanium PVD coating can protect a diamond nanoindenter during measurements between the temperatures of 400-750°C.

There are two unique contributions that this thesis makes to the current science of nanoindentation. First, in using a diamond nanoindenter with a titanium PVD coating 0.50 $\mu$m thick, it demonstrates that coated nanoindenters can be used for measurements. Therefore, there is an alternative means of enhancing nanoindentation in comparison to the current approach of changing the nanoindenter material. Second, it demonstrates that coating a diamond nanoindenter with titanium by PVD extends the operational temperature range that diamond can be used from a maximum of 400°C to 750°C. Thus, the titanium PVD coating has shown a way of mitigating the diamond breakdown mechanism while maintaining functionality, while also increasing functionality and durability for elevated temperature applications.

Secondary contributions from the thesis results are:

- The assessment of the adhesion of titanium coatings to diamond in the temperature range of 400-750°C.
- The methodology of testing coating to determine the best coating options.

While this work establishes the proof of concept, recommended future work would be to determine the durability of the coating: how many nanoindentations can be performed, and what impact does the temperature have on this number? Other development ideas involve looking at multilayered coatings which build on the adhesion of the TiC interlayer and provide higher oxidation protection. Elements such as chromium and tungsten are recommended due to their high temperature stability properties.

# Appendix A

# Indenter and Nanoindenter Friction

## A.1 Literature Review

In a literature review on friction in nanoindentation, only one paper was found where it was concluded that friction should be considered (Zhao *et al.*, 2003). A more useful and comprehensive study of friction was performed by Hankins (Hankins, 1925) on ball and conical indenters.

## A.2 Analysis of Friction for Nanoindentation

What Hankins did was a simple force balance to describe the results of the tests performed, which showed that there was a constant yield pressure for indentation. A diagram of the force balance can be seen in figure A.1, where $W$ is the normal load, $P$ is the yield pressure for indentation, $\mu$ is the coefficient of friction, $\alpha$ is the angle

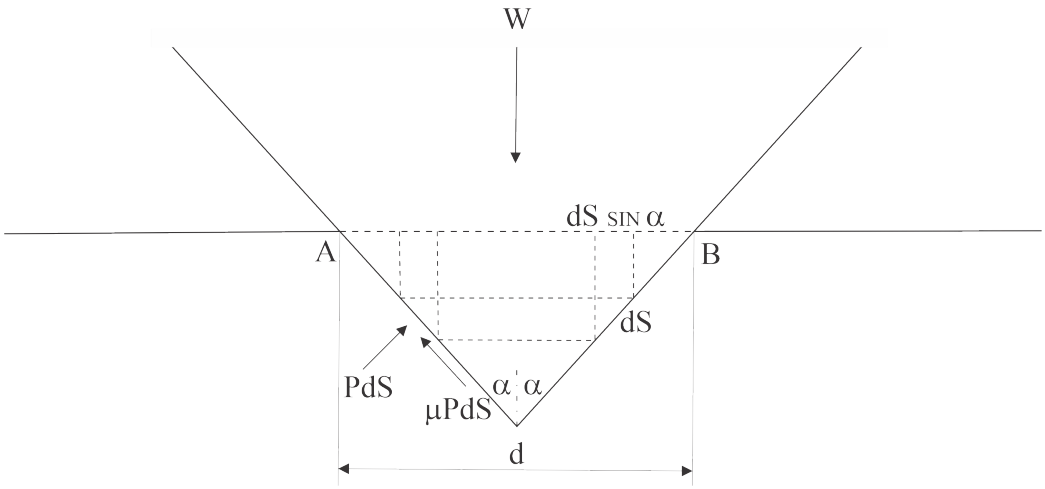


Figure A.1: Role of friction between a conical indenter and the deformed metal as Treated by Hankins (Hankins, 1925) and illustrated by (Tabor, 1951)

of the indenter, and $dS$ is an element of the cone surface area. Applying a vertical force balance,

$$W = \int dW = \int (PdS \sin\alpha + \mu PdS \cos\alpha) \tag{A.1}$$

$$= P(1 + \mu \cot\alpha) \int \sin\alpha dS. \tag{A.2}$$

As noted from figure A.1, $dS \sin\alpha$ is the projection of the area $dS$ on the section $AB$,

$$dS \sin\alpha = \frac{\pi d^2}{4}. \tag{A.3}$$

Substituting this into equation A.1,

$$W = P(1 + \mu \cot\alpha) \frac{\pi d^2}{4} \tag{A.4}$$

$$P = \frac{4W}{\pi d^2} \left( \frac{1}{1 + \mu \cot\alpha} \right). \tag{A.5}$$

Now, when there is no friction, the yield pressure, $P_o$, is

$$P_o = \frac{4W}{\pi d^2}. \tag{A.6}$$

Substituting this into equation A.4 results in

$$P = P_o \left( \frac{1}{1 + \mu \cot \alpha} \right). \tag{A.7}$$

Tabor (Tabor, 1951) notes that this formula breaks down at 90° (i.e., a flat punch), but there is good correlation to experimental results when there is a point to the indenter (i.e., less than 90°).

When compared to the nanoindentation mathematics in section 1.2.1, it is clear that the hardness calculation for nanoindentation in (1.34) is the same as (A.6). Applying the equivalent indenter angle of 70.3° (used in the nanoindentation equations as a conical approximation of a Berkovich indenter) and coefficient of friction of diamond between 0.10 and 0.15 to (A.6) results in an approximately 5% reduction in hardness. Additionally, this reduction would also apply to the nanoindentation loading and unloading curve, thus impacting the stiffness value.

# Appendix B

# Round 1 & Round 2 Comparison

During the experimental phase it was determined that the first round of experiments had some contamination by 575°C. Based on the methodology of the experiments and how the contamination presented itself on the surface, it is presumed that the contamination is the glue that holds the diamond to the steel stub, thus the second round of experiments had a high temperature cement applied to the samples, coating the edge of the diamond to the surface of the steel stub, while leaving the coated surface of the diamond exposed for the purposes of the experiments. However, experience from the first round of experiments showed that not much changed in terms of the elements measured by EDS at 425°C, thus the second round of experiments began at 500°C and went to 650°C instead of 575°C of round 1. It is therefore of interest to determine if it can be justified to used some of the results from the first round of experiments. In order to do that, the data set from the EDS point analysis was divided up, first by the 4 coating types, then by the 4 elements of interest (Al, C, O and Ti), and then by the first 3 types of the EDS point analysis. To compare round 1 and round 2, the values are then graphed by atomic % and temperature,

with a linear regression line through them.

## B.1 Comparison of Ti coating 0.5 - 0.6 $\mu$m Thick

The graphs of the Ti coating 0.5 - 0.6 $\mu$m thick are as follows.

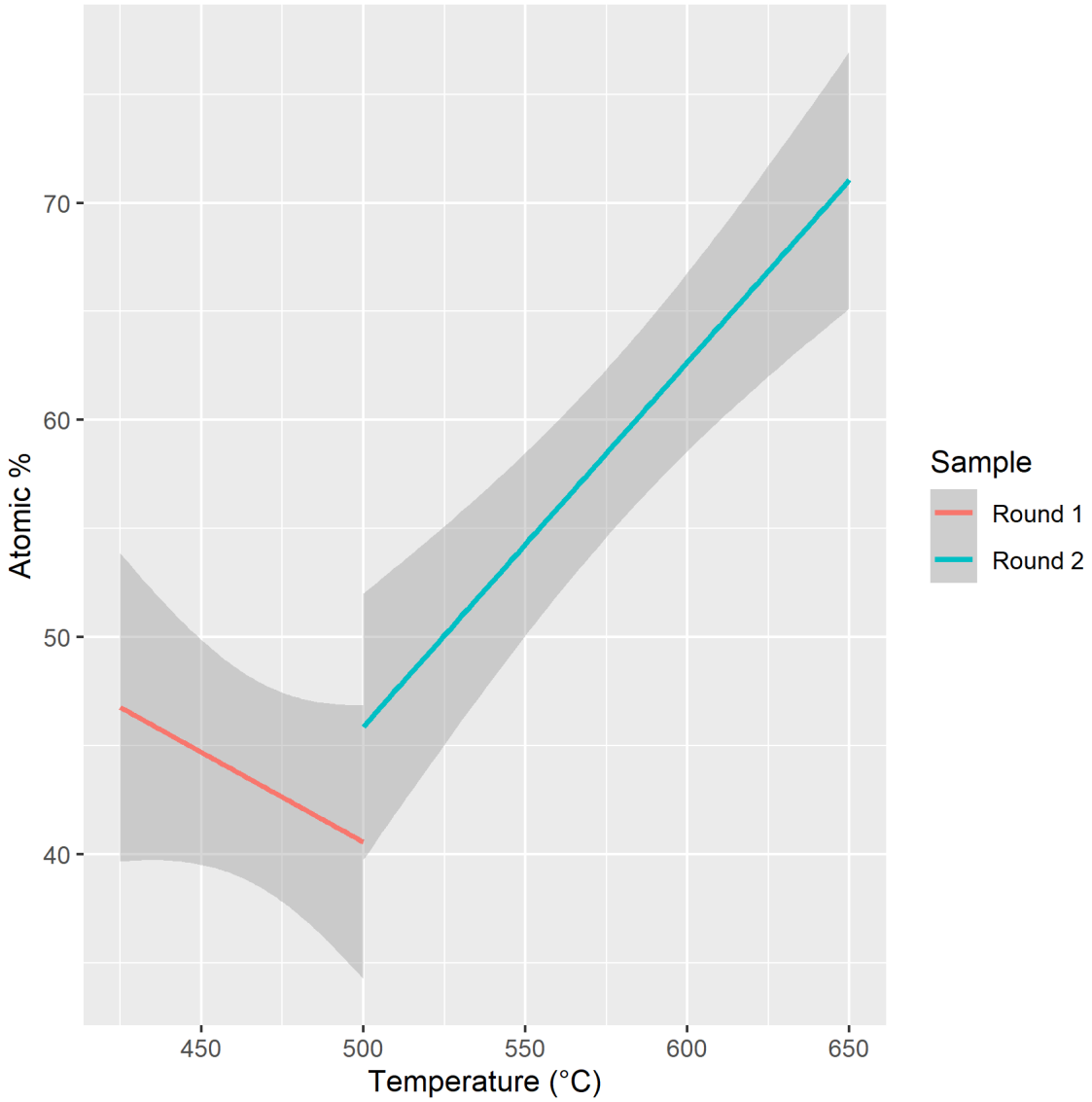


Figure B.2: Comparison of round 1 & round 2 Ti coating 0.5 - 0.6 $\mu$m thick, element O

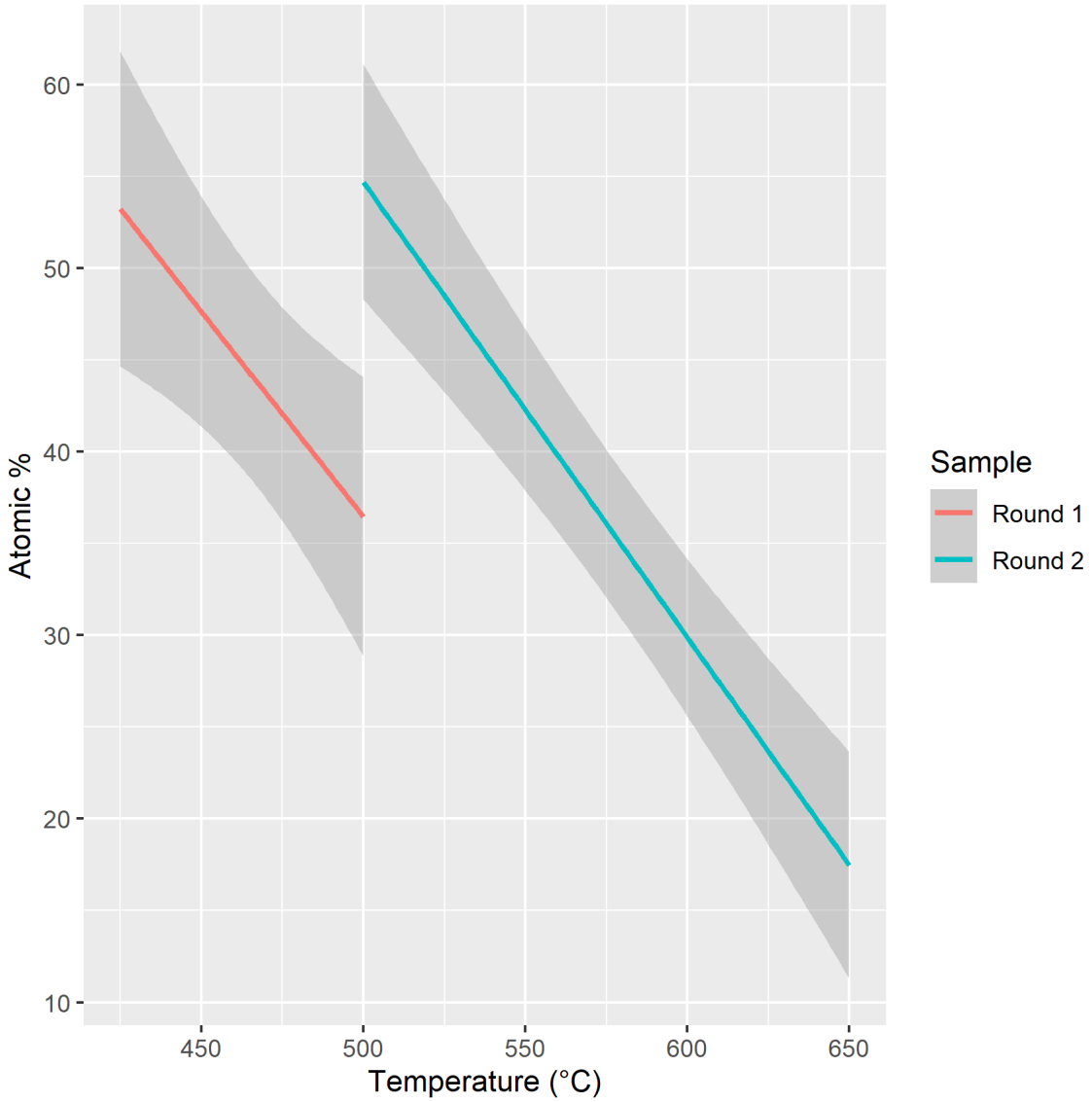


Figure B.3: Comparison of round 1 & round 2 Ti coating 0.5 - 0.6 $\mu$m thick, element Ti

## B.2 Comparison of Ti coating 1.0 - 1.5 $\mu$m Thick

The graphs of the Ti coating 1.0 - 1.5 $\mu$m thick are as follows.

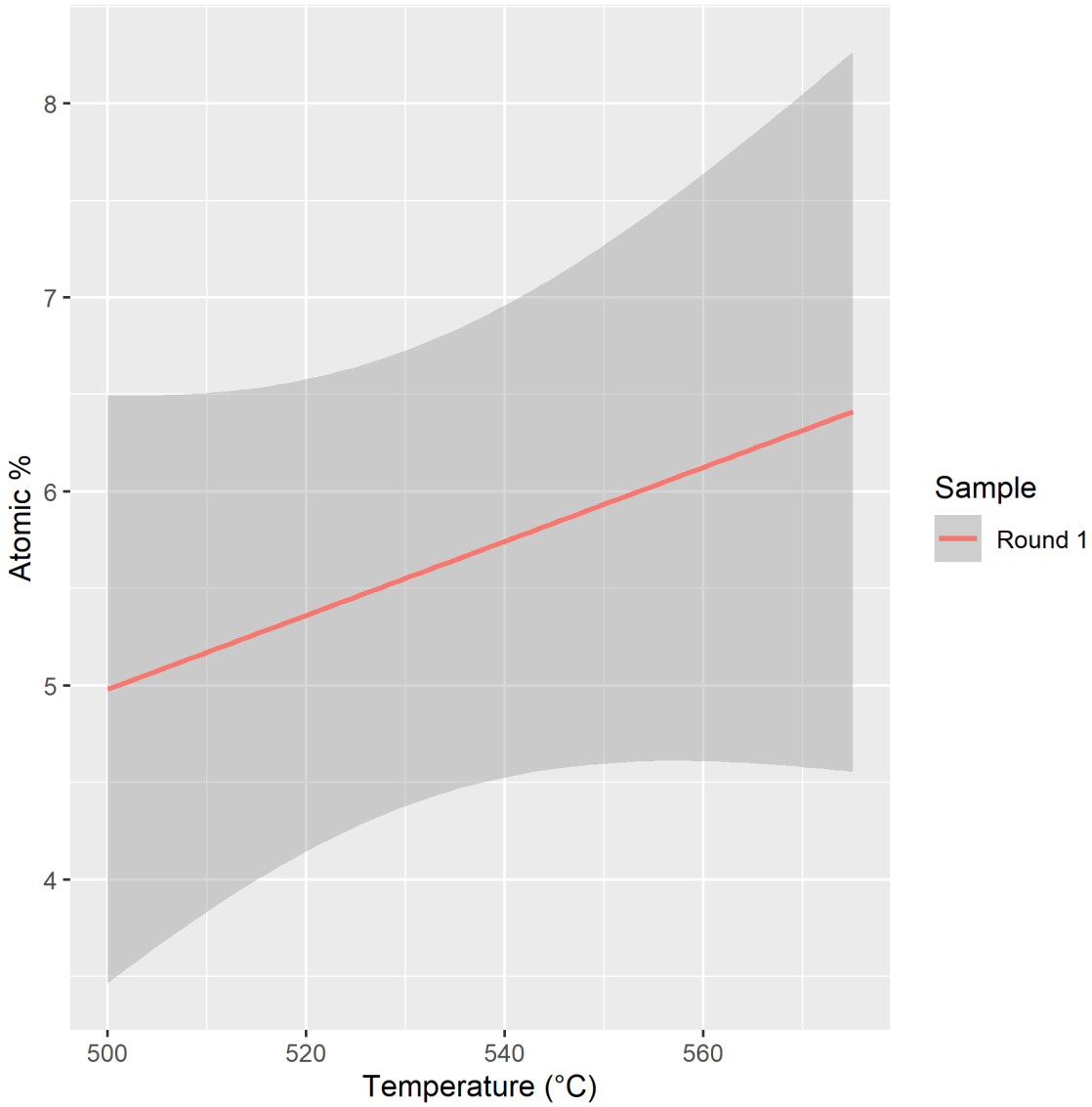


Figure B.4: Comparison of round 1 & round 2 Ti coating 1.0 - 1.5 $\mu$m thick, element C

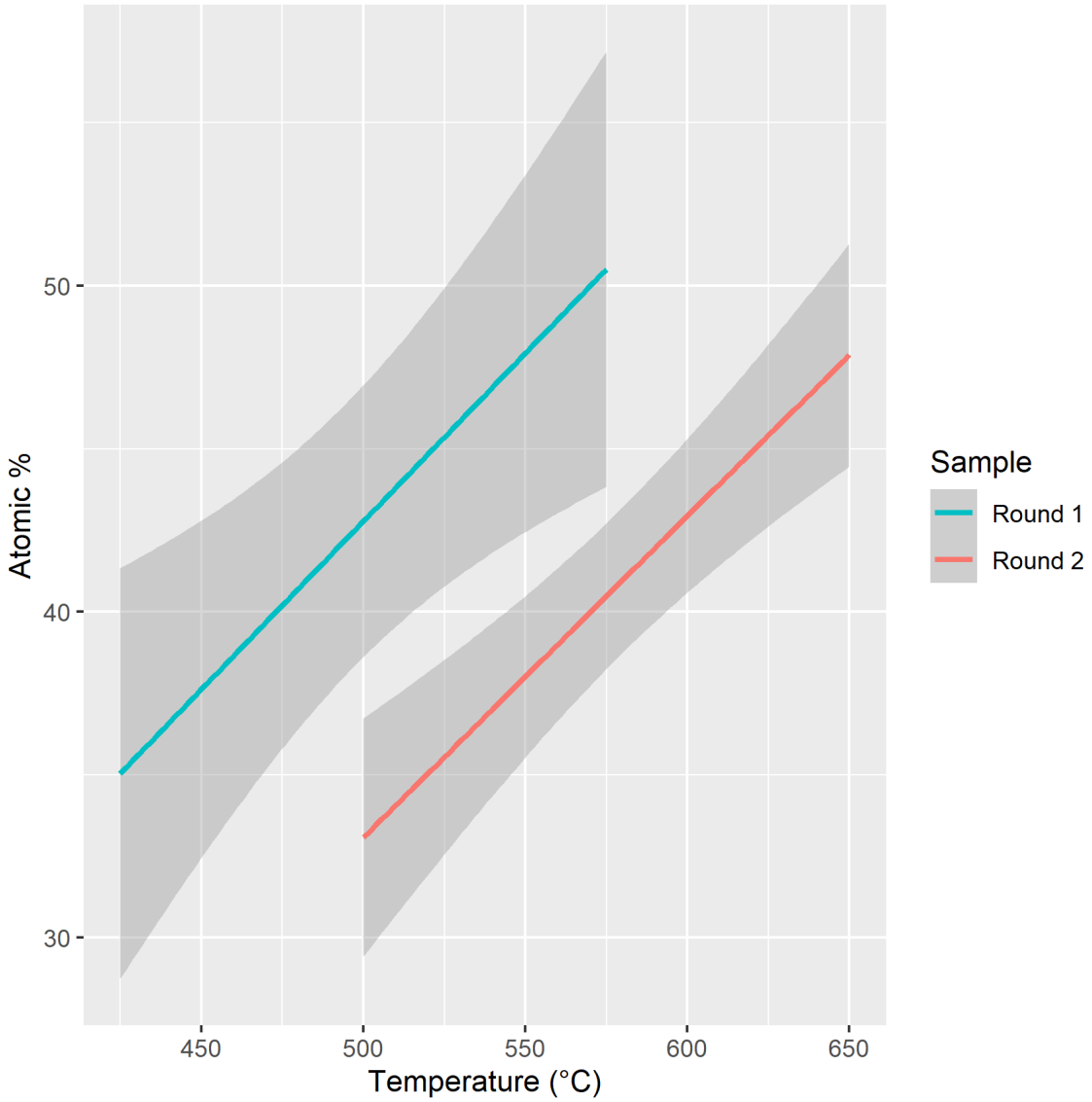


Figure B.5: Comparison of round 1 & round 2 Ti coating 1.0 - 1.5 $\mu$m thick, element O

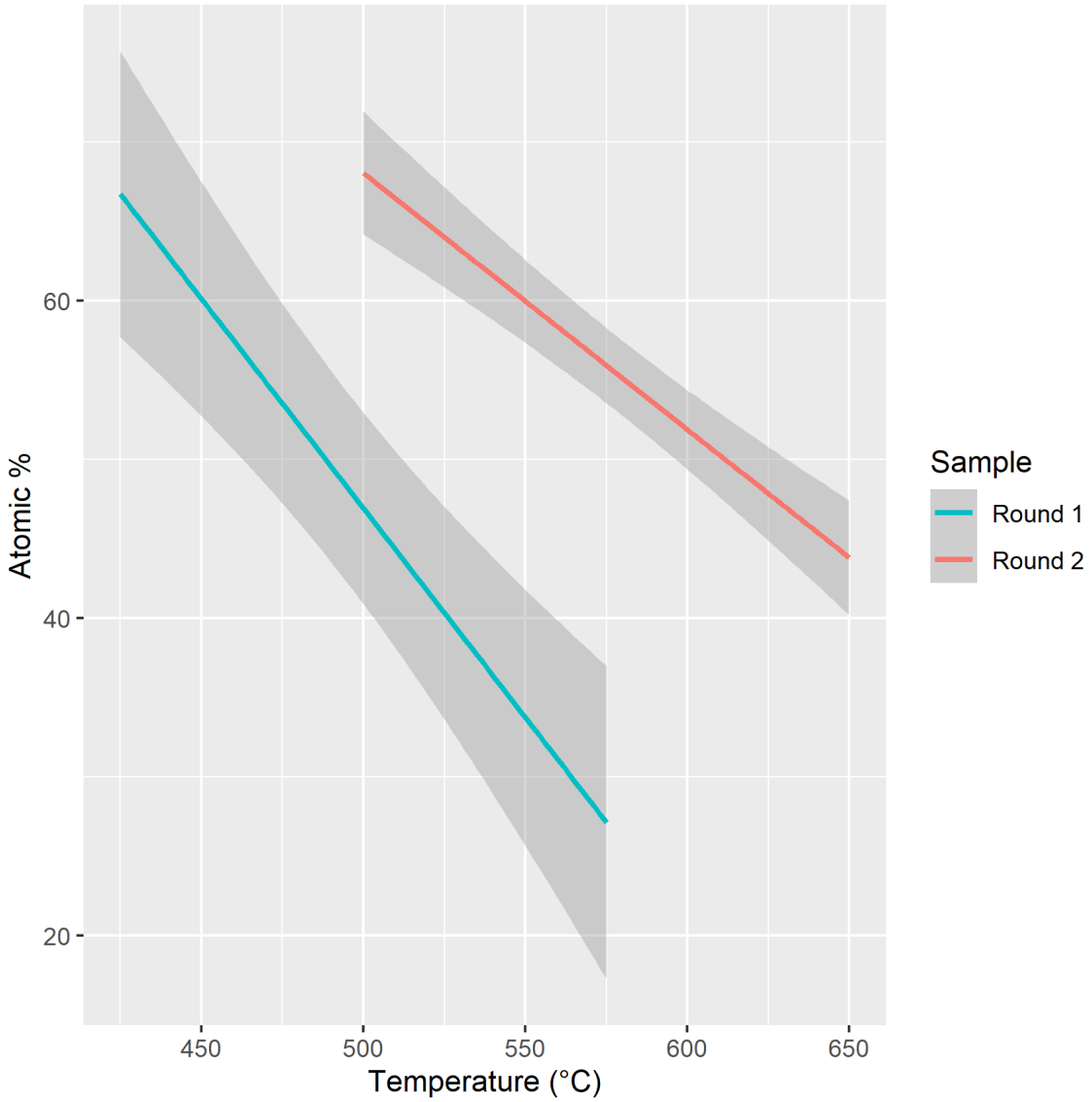


Figure B.6: Comparison of round 1 & round 2 Ti coating 1.0 - 1.5 $\mu$m thick, element Ti

## B.3 Comparison of TiAl 50:50 coating 1.0 - 1.5 $\mu$m Thick

Due to round 1 contamination of the TiAl 50:50 coating 1.0 - 1.5 $\mu$m thick, it is not possible to compare round 1 and round 2 results.

## B.4 Comparison of TiAl 40:60 coating 1.0 - 1.5 $\mu$m Thick

Due to round 1 contamination of the TiAl 40:60 coating 1.0 - 1.5 $\mu$m thick, it is not possible to compare round 1 and round 2 results.

## B.5 Round 1 & Round 2 Comparison Conclusion

For the elements and types where there is data across at least 2 temperatures, what was found is that round 1 and round 2 results do not have the same atomic % at temperatures that they overlapped. Furthermore, the slopes of the lines are not parallel as well. From this it can be concluded that round 1 and round 2 are separate data sets and can't be used together. Additionally, it also seems to indicate that there was more going on at 425°C than was originally thought.

# Appendix C

# Comparison of Topological Features

The purpose of the type comparison is to see if there are differences in the elemental composition of the features of the surface, and also whether that composition changes with temperature. This analysis will only look at round 2 results, where the data will be separated by coating, and then by the elements, only looking at Ti, O, and Al for the TiAl coatings. Box plots were created to compare the types for a specific temperature, and then a line graph over all the temperatures to see the variation by temperature and the trend with temperature change.

## C.1 Comparison of Ti Coating 0.5 - 0.6 $\mu$m Thick

For the Ti coating 0.5 - 0.6 $\mu$m thick, the SEM images were examined for general consistent features and then divided into general features. An example of how that is performed can be seen by comparing figure C.7 and table C.1, which shows the

breakdown at 500°C. This is performed at 575°C and 650°C as well, which are then graphed in box plots in figures C.8 to C.10 and analysed via linear regression in figure C.11.

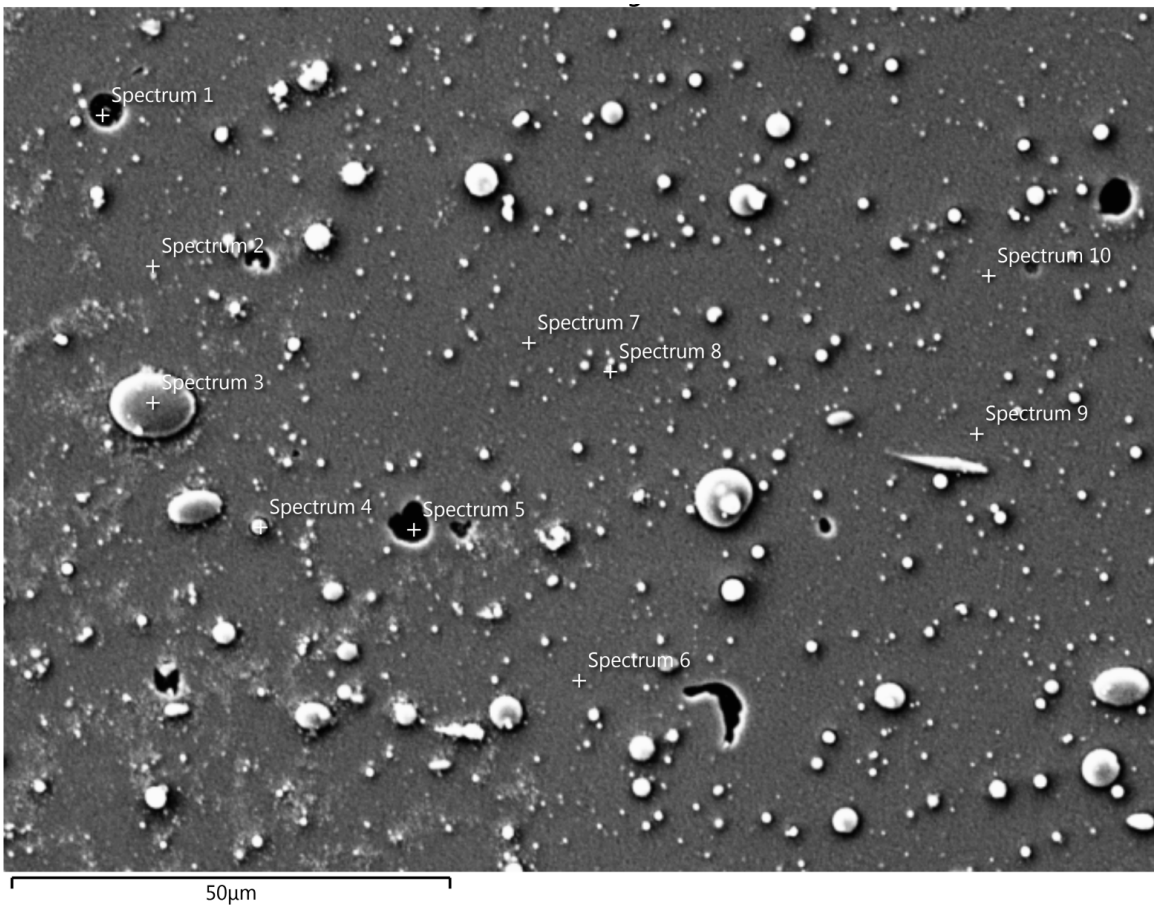


Figure C.7: Ti coating 0.5 - 0.6 $\mu$m thick at 500°C EDS locations

Table C.1: Ti coating 0.5 - 0.6 $\mu$m thick at 500°C topology

| **Feature No.** | **Feature Type** | **Spectrum** |
|---|---|---|
| 1 | Coating | 2, 6, 7, 9, 10 |
| 2 | Holes | 1, 5, 8 |
| 3 | Surface Drops | 3, 4 |

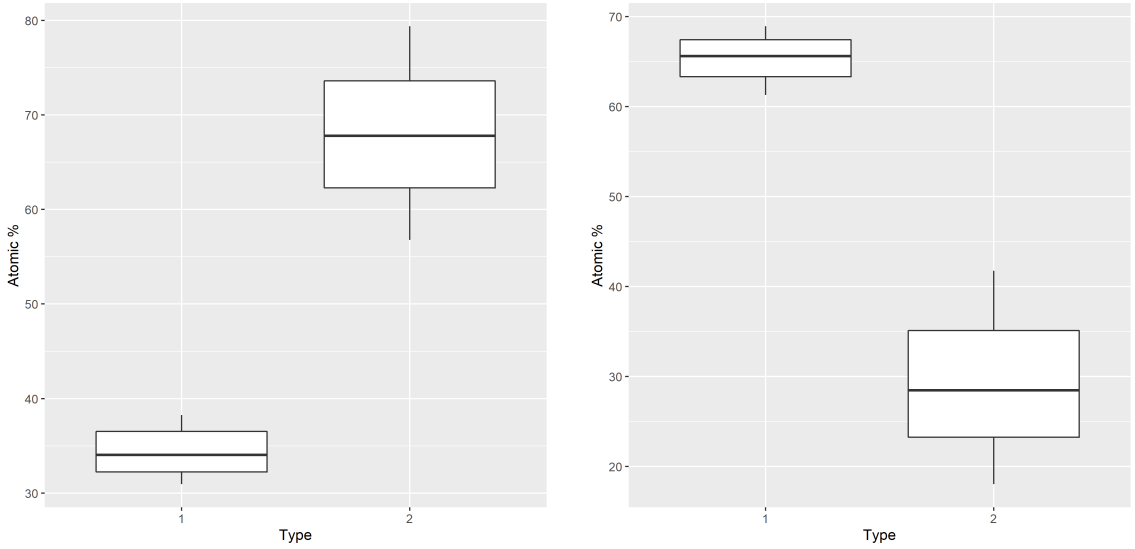


(a) O boxplot (b) Ti boxplot

Figure C.8: Ti coating 0.5 - 0.6 $\mu$m thick at 500°C boxplot type comparison

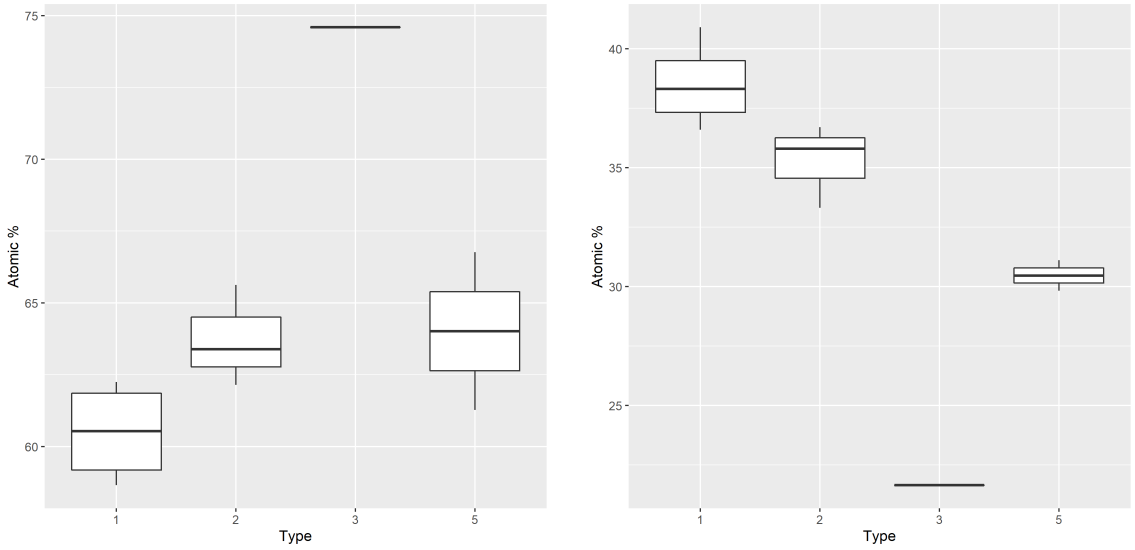


(a) O boxplot (b) Ti boxplot

Figure C.9: Ti coating 0.5 - 0.6 $\mu$m thick at 575°C boxplot type comparison

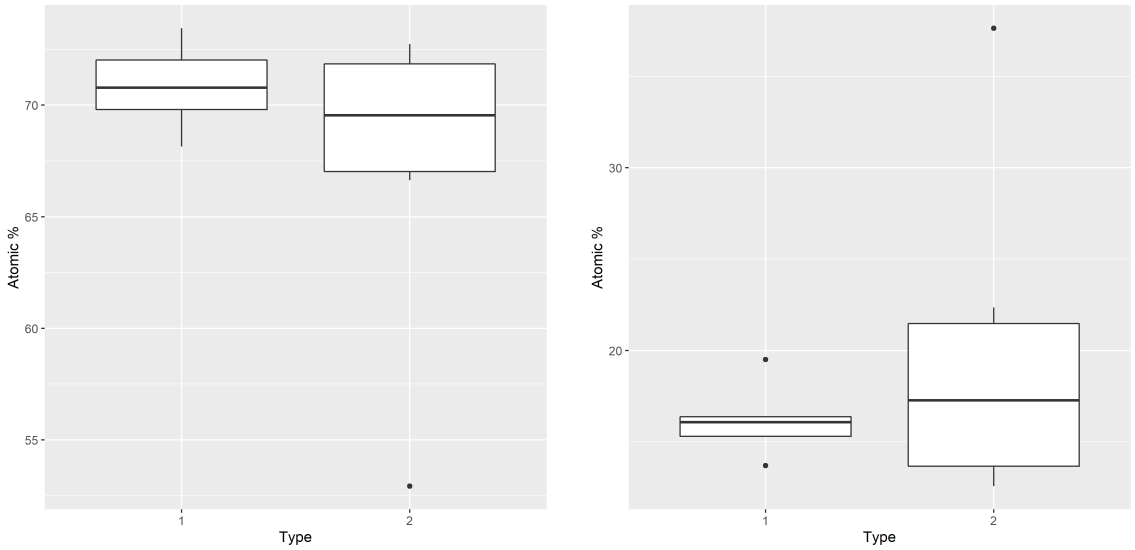


(a) O boxplot (b) Ti boxplot

Figure C.10: Ti coating 0.5 - 0.6 $\mu$m thick at 650°C boxplot type comparison

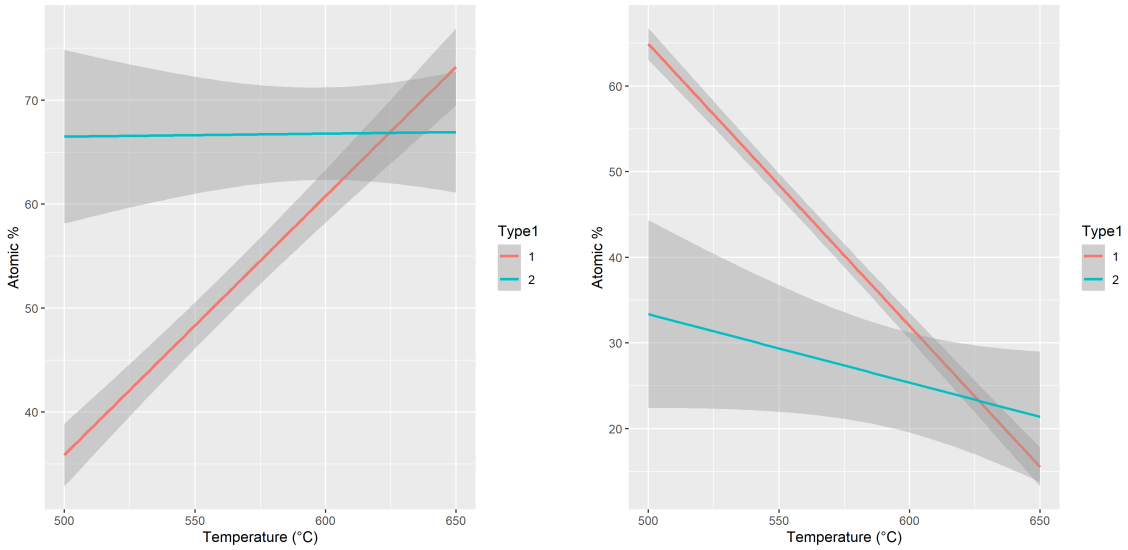


(a) O (b) Ti

Figure C.11: Ti coating 0.5 - 0.6 $\mu$m thick linear regression type comparison

## C.2 Comparison of Ti coating 1.0 - 1.5 $\mu$m Thick

For the Ti coating 1.0 - 1.5 $\mu$m thick, the SEM images were examined for general consistent features and then divided into general features. An example of how that is performed can be seen by comparing figure C.12 and table C.2, which shows the breakdown at 500°C. This is performed at 575°C and 650°C as well, which are then graphed in box plots in figures C.13 to C.15 and analysed via linear regression in figure C.16.


Figure C.12: Ti coating 1.0 - 1.5 $\mu$m thick at 500°C EDS locations

Table C.2: Ti coating 1.0 - 1.5 $\mu$m thick at 500°C topology

| **Feature No.** | **Feature Type** | **Spectrum** |
|---|---|---|
| 1 | Coating | 33, 36, 38, 40, 42 |
| 2 | Small Drops | 34, 39, 41 |
| 3 | Large Drops | 35, 37 |
| 4 | Holes | 32 |

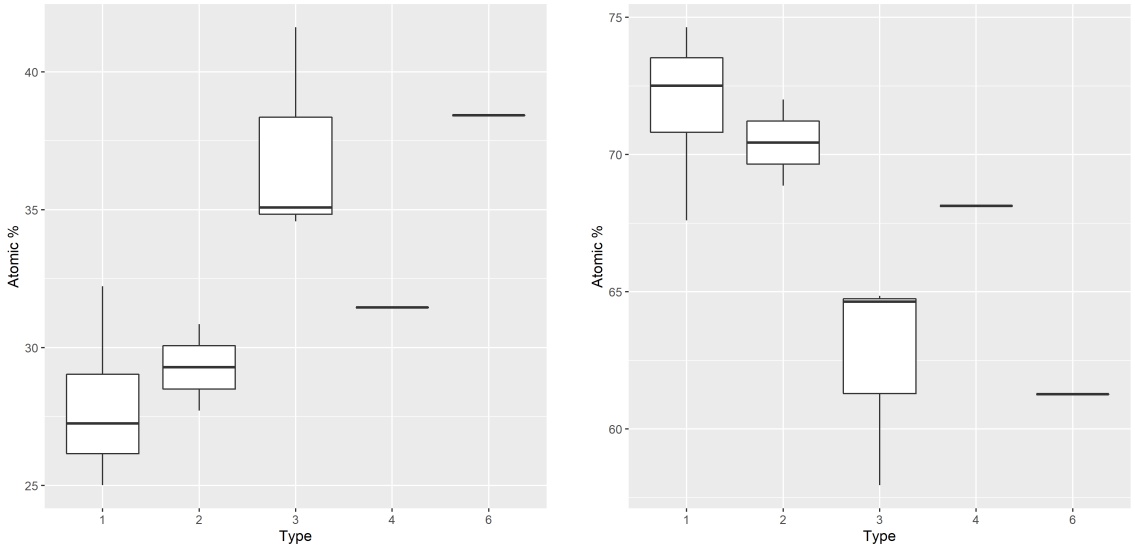


(a) O boxplot (b) Ti boxplot

Figure C.13: Ti coating 1.0 - 1.5 $\mu$m thick at 500°C boxplot type comparison

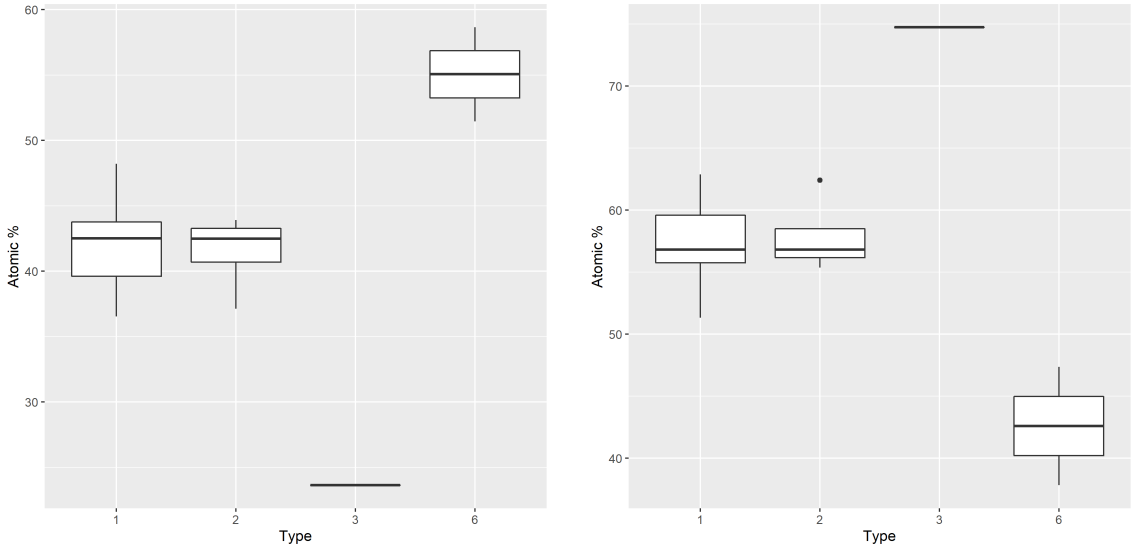


(a) O boxplot (b) Ti boxplot

Figure C.14: Ti coating 1.0 - 1.5 $\mu$m thick at 575°C boxplot type comparison

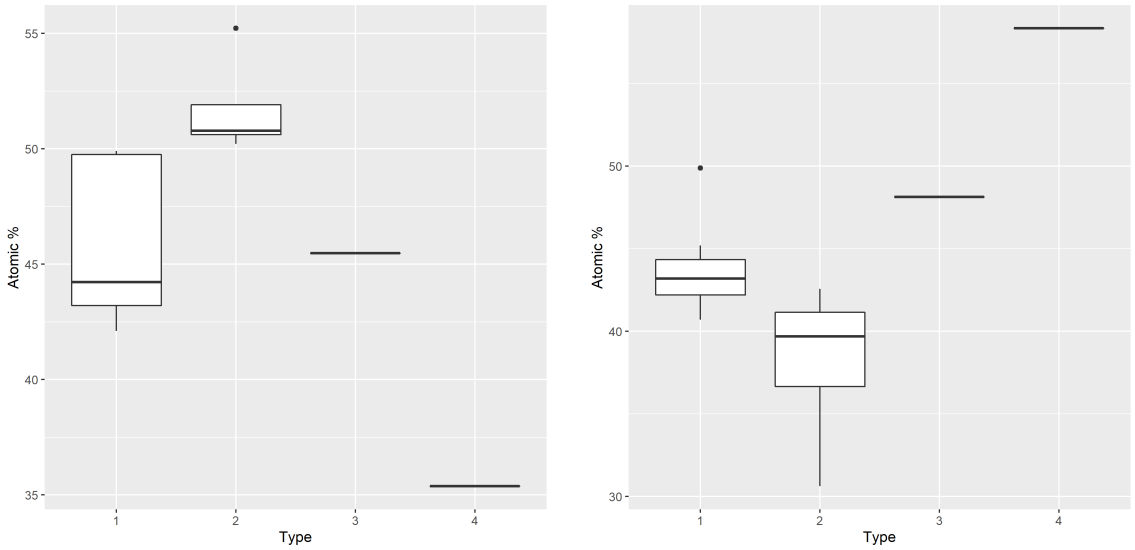


(a) O boxplot (b) Ti boxplot

Figure C.15: Ti coating 1.0 - 1.5 $\mu$m thick at 650°C boxplot type comparison

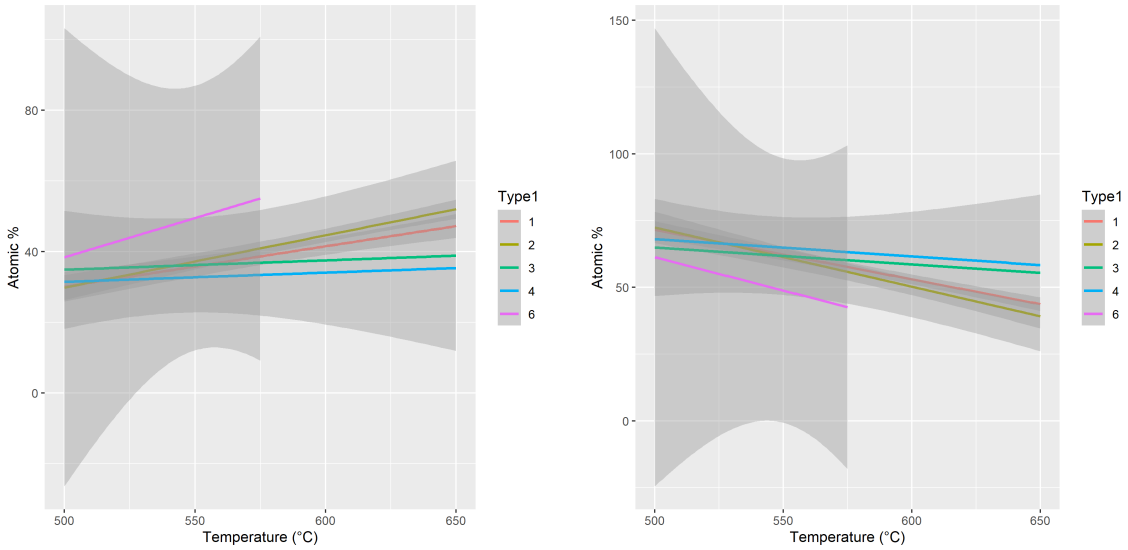


(a) O (b) Ti

Figure C.16: Ti coating 1.0 - 1.5 $\mu$m thick linear regression type comparison

## C.3 Comparison of TiAl 50:50 coating 1.0 - 1.5 $\mu$m Thick

For the TiAl 50:50 coating 1.0 - 1.5 $\mu$m thick, the SEM images were examined for general consistent features and then divided into general features. An example of how that is performed can be seen by comparing figure C.17 and table C.3, which shows the breakdown at 500°C. In comparison to the titanium only coatings, there are a lot more droplet like features on the surface, which also tend to be smaller, opposed to the larger, but less frequent droplet features in the titanium coatings. The breakdown of the features is also performed at 575°C and 650°C, which are then graphed in box plots in figures C.18 to C.20 and analysed via linear regression in figure C.21.

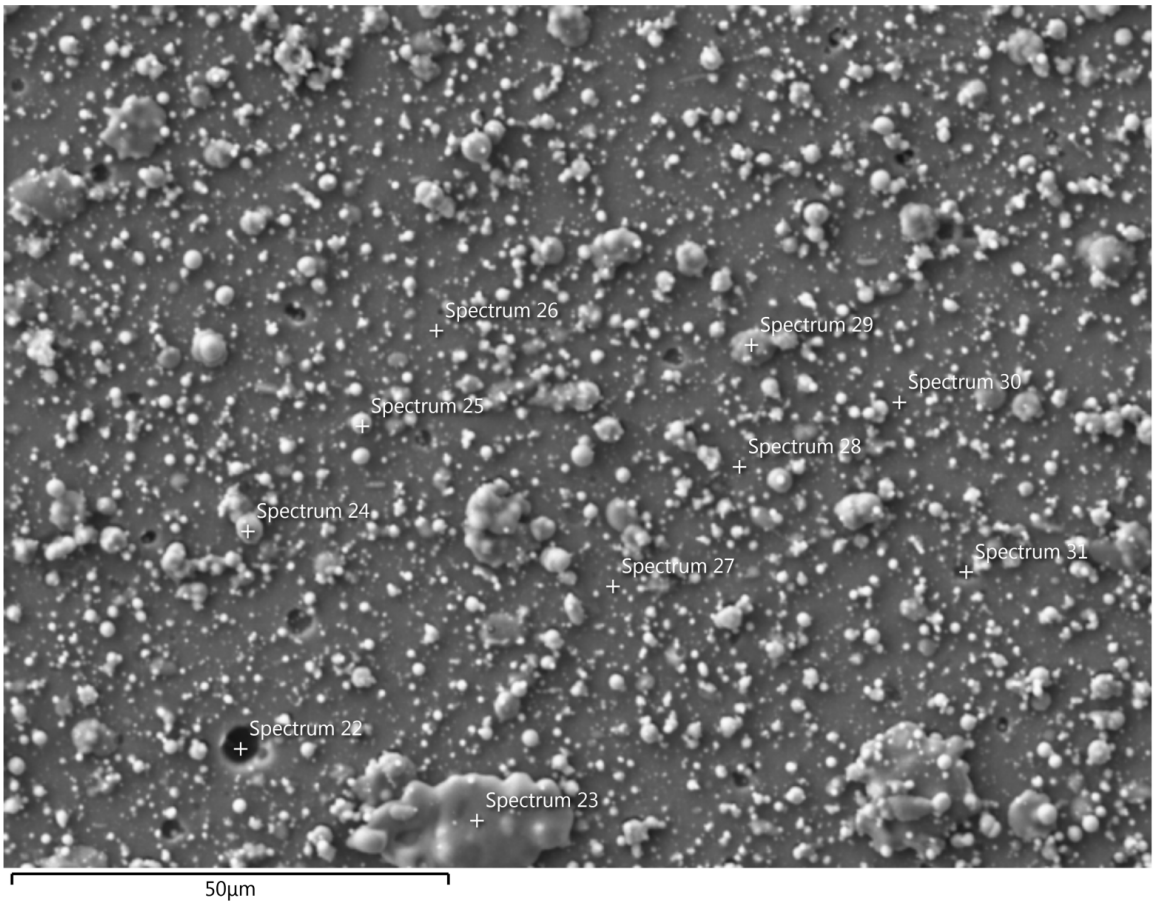


Figure C.17: TiAl 50:50 coating 1.0 - 1.5 $\mu$m thick at 500°C EDS locations

Table C.3: TiAl 50:50 coating 1.0 - 1.5 $\mu$m thick at 500°C topology

| **Feature No.** | **Feature Type** | **Spectrum** |
|---|---|---|
| 1 | Coating | 26, 27, 28, 30 |
| 2 | Small Drops | 24, 25, 29 |
| 3 | Large Drops | 23 |
| 4 | Holes | 22, 31 |

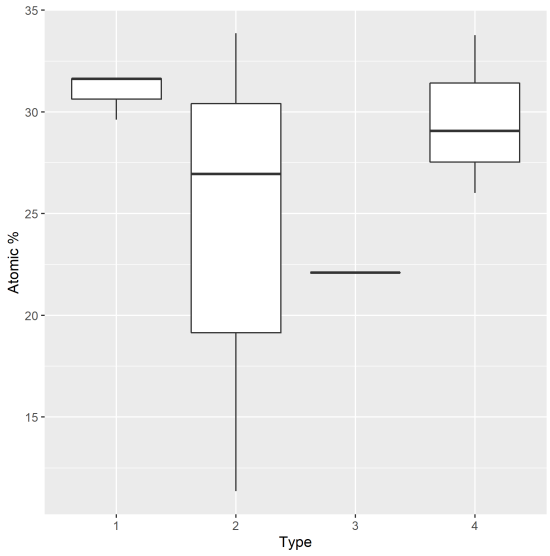


(a) Al boxplot

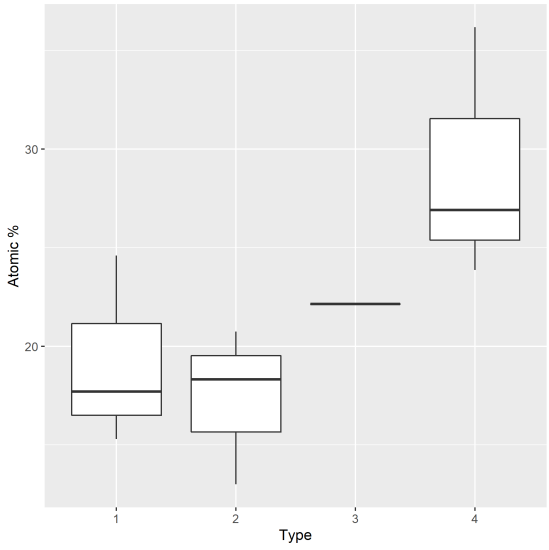


(b) O boxplot

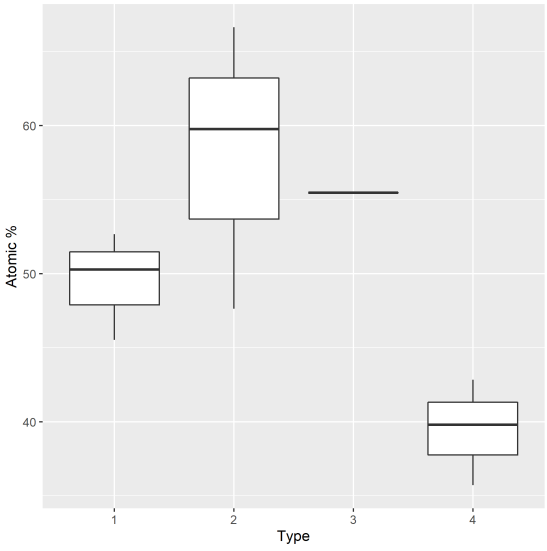


(c) Ti boxplot

Figure C.18: TiAl 50:50 coating 1.0 - 1.5 $\mu$m thick at 500°C boxplot type comparison

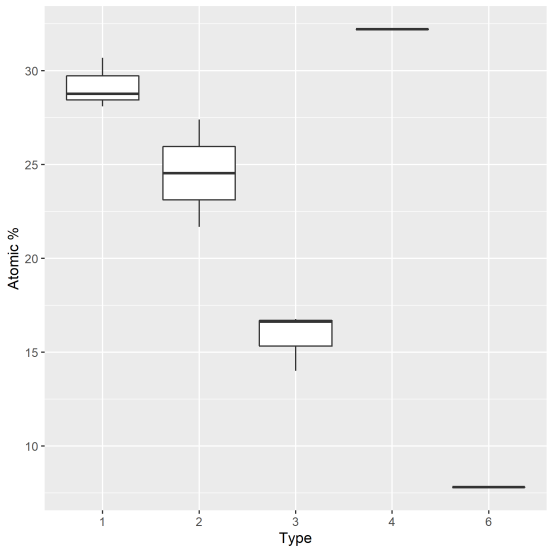


(a) Al boxplot

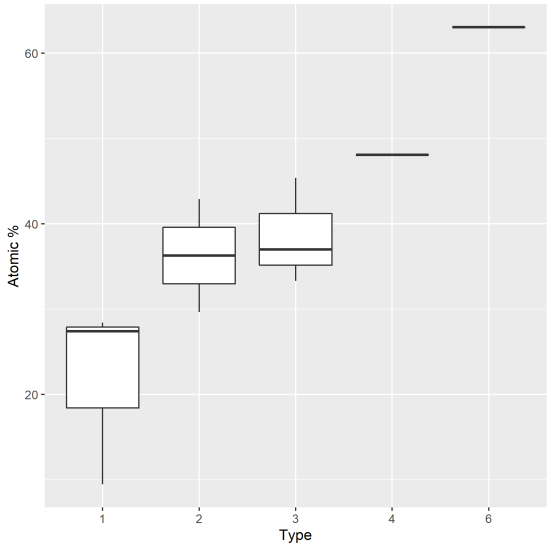


(b) O boxplot

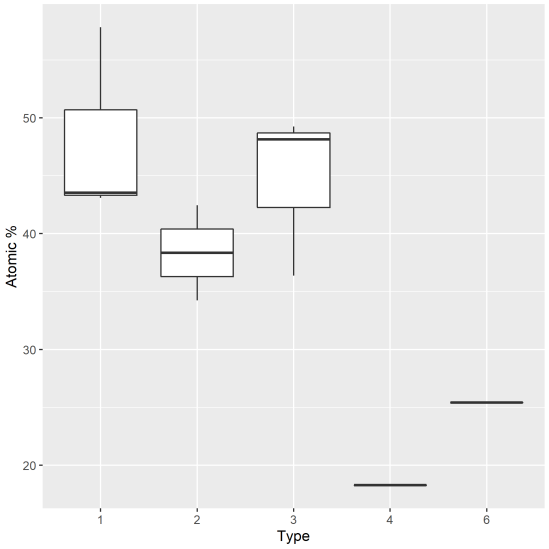


(c) Ti boxplot

Figure C.19: TiAl 50:50 coating 1.0 - 1.5 $\mu$m thick at 575°C boxplot type comparison

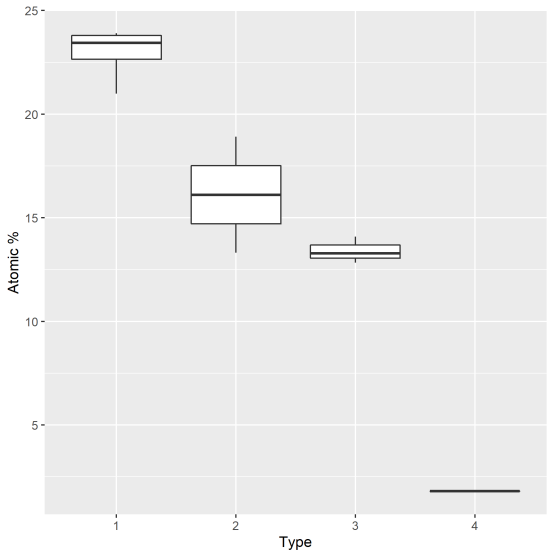


(a) Al boxplot

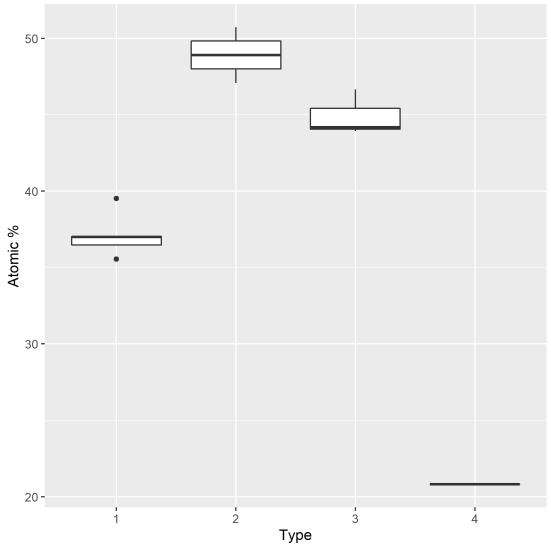


(b) O boxplot

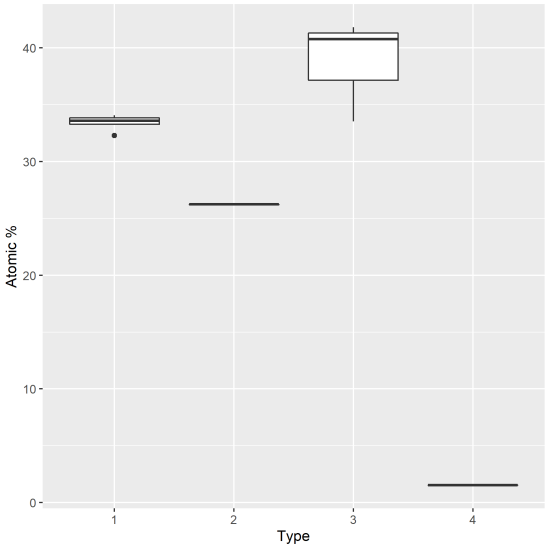


(c) Ti boxplot

Figure C.20: TiAl 50:50 coating 1.0 - 1.5 $\mu$m thick at 650°C boxplot type comparison

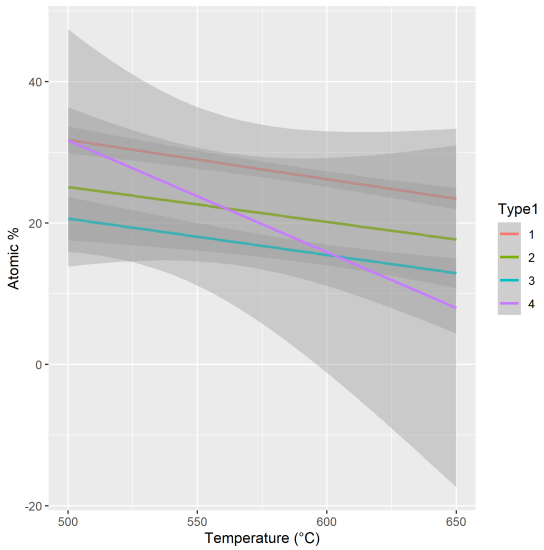


(a) Al

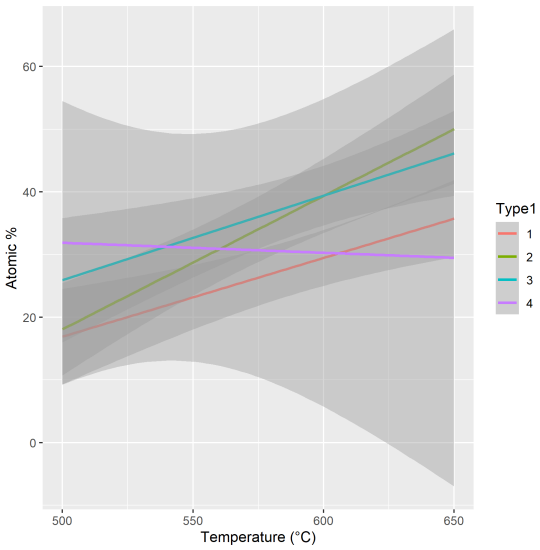


(b) O

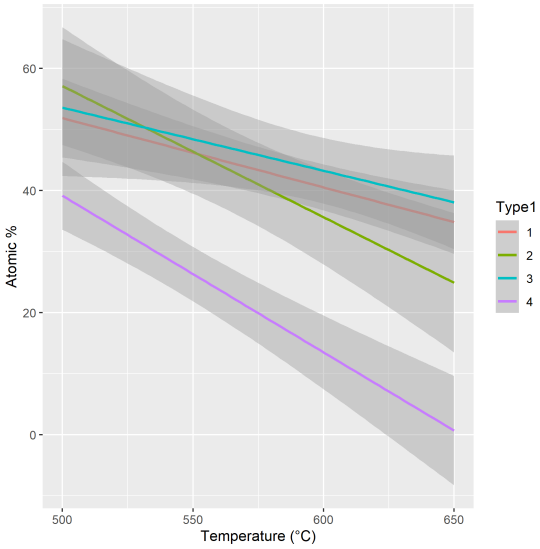


(c) Ti

Figure C.21: TiAl 50:50 coating 1.0 - 1.5 $\mu$m thick linear regression type comparison

## C.4 Comparison of TiAl 40:60 coating 1.0 - 1.5 $\mu$m Thick

For the TiAl 40:60 coating 1.0 - 1.5 $\mu$m thick, the SEM images were examined for general consistent features and then divided into general features. An example of how that is performed can be seen by comparing figure C.22 and table C.4, which shows the breakdown at 500°C. This is performed at 575°C and 650°C as well, which are then graphed in box plots in figures C.23 to C.25 and analysed via linear regression in figure C.26.

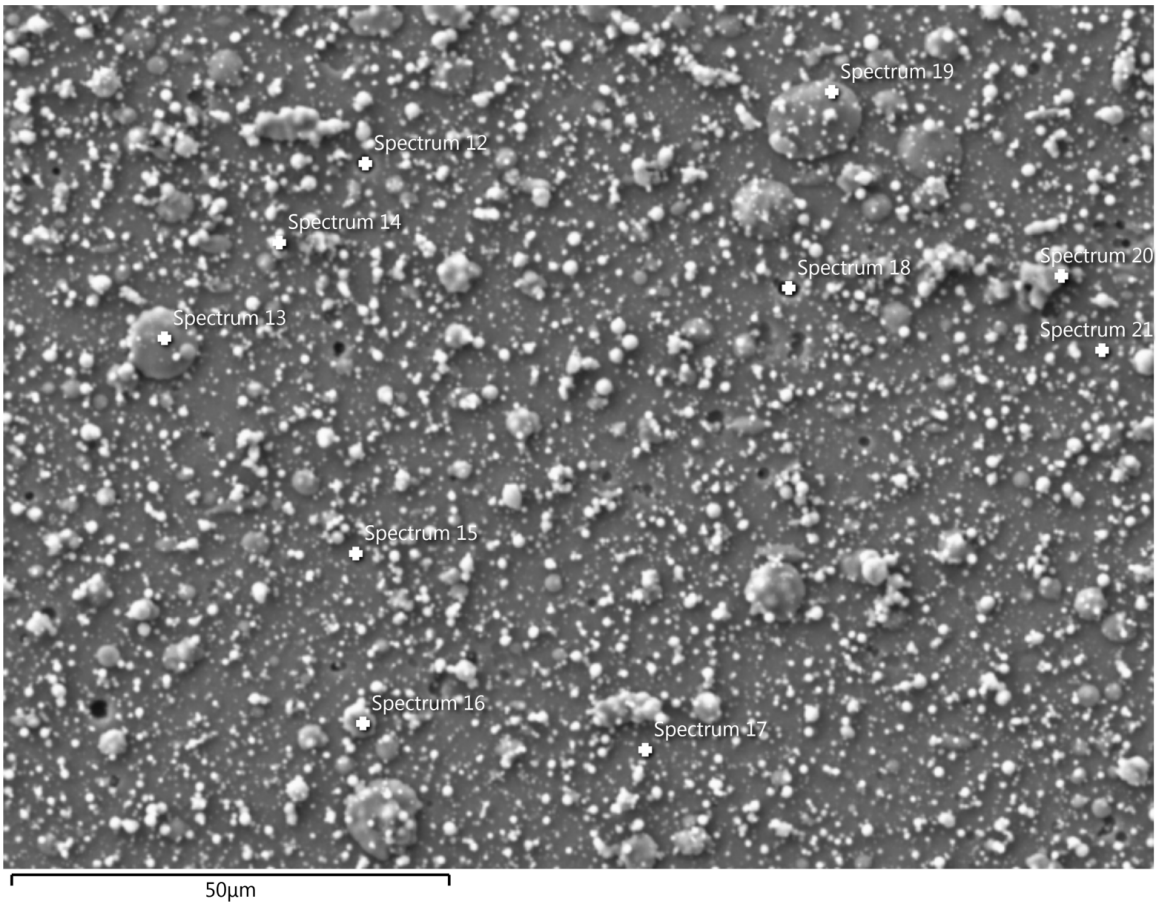


Figure C.22: TiAl 40:60 coating 1.0 - 1.5 $\mu$m thick at 500°C EDS locations

Table C.4: TiAl 40:60 coating 1.0 - 1.5 $\mu$m thick at 500°C topology

| **Feature No.** | **Feature Type** | **Spectrum** |
|---|---|---|
| 1 | Coating | 15, 17, 21 |
| 2 | Small Drops | 14, 16 |
| 3 | Large Drops | 13, 19, 20 |
| 4 | Holes | 12, 18 |

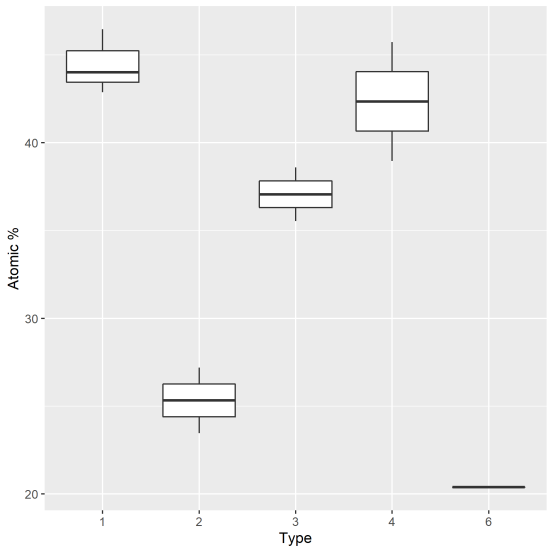


(a) Al boxplot

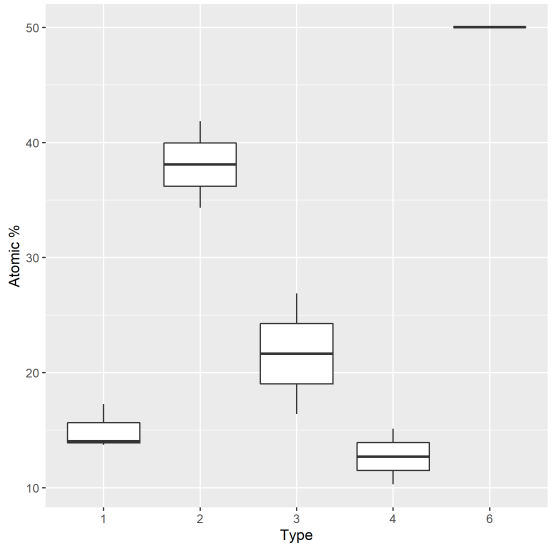


(b) O boxplot

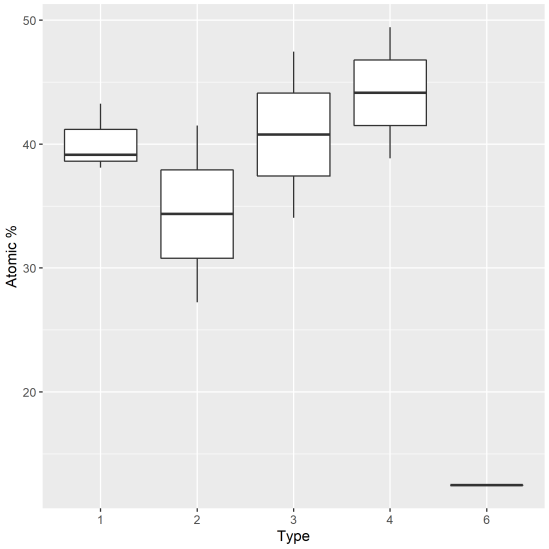


(c) Ti boxplot

Figure C.23: TiAl 40:60 coating 1.0 - 1.5 $\mu$m thick at 500°C boxplot type comparison

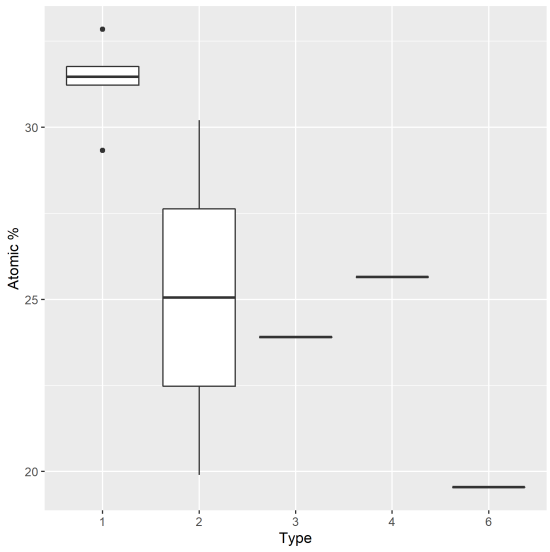


(a) Al boxplot

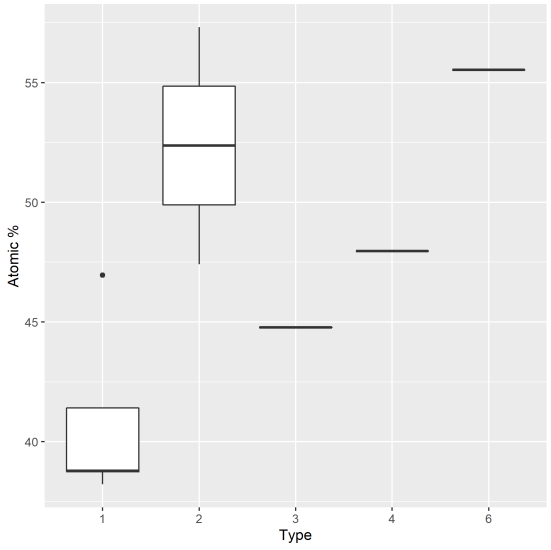


(b) O boxplot

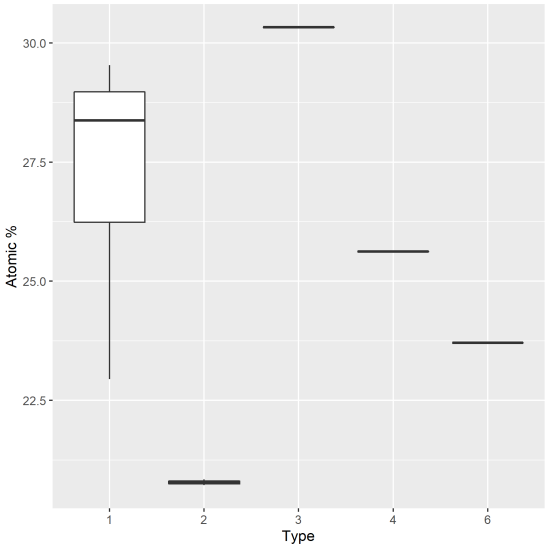


(c) Ti boxplot

Figure C.24: TiAl 40:60 coating 1.0 - 1.5 $\mu$m thick at 575°C boxplot type comparison

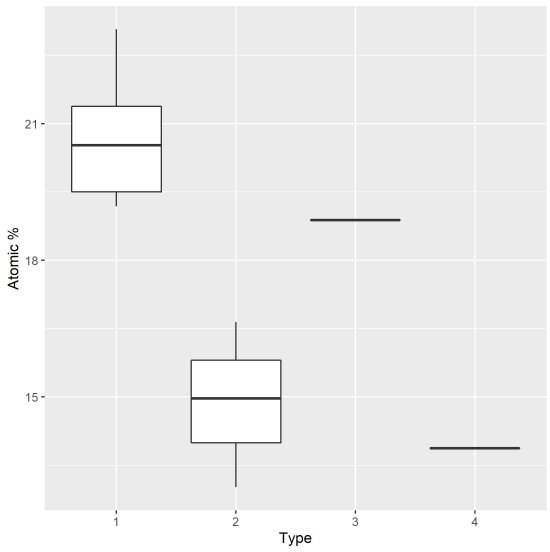


(a) Al boxplot

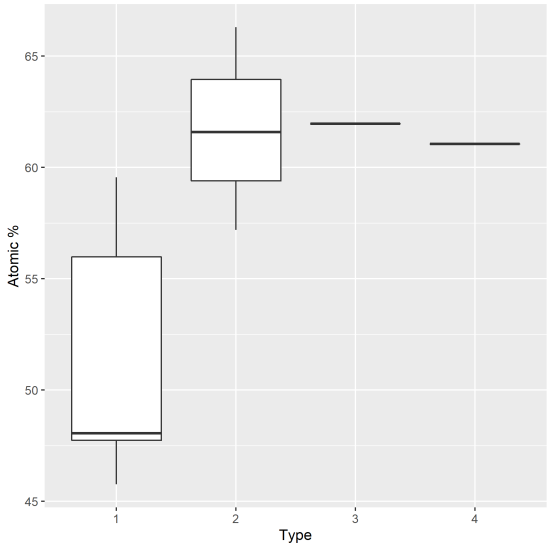


(b) O boxplot

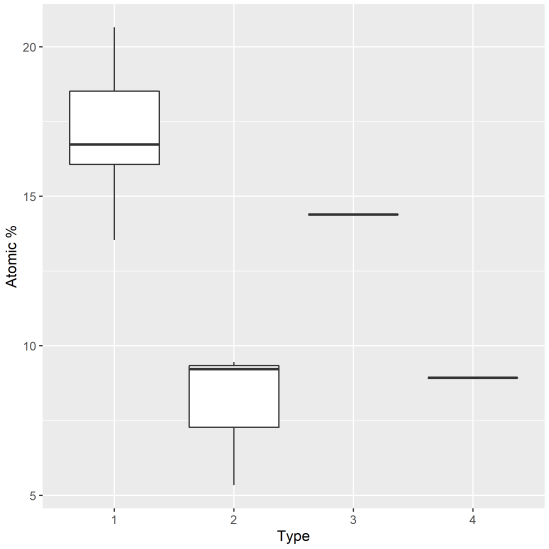


(c) Ti boxplot

Figure C.25: TiAl 40:60 coating 1.0 - 1.5 $\mu$m thick at 650°C boxplot type comparison

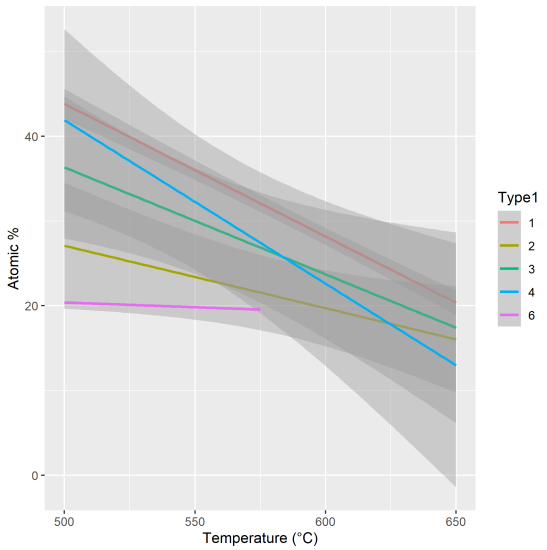


(a) Al

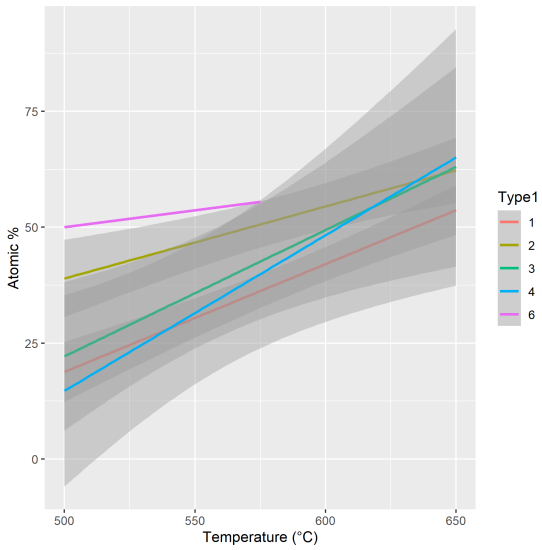


(b) O

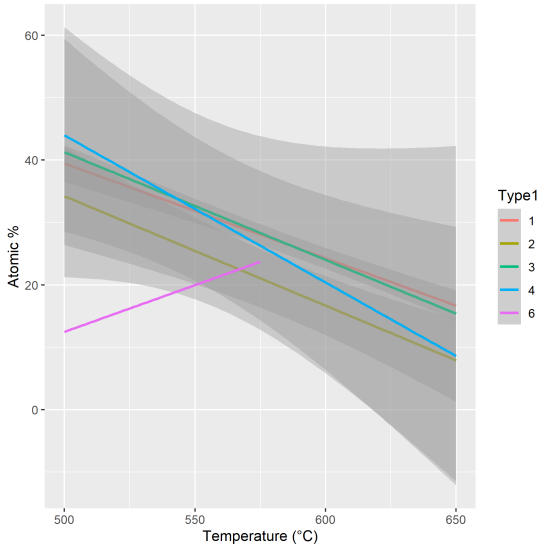


(c) Ti

Figure C.26: TiAl 40:60 coating 1.0 - 1.5 $\mu$m thick linear regression type comparison

## C.5 Conclusion to Comparison of Types

From the analysis of the elements present in the different features of the surface based on the SEM images, there are a couple conclusions. First, the variation is similar between the different features of the surface. Second, the average element concentration per element type is comparable between different features. It can therefore be concluded that in spite of visual difference of the surface, there is not enough variation between the features in terms of element concentration to merit their separation.

# Appendix D

# EDS Maps

The EDS maps are located here for reference.

## D.1 EDS Maps for Ti Only 0.5 - 0.6 $\mu$m Thick

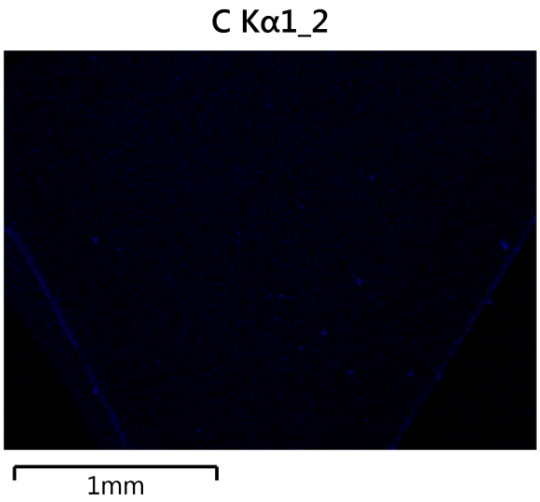


(a) C map

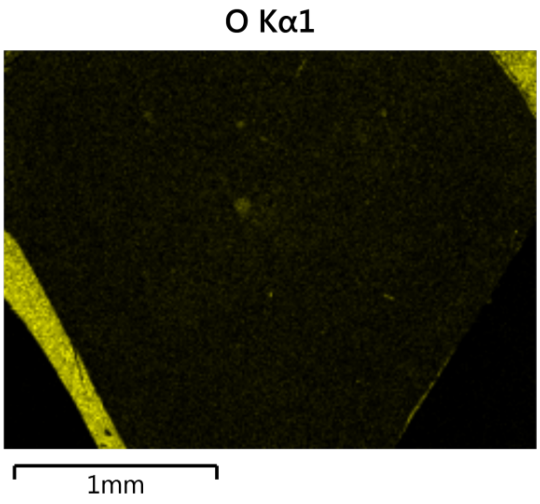


(b) O map

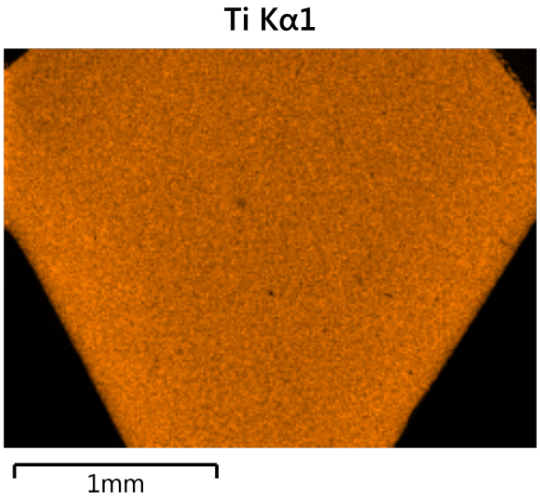


(c) Ti map

Figure D.27: Ti coating 0.5 - 0.6 $\mu$m thick at 500°C EDS element map analysis

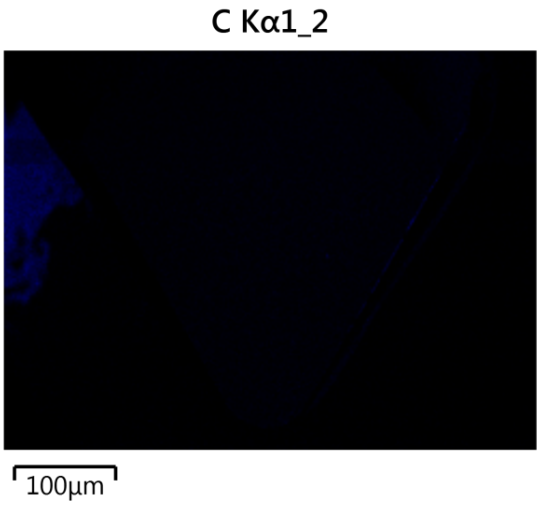


(a) C map

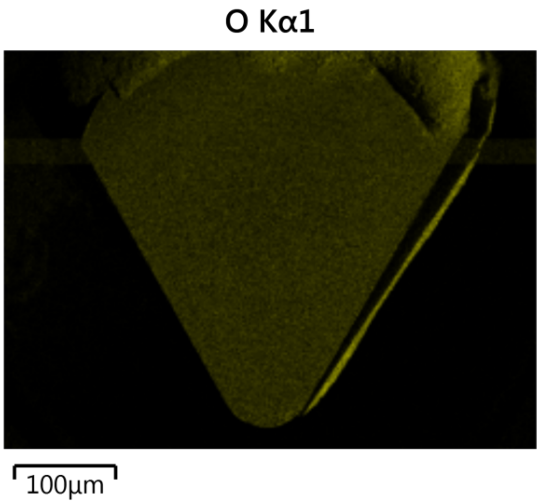


(b) O map

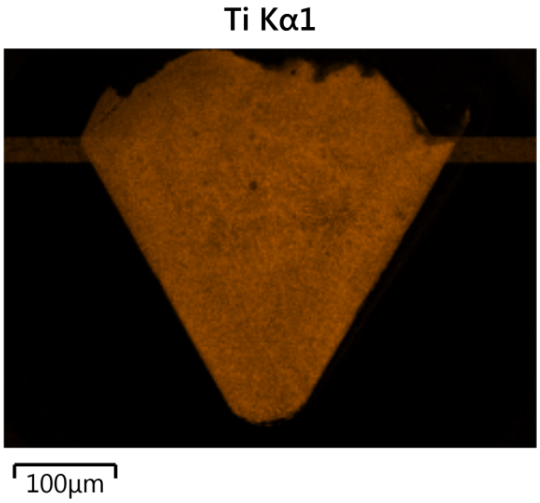


(c) Ti map

Figure D.28: Ti coating 0.5 - 0.6 $\mu$m thick at 575°C EDS element map analysis

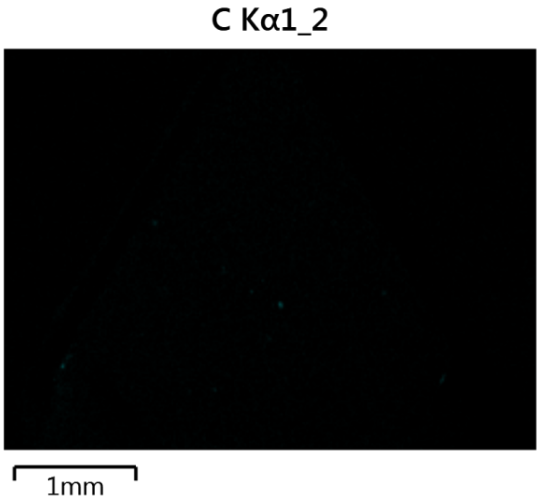


(a) C map

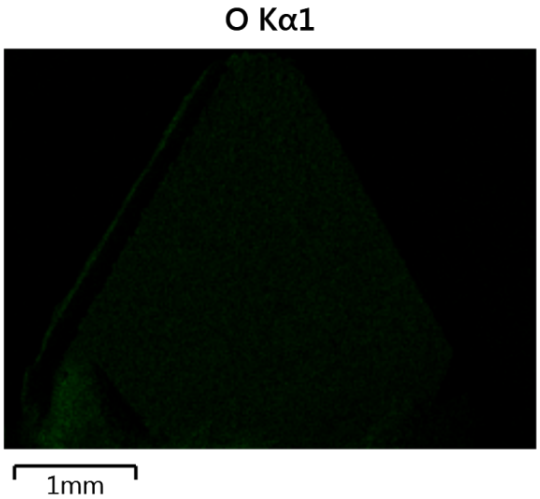


(b) O map

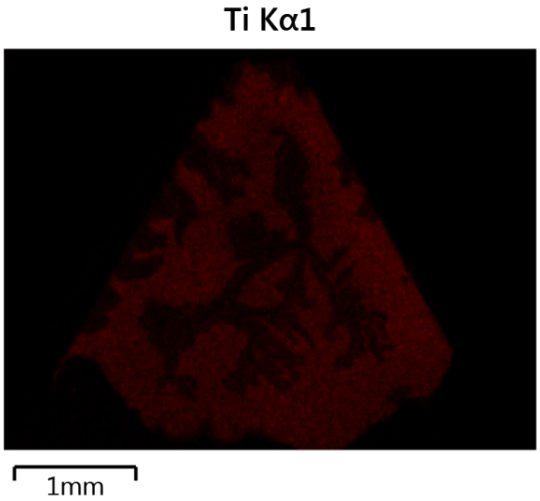


(c) Ti map

Figure D.29: Ti coating 0.5 - 0.6 $\mu$m thick at 650°C EDS element map analysis

## D.2 EDS Maps for Ti Only 1.0 - 1.5 $\mu$m Thick

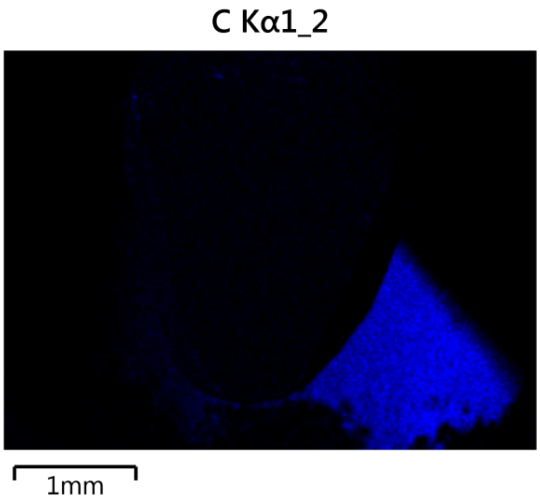


(a) C map

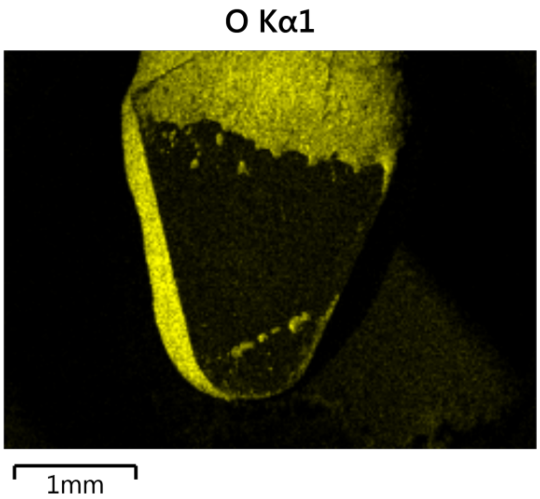


(b) O map

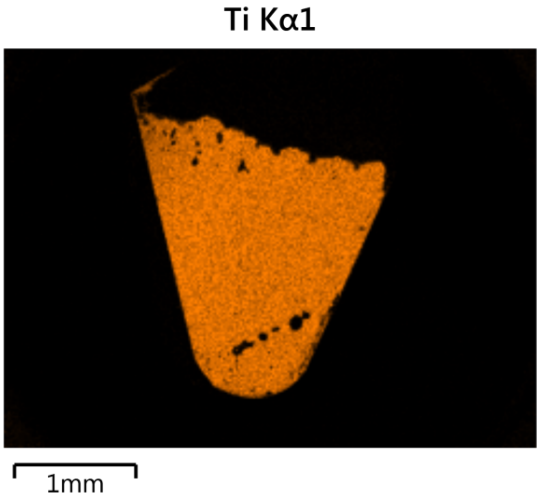


(c) Ti map

Figure D.30: Ti coating 1.0 - 1.5 $\mu$m thick at 500°C EDS element map analysis

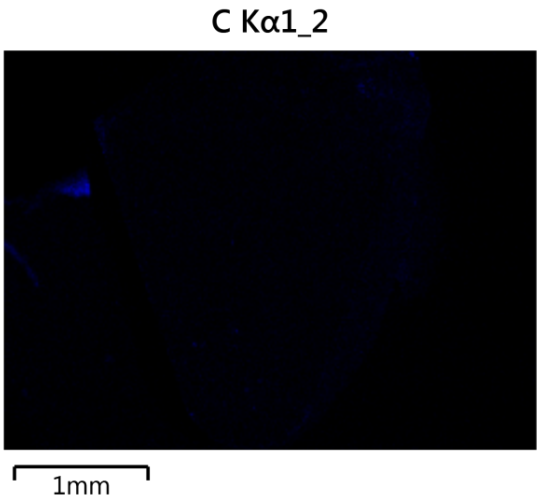


(a) C map

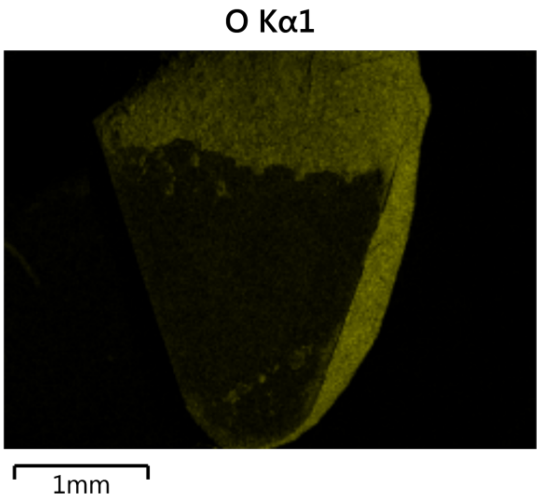


(b) O map

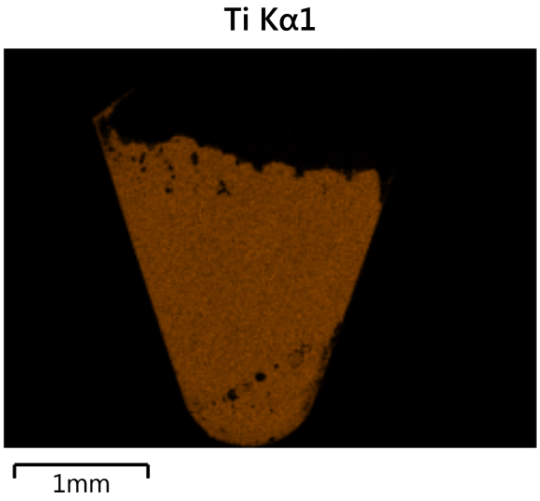


(c) Ti map

Figure D.31: Ti coating 1.0 - 1.5 $\mu$m thick at 575°C EDS element map analysis

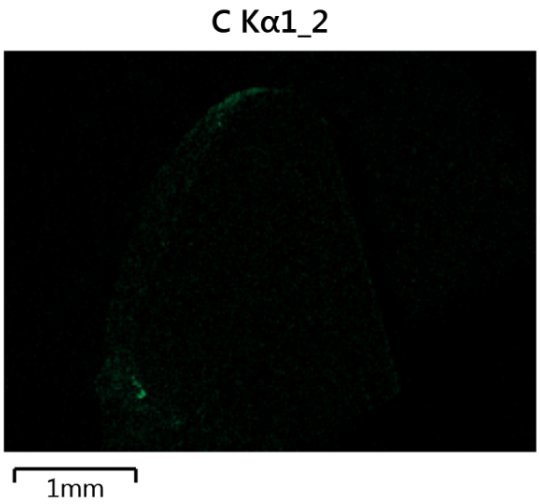


(a) C map

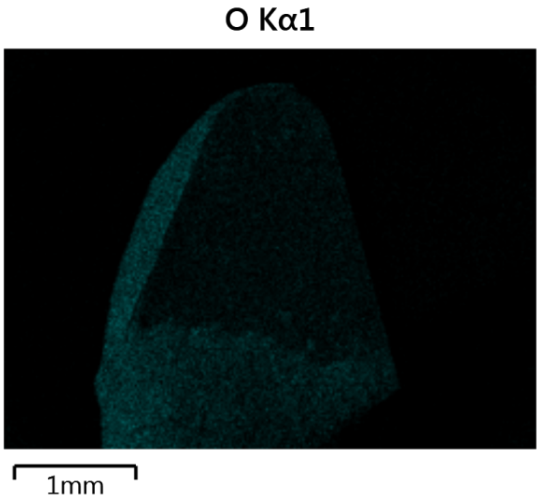


(b) O map

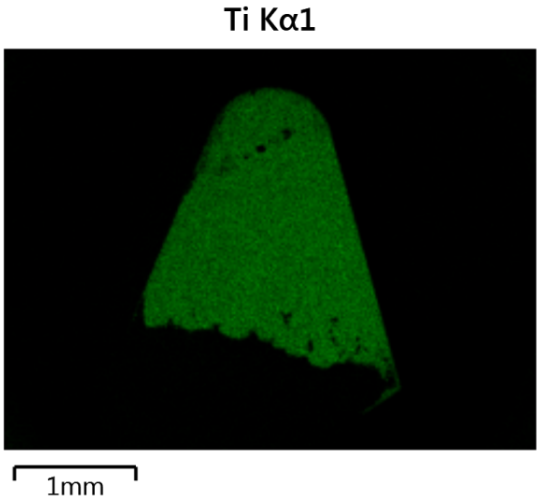


(c) Ti map

Figure D.32: Ti coating 1.0 - 1.5 $\mu$m thick at 650°C EDS element map analysis

## D.3 EDS Maps for TiAl 50:50 1.0 - 1.5 $\mu$m Thick

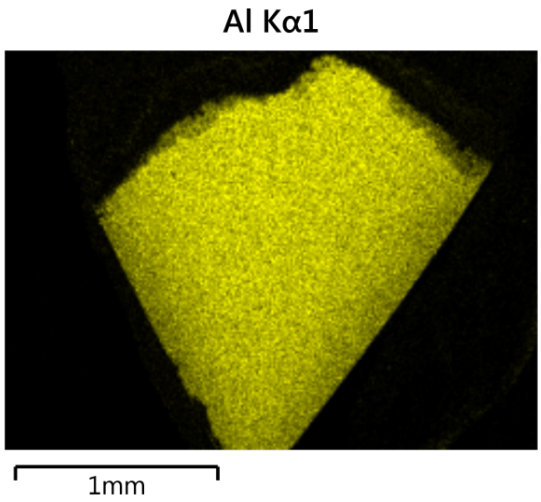


(a) Al map

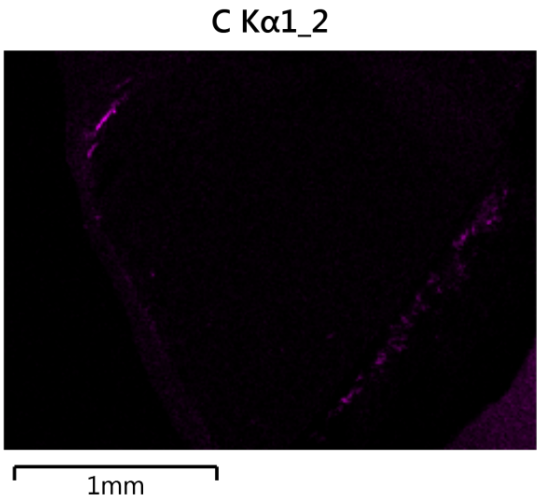


(b) C map

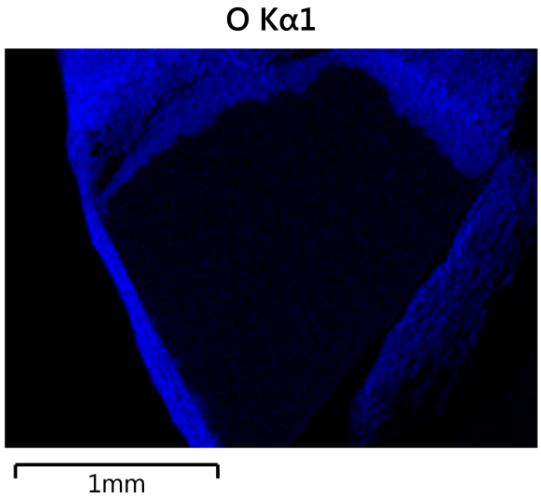


(c) O map

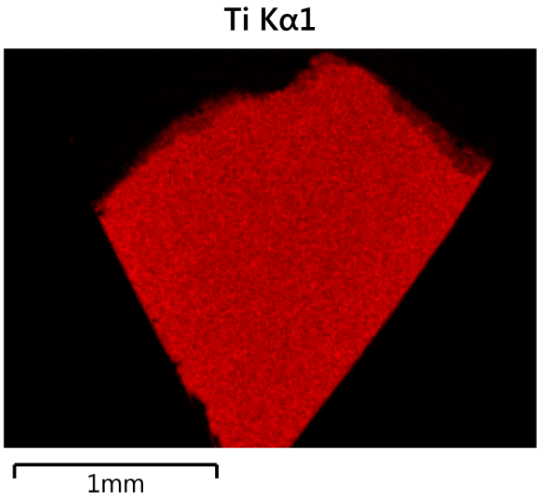


(d) Ti map

Figure D.33: TiAl coating 1.0 - 1.5 $\mu$m thick at 500°C EDS element map analysis

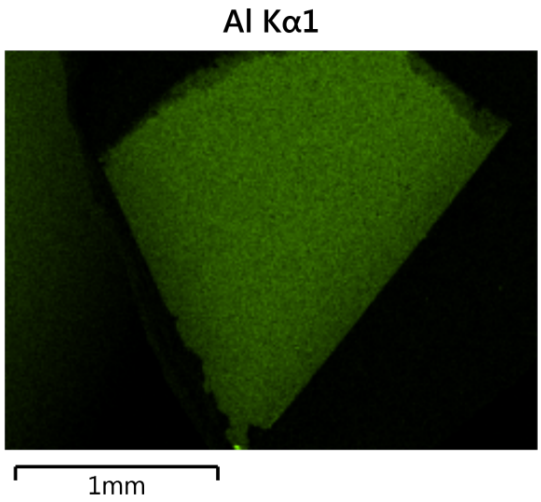


(a) Al map

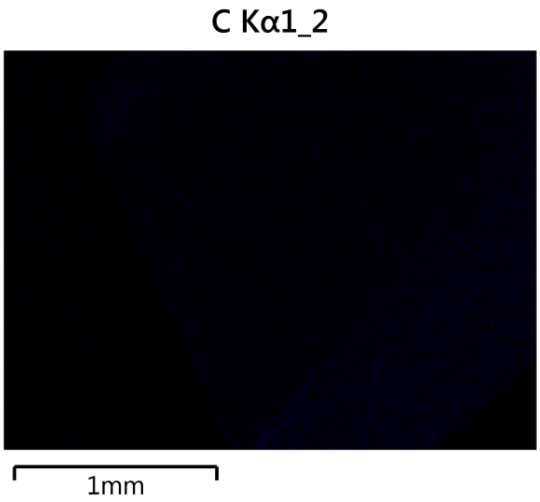


(b) C map

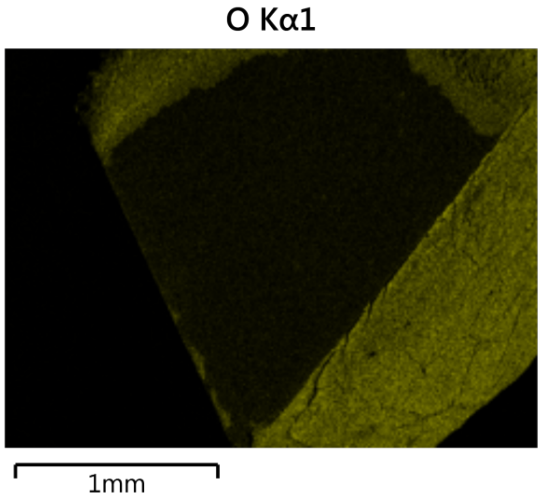


(c) O map

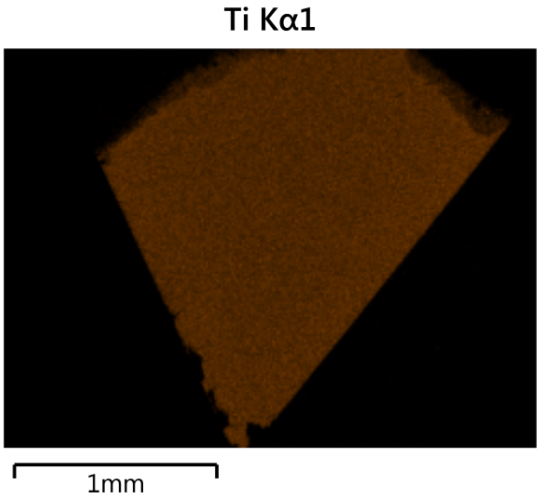


(d) Ti map

Figure D.34: TiAl coating 1.0 - 1.5 $\mu$m thick at 575°C EDS element map analysis

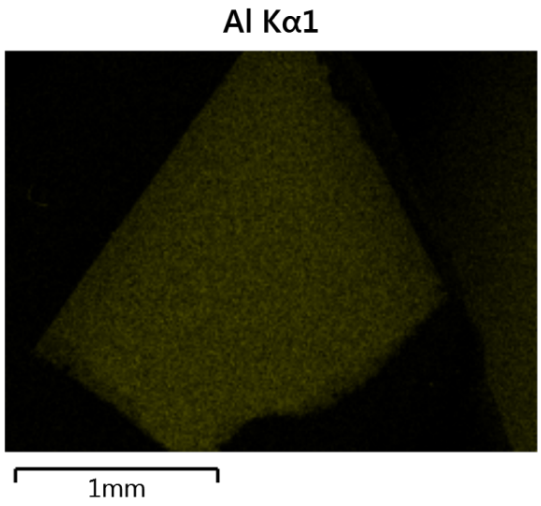


(a) Al map

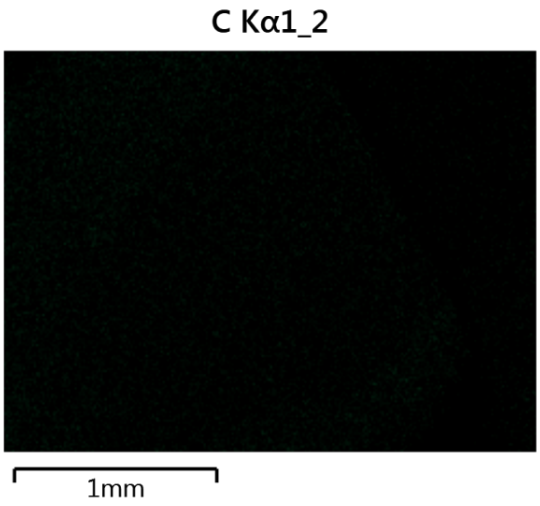


(b) C map

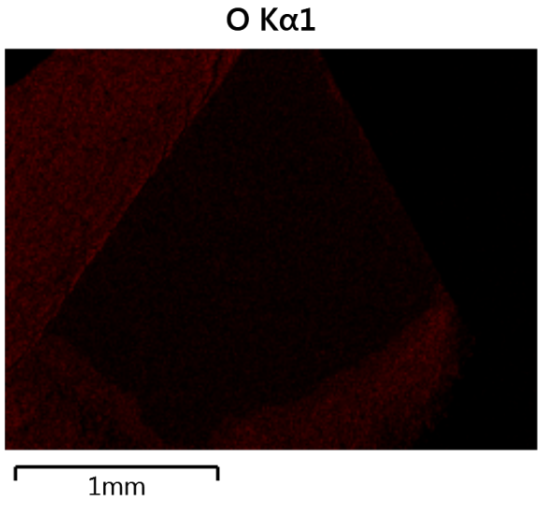


(c) O map

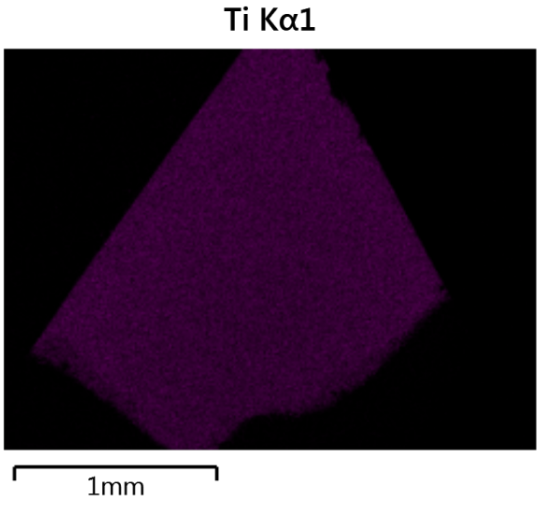


(d) Ti map

Figure D.35: TiAl coating 1.0 - 1.5 $\mu$m thick at 650°C EDS element map analysis

## D.4 EDS Maps for TiAl 40:60 1.0 - 1.5 $\mu$m Thick

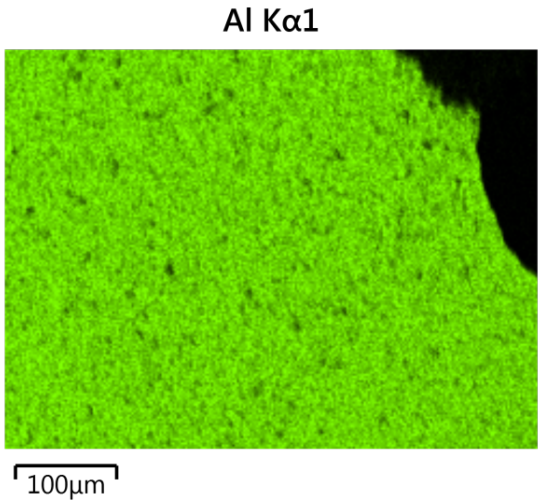


(a) Al map

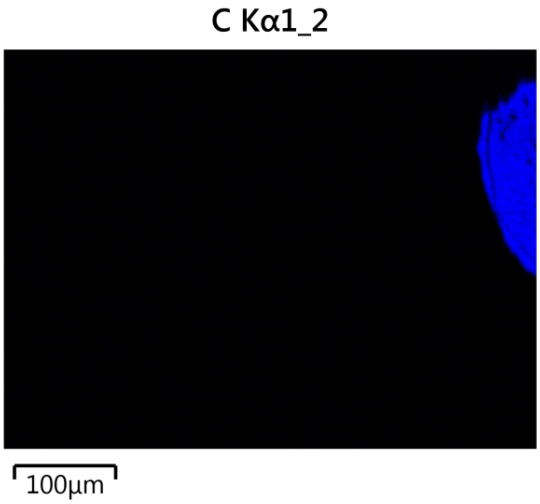


(b) C map

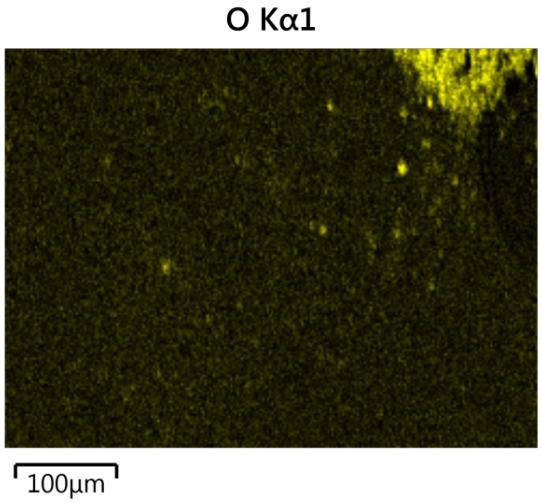


(c) O map

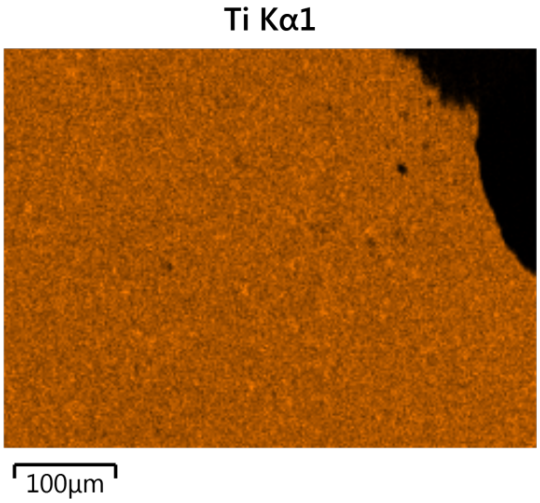


(d) Ti map

Figure D.36: TiAl 40:60 coating 1.0 - 1.5 $\mu$m thick at 500°C EDS element map analysis

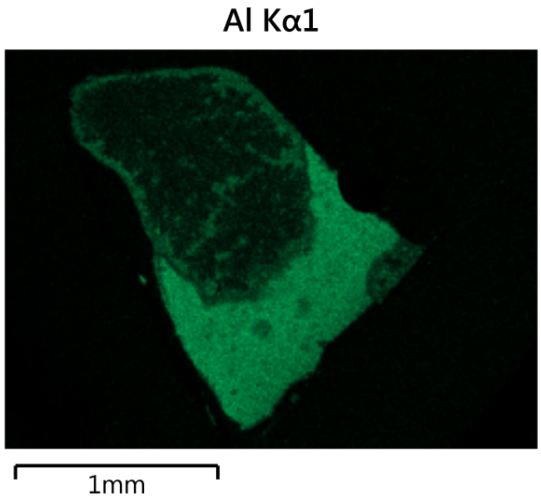


(a) Al map

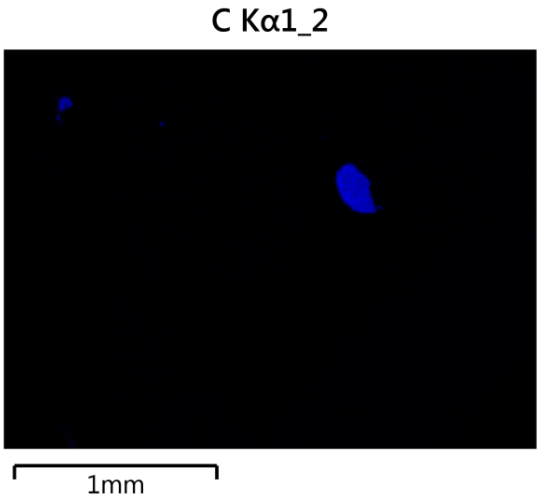


(b) C map

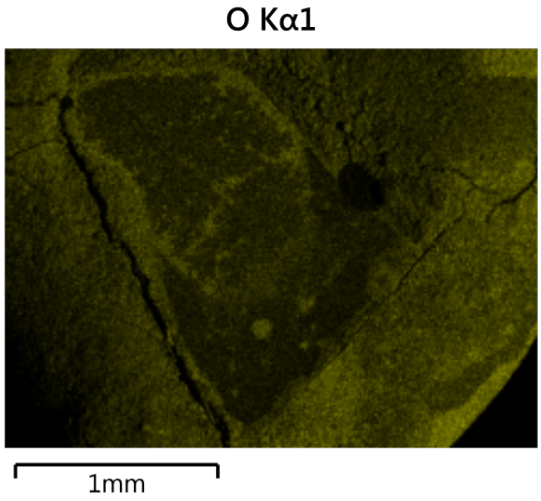


(c) O map

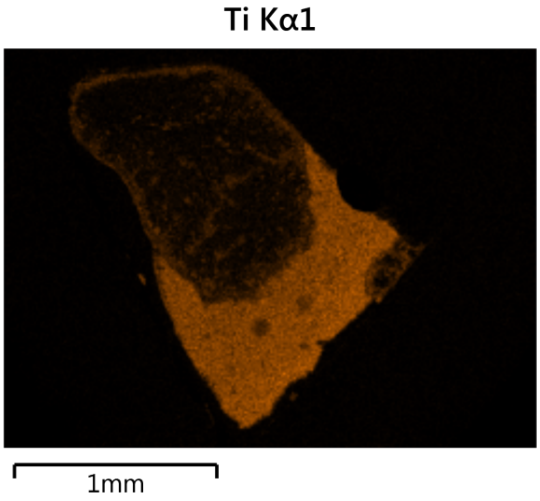


(d) Ti map

Figure D.37: TiAl 40:60 coating 1.0 - 1.5 $\mu$m thick at 575°C EDS element map analysis

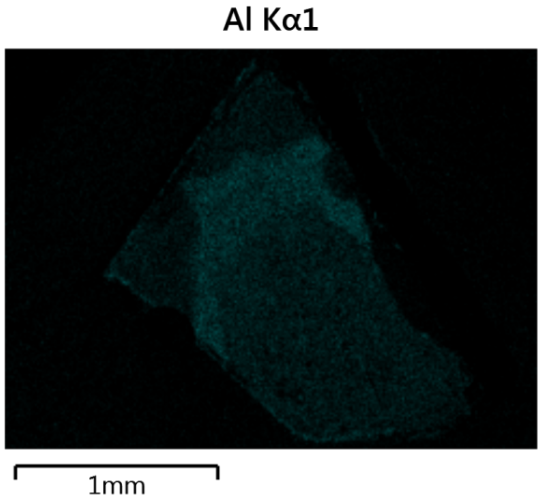


(a) Al map

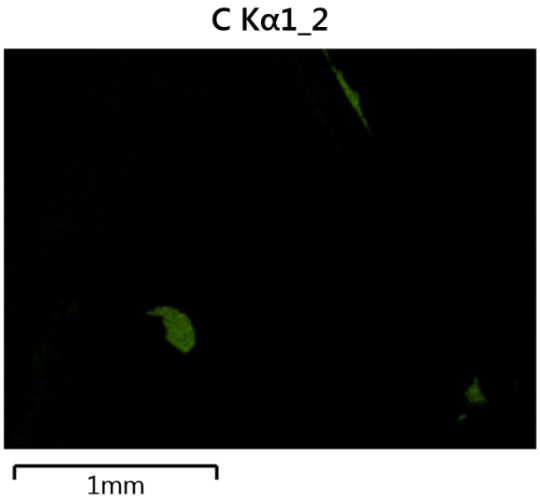


(b) C map

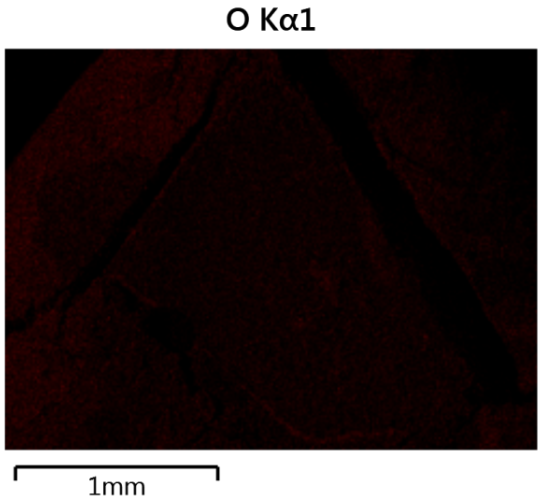


(c) O map

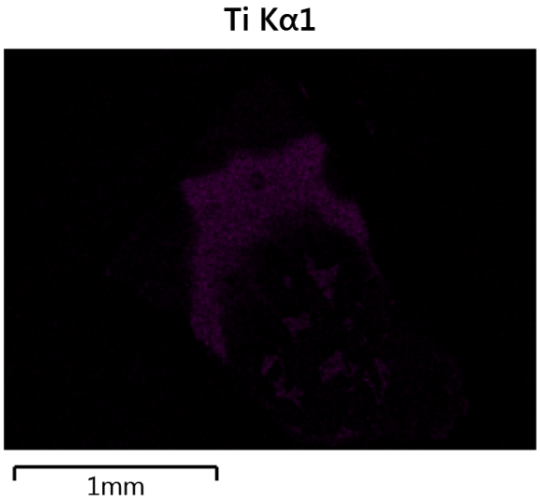


(d) Ti map

Figure D.38: TiAl 40:60 coating 1.0 - 1.5 $\mu$m thick at 650°C EDS element map analysis

# Bibliography

Arvieu, C., Manaud, J.-P., and Quenisset, J.-M. (2004). Interaction between titanium and carbon at moderate temperatures. *Journal of Alloys and Compounds*, **368**(1-2), 116–122.

Attia, M. H., Cameron, a., and Kops, L. (2002). Distortion in Thermal Field Around Inserted Thermocouples in Experimental Interfacial Studies, Part 4: End Effect. *Journal of Manufacturing Science and Engineering*, **124**(1), 135.

Berman, R. and Simon, S. F. (1955). On the Graphite-Diamond Equilibrium. *Berichte der Bunsengesellschaft für physikalische Chemie*, **59**(5), 333–338.

Bikulcius, G., Juodiene, T., and Sukiene, V. (1994). Investigation of wear of alloys based on gold. *Surface and Coatings Technology*, **64**(3), 149–154.

Bolshakov, A. and Pharr, G. M. (1998). Influences of pileup on the measurement of mechanical properties by load and depth sensing indentation techniques. *Journal of Materials Research*, **13**(04), 1049–1058.

Boussinesq, J. (1885). *Application des potentiels à l'étude de l'équilibre et du mouvement des solides élastiques: principalement au calcul des déformations et des pressions que produisent, dans ces solides, des efforts quelconques exercés sur une*

*petite partie de leur surface ou de leur intérieur: mémoire suivi de notes étendues sur divers points de physique, mathematique et d'analyse*, volume 4. Gauthier-Villars.

Bouzakis, K.-D., Michailidis, N., Skordaris, G., Bouzakis, E., Biermann, D., and M'Saoubi, R. (2012). Cutting with coated tools: Coating technologies, characterization methods and performance optimization. *CIRP annals*, **61**(2), 703–723.

Brinell, J. (1900). 2ième congres. *Internationale Métheodes d'Essai, Paris*.

Cheng, Y. T. and Cheng, C. M. (1998). Relationships between hardness, elastic modulus, and the work of indentation. *Applied Physics Letters*, **73**(5), 614–616.

das Chagas, V. M., Pecanha, M. P., da Silva Guimarães, R., dos Santos, A. A. A., de Azevedo, M. G., and Filgueira, M. (2019). The influence of titanium carbide (tic) coating over the thermal damage processes in diamonds. *Journal of Alloys and Compounds*, **791**, 438–444.

Davies, G. and Evans, T. (1972). Graphitization of diamond at zero pressure and at a high pressure. *Proceedings of the Royal Society A: Mathematical, Physical and Engineering Sciences*, **328**(1574), 413–427.

Davies, M., Ueda, T., M'Saoubi, R., Mullany, B., and a.L. Cooke (2007). On The Measurement of Temperature in Material Removal Processes. *CIRP Annals - Manufacturing Technology*, **56**(2), 581–604.

De Barros, M., Serin, V., Vandenbulcke, L., Botton, G., Andreazza, P., and Phaneuf, M. (2002). Characterisation of smooth fine-grained diamond coatings on titanium

alloy by tem/eels, raman spectroscopy and x-ray diffraction. *Diamond and related materials*, **11**(8), 1544–1551.

Doerner, M. F. and Nix, W. D. (1986). A method for interpreting the data from depth-sensing indentation instruments. *Journal of Materials Research*, **1**(4), 601–609.

Egan, D. and Engels, J. (2004). The use of coated diamonds in diamond impregnated tools. *Industrial Diamond Review*, **64**(4), 34–37.

Endler, I., Leonhardt, A., Scheibe, H.-J., and Born, R. (1996). Interlayers for diamond deposition on tool materials. *Diamond and related materials*, **5**(3-5), 299–303.

Everitt, N. M. (1990). *Indentation creep and anisotropy in magnesium oxide and germanium*. Ph.D. thesis, University of Oxford.

Faraday, M. (1857). The Bakerian Lecture: Experimental Relations of Gold (and Other Metals) to Light. *Philosophical Transactions of the Royal Society of London*, **147**(January), 145.

Fischer-Cripps, A. C. (2011). *Nanoindentation*. Springer, New York, NY, 3rd edition.

Fox-Rabinovich, G., Beake, B., Yamamoto, K., Aguirre, M., Veldhuis, S., Dosbaeva, G., Elfizy, A., Biksa, A., and Shuster, L. (2010a). Structure, properties and wear performance of nano-multilayered TiAlCrSiYN/TiAlCrN coatings during machining of Ni-based aerospace superalloys. *Surface and Coatings Technology*, **204**(21-22), 3698–3706.

Fox-Rabinovich, G., Endrino, J., Agguire, M., Beake, B., Veldhuis, S., Kovalev, A., Gershman, I., Yamamoto, K., Losset, Y., Wainstein, D., and Rashkovskiy, A.

(2012). Mechanism of adaptability for the nano-structured TiAlCrSiYN-based hard physical vapor deposition coatings under extreme frictional conditions. *Journal of Applied Physics*, **111**(6).

Fox-Rabinovich, G. S., Yamamoto, K., Beake, B. D., Kovalev, A. I., Aguirre, M. H., Veldhuis, S. C., Dosbaeva, G. K., Wainstein, D. L., Biksa, A., and Rashkovskiy, A. (2010b). Emergent behavior of nano-multilayered coatings during dry high-speed machining of hardened tool steels. *Surface & Coatings Technology*, **204**, 3425–3435.

Fu, Y., Yan, B., and Loh, N. L. (2000). Effects of pre-treatments and interlayers on the nucleation and growth of diamond coatings on titanium substrates. *Surface and Coatings Technology*, **130**(2-3), 173–185.

Galanov, B. and Dub, S. (2017). Critical comments to the oliver–pharr measurement technique of hardness and elastic modulus by instrumented indentations and refinement of its basic relations. *Journal of Superhard Materials*, **39**(6), 373–389.

Gibson, J. S. K.-L., Schroders, S., Zehnder, C., and Korte-Kerzel, S. (2017). On extracting mechanical properties from nanoindentation at temperatures up to 1000$^o$c. *Extreme Mechanics Letters*, **17**, 43–49.

Glezen, J. H., Naseem, H. A., Brown, W. D., Schaper, L. W., and Malshe, A. P. (1999). Method of electroplating a substrate, and products made thereby. US Patent 5,873,992.

Greene, K., Egan, D., Kelly, S., Nailer, S., and Melody, S. (2006). Metal coatings on synthetic diamond and their application areas. *Industrial Diamond Review*, **66**(1).

Hankins, G. A. (1925). Hardness Tests Research: Report on the Effects of Adhesion between the Indenting Tool and the Material in Ball and Cone Indentation Hardness Tests. *Proceedings of the Institution of Mechanical Engineers*, **108**(1), 611–645.

Harris, A. J., Beake, B. D., Armstrong, D. E. J., and Davies, M. I. (2016). Development of High Temperature Nanoindentation Methodology and its Application in the Nanoindentation of Polycrystalline Tungsten in Vacuum to 950 °C. *Experimental Mechanics*, pages 1–12.

Hay, J. C., Bolshakov, A., and Pharr, G. M. (1999). A critical examination of the fundamental relations used in the analysis of nanoindentation data. *Journal of Materials Research*, **14**(06), 2296–2305.

Hertz, H. (1896a). On the Contact of Elastic Solids, 1881. In *Miscellaneous papers - Primary Source Edition*, chapter 5, pages 146–162. Macmillan and Co., Ltd.

Hertz, H. (1896b). On the Contact of Rigid Elastic Solids and on Hardness, 1882. In *Miscellaneous papers - Primary Source Edition*, chapter 6, pages 163–183. Macmillan and Co., Ltd.

Howe, J. (2001). *The oxidation of diamond*. Ph.D. thesis, New York State College of Ceramics at Alfred University. Kazuo Inamori ....

Iacovangelo, C. and Jerabek, E. (1993). Metallizing cvd diamond for electronic applications. *Microelectronics 1994*, **2105**, 132.

Kanaya, K. and Okayama, S. (1972). Penetration and energy-loss theory of electrons in solid targets. *Journal of Physics D: Applied Physics*, **5**(1), 43.

Khmelnitsky, R. A. and Gippius, A. A. (2014). Transformation of diamond to graphite under heat treatment at low pressure. *Phase Transitions*, **87**(2), 175–192.

King, R. (1987). Elastic analysis of some punch problems for a layered medium. *International Journal of Solids and Structures*, **23**(12), 1657–1664.

Klocke, F., Michailidis, N., Bouzakis, K.-D., Witty, M., Gerardis, S., Lili, E., and Pappa, M. (2010). Investigation of coated tools' cutting performance in milling Ti6Al4V and its correlation to the temperature dependent impact resistance of the film. *Production Engineering*, **4**(5), 509–514.

Koester, R. and Moak, D. (1967). Hot hardness of selected borides, oxides, and carbides to 1900 c. *Journal of the American Ceramic Society*, **50**(6), 290–296.

Korte, S., Stearn, R. J., Wheeler, J. M., and Clegg, W. J. (2012). High temperature microcompression and nanoindentation in vacuum. *Journal of Materials Research*, **27**(01), 167–176.

Lee, M. (1983). High temperature hardness of tungsten carbide. *Metallurgical Transactions A*, **14**(8), 1625–1629.

Lo, R. Y. and Bogy, D. B. (1999). Compensating for elastic deformation of the indenter in hardness tests of very hard materials. *Journal of materials research*, **14**(6), 2276–2282.

Loffler, F. H. W. (1994). Systematic approach to improve the performance of PVD coatings for tool applications. *Surface and Coatings Technology*, **68/69**(0), 729–740.

Loubet, J., Georges, J., Marchesini, O., and Meille, G. (1984). Vickers indentation curves of magnesium oxide (MgO). *Journal of tribology*, **106**(1), 43–48.

Love, A. E. H. (1929). The stress produced in a semi-infinite solid by pressure on part of the boundary. *Philosophical Transactions of the Royal Society of London. Series A, Containing Papers of a Mathematical or Physical Character*, **228**, 377–420.

Love, A. E. H. (1939). Boussinesq's problem for a rigid cone. *The Quarterly Journal of Mathematics*, (1), 161–175.

Lucas, B. and Oliver, W. (1995). Time dependent indentation testing at non-ambient temperatures utilizing the high temperature mechanical properties microprobe. *Materials Research Society Symposium - Proceedings*, **356**, 645 – 650.

Ludwik, P. (1908). Die Kegelprobe. In *Die Kegelprobe*, pages 3–17. Springer.

Meyer, E. (1908). Contribution to the knowledge of hardness and hardness testing. *Zeitschrift Des Vereines Deutscher Ingenieure*, **52**, 740–835.

Mukhanov, V. A., Kurakevych, O. O., and Solozhenko, V. L. (2009). Hardness of materials at high temperature and high pressure. *Philosophical Magazine*, **89**(25), 2117–2127.

Naidich, Y., Umanskii, V., and Lavrinenko, I. (1984). Metal and alloy bond strengths to diamond. *Ind. Diamond Rev.*, **44**(505), 327–331.

Ning, L., Veldhuis, S., and Yamamoto, K. (2008). Investigation of wear behavior and chip formation for cutting tools with nano-multilayered TiAlCrN/NbN PVD coating. *International Journal of Machine Tools and Manufacture*, **48**(6), 656–665.

Ning, Y., Rahman, M., and Wong, Y. S. (2001). Investigation of chip formation in high speed end milling. *Journal of Materials Processing Technology*, **113**(1), 360–367.

Oliver, W. C. and Pharr, G. M. (1992). An improved technique for determining hardness and elastic modulus using load and displacement sensing indentation experiments. *Journal of Materials Research*, **7**(6), 1564–1583.

Oliver, W. C. and Pharr, G. M. (2004). Measurement of hardness and elastic modulus by instrumented indentation: Advances in understanding and refinements to methodology. *Journal of Materials Research*, **19**(1), 3–20.

Peng, X. and Clyne, T. (1997). Formation and adhesion of hot filament cvd diamond films on titanium substrates. *Thin solid films*, **293**(1-2), 261–269.

Pervaiz, S., Rashid, A., Deiab, I., and Nicolescu, M. (2014). Influence of Tool Materials on Machinability of Titanium- and Nickel-Based Alloys: A Review. *Materials and Manufacturing Processes*, **29**(3), 219–252.

Pethica, J. B., Hutchings, R., and Oliver, W. C. (1983). HARDNESS MEASUREMENT AT PENETRATION DEPTHS AS SMALL AS 20 NM. *Philosophical Magazine A: Physics of Condensed Matter, Structure, Defects and Mechanical Properties*, **48**(4), 593–606.

Pharr, G. M. and Bolshakov, a. (2002). Understanding nanoindentation unloading curves. *Journal of Materials Research*, **17**(10), 2660–2671.

Pharr, G. M., Oliver, W. C., and Brotzen, F. R. (1992). On the generality of the

relationship among contact stiffness, contact area, and elastic modulus during indentation. *Journal of Materials Research*, **7**(3), 613–617.

Polini, R., Mantini, F. P., Barletta, M., Valle, R., and Casadei, F. (2006). Hot filament chemical vapour deposition and wear resistance of diamond films on wc-co substrates coated using pvd-arc deposition technique. *Diamond and related materials*, **15**(9), 1284–1291.

Pring, J. N. and Fielding, W. (1909). The Preparation at High Temperatures of Some Refractory Metals From Their Chlorides. *Journal of the Chemical Society*, **95**, 1497–1506.

Quinto, D. T., Wolfe, G. J., and Jindal, P. C. (1987). High temperature microhardness of hard coatings produced by physical and chemical vapor deposition. *Thin solid films*, **153**(1-3), 19–36.

Rech, J., Battaglia, J., and Moisan, A. (2005). Thermal influence of cutting tool coatings. *Journal of Materials Processing Technology*, **159**(1), 119–124.

Rosa, M. C. G., Peçanha, M. P., and Filgueira, M. (2015). Thermal damage in diamonds: the protective effect of titanium coating. *Materials Research*, **18**(4), 683–689.

Silva, F., Baptista, A., Pereira, E., Teixeira, V., Fan, Q., Fernandes, A., and Costa, F. (2002). Microwave plasma chemical vapour deposition diamond nucleation on ferrous substrates with ti and cr interlayers. *Diamond and Related Materials*, **11**(9), 1617–1622.

Smith, R. and Sandland, G. (1925). Some notes on the use of a diamond pyramid for hardness testing. *J. Iron Steel Inst*, **111**, 285–294.

Sneddon, I. (1951). *Fourier Transforms, International Series in Pure and Applied Mathematics*. McGraw-Hill.

Sneddon, I. N. (1946). Boussinesq's problem for a flat-ended cylinder. In *Mathematical Proceedings of the Cambridge Philosophical Society*, volume 42, pages 29–39. Cambridge Univ Press.

Sneddon, I. N. (1948). Boussinesq's problem for a rigid cone. In *Mathematical Proceedings of the Cambridge Philosophical Society*, volume 44, pages 492–507. Cambridge Univ Press.

Sneddon, I. N. (1960). The elementary solution of dual integral equations. In *Proceedings of the Glasgow Mathematical Association*, volume 4, pages 108–110. Cambridge Univ Press.

Sneddon, I. N. (1965). The Relation Between Load and Penetration in the Axisymmetric Boussinesq Problem for a Punch of Arbitrary Profile. *International Journal of Engineering Science*, **3**(1), 47–57.

Sproul, W. D. (1996). Physical vapor deposition tool coatings. *Surface and Coatings Technology*, **81**(1), 1–7.

Stilwell, N. A. and Tabor, D. (1961). Elastic Recovery of Conical Indentations. *Proceedings of the Physical Society*, **78**(2), 169–179.

Syed Asif, S. and Pethica, J. (1998). Nano-scale indentation creep testing at non-ambient temperature. *The Journal of Adhesion*, **67**(1-4), 153–165.

Tabor, D. (1948). A simple theory of static and dynamic hardness. *Proceedings of the Royal Society of London. Series A. Mathematical and Physical Sciences*, **192**(1029), 247–274.

Tabor, D. (1951). *The Hardness of Metals*. Clarendon Press.

Tadao, I., Tomohisa, K., Osamu, K., and Hitoshi, M. (1997). Grinding ability of tungsten-coated diamond composite sintered tool. *Trans Jpn Soc Mech Eng*, pages 2694–2700.

Timoshenko, S. (1951). *Theory of elasticity*. Engineering societies monographs. McGraw-Hill, New York, 2nd ed. edition.

Trenkle, J. C., Packard, C. E., and Schuh, C. A. (2010). Hot nanoindentation in inert environments. *Review of Scientific Instruments*, **81**.

Trent, E. M. and Wright, P. K. (2000). *Metal Cutting*. Butterworth-Heinemann, Woburn, MA, USA, 4 edition.

Urbonaite, S., Wachtmeister, S., Mirguet, C., Coronel, E., Zou, W., Csillag, S., and Svensson, G. (2007). Eels studies of carbide derived carbons. *Carbon*, **45**(10), 2047–2053.

Venkatesh, V., Zhou, D., Xue, W., and Quinto, D. (1993). A Study of Chip Surface Characteristics during the Machining of Steel*. *CIRP Annals-Manufacturing Technology*, **42**(1), 631–636.

Wang, Y. H., Zang, J. B., Wang, M. Z., and Zheng, Y. (2003). Relationship of interface microstructure and adhesion strength between ti coating and diamond. In *Key Engineering Materials*, volume 250, pages 41–45. Trans Tech Publ.

Webb, S. W. (1999). Diamond retention in sintered cobalt bonds for stone cutting and drilling. *Diamond and Related Materials*, **8**(11), 2043–2052.

Wheeler, J., Armstrong, D., Heinz, W., and Schwaiger, R. (2015). High temperature nanoindentation: The state of the art and future challenges. *Current Opinion in Solid State and Materials Science*.

Wheeler, J. M. and Michler, J. (2013). Invited Article: Indenter materials for high temperature nanoindentation. *The Review of Scientific Instruments*, **84**.

Wheeler, J. M., Oliver, R. A., and Clyne, T. W. (2010a). AFM observation of diamond indenters after oxidation at elevated temperatures. *Diamond & Related Materials*, **19**(11), 1348–1353.

Wheeler, J. M., Collier, C. A., Paillard, J. M., and Curran, J. A. (2010b). Evaluation of micromechanical behaviour of plasma electrolytic oxidation (PEO) coatings on Ti-6Al-4V. *Surface & Coatings Technology*, **204**(21-22), 3399–3409.

Yu, X., Zhao, X.-a., Liu, Y.-y., Hua, M., and Jiang, X. (2014). The effects of ti carbonization on the nucleation and oriented growth of diamond films on cemented carbide. *ACS applied materials & interfaces*, **6**(7), 4669–4677.

Zhang, X.-F. and Lu, A.-X. (2007). Effects of titanium coating on property of diamond. *Transactions of Nonferrous Metals Society of China*, **17**(4), 715–719.

Zhao, Y.-P., Shi, X., and Li, W. J. (2003). *Reviews on Advanced Materials Science*, **5**(4), 348–353.